TU/e EINDHOVEN UNIVERSITY OF TECHNOLOGY

Understanding Allosteric Modulation of Nuclear Receptors by Engineering Proteins and Assays

Citation for published version (APA):
Leijten-van de Gevel, I. A. (2022). *Understanding Allosteric Modulation of Nuclear Receptors by Engineering Proteins and Assays*. [Phd Thesis 1 (Research TU/e / Graduation TU/e), Biomedical Engineering]. Eindhoven University of Technology.

Document status and date:
Published: 25/05/2022

Document Version:
Publisher's PDF, also known as Version of Record (includes final page, issue and volume numbers)

Please check the document version of this publication:

• A submitted manuscript is the version of the article upon submission and before peer-review. There can be important differences between the submitted version and the official published version of record. People interested in the research are advised to contact the author for the final version of the publication, or visit the DOI to the publisher's website.
• The final author version and the galley proof are versions of the publication after peer review.
• The final published version features the final layout of the paper including the volume, issue and page numbers.

Link to publication

General rights
Copyright and moral rights for the publications made accessible in the public portal are retained by the authors and/or other copyright owners and it is a condition of accessing publications that users recognise and abide by the legal requirements associated with these rights.

• Users may download and print one copy of any publication from the public portal for the purpose of private study or research.
• You may not further distribute the material or use it for any profit-making activity or commercial gain
• You may freely distribute the URL identifying the publication in the public portal.

If the publication is distributed under the terms of Article 25fa of the Dutch Copyright Act, indicated by the "Taverne" license above, please follow below link for the End User Agreement:

www.tue.nl/taverne

Take down policy
If you believe that this document breaches copyright please contact us at:

openaccess@tue.nl

providing details and we will investigate your claim.

Download date: 05. Oct. 2023

Understanding Allosteric Modulation of Nuclear Receptors by Engineering Proteins and Assays

PROEFSCHRIFT

ter verkrijging van de graad van doctor aan de Technische Universiteit Eindhoven, op gezag van de rector magnificus prof.dr.ir. F.P.T. Baaijens, voor een commissie aangewezen door het College voor Promoties, in het openbaar te verdedigen op woensdag 25 mei 2022 om 16:00 uur

door

Iris Amber Leijten – van de Gevel

geboren te Rosmalen

Dit proefschrift is goedgekeurd door de promotoren en de samenstelling van de promotiecommissie is als volgt:

voorzitter:	prof.dr. M. Merkx
1e promotor:	prof.dr.ir. L. Brunsveld
2e promotor:	dr. C. Ottmann
leden:	prof.dr. W.T. Zwart
	prof.dr.rer.nat.habil. D. Merk
	dr. E. Kalkhoven
	dr. F. Grisoni
	dr. S. van Zanten

Het onderzoek of ontwerp dat in dit proefschrift wordt beschreven is uitgevoerd in overeenstemming met de TU/e Gedragscode Wetenschapsbeoefening

“A scientist in his laboratory is not a mere technician: he is also a child confronting natural phenomena that impress him as though they were fairy tales.”

Marie Curie

I.A. Leijten-van de Gevel ©

Cover design: ICMS Animation Studio, TU/e

Printed by: ADC Dereumaux – the Netherlands

A catalogue record is available from the Eindhoven University of Technology Library ISBN: 978-90-386-5504-8

This work has been financially supported by the Dutch Ministry of Education, Culture and Science (Gravity program 024.001.035)

Table of contents

Chapter 1

Allosteric Modulation of Nuclear Receptors

Abstract

Nuclear Receptors (NRs) are multi-domain proteins, whose natural regulation occurs via ligands for a classical, orthosteric, binding pocket and via intra-and inter-domain allosteric mechanisms. Allosteric modulation of NRs via synthetic small molecules has recently emerged as an interesting entry to address the need for small molecules targeting NRs in pathology, via novel modes of action and with beneficial profiles. In this chapter the general concept of allosteric modulation in drug discovery is first discussed, serving as a background and inspiration for NRs. Subsequently, the obtained insights serve as a basis for recommendations for the next steps to take in allosteric small molecular targeting of NRs. More specifically, this chapter serves as an introduction for investigating the mechanisms behind the allosteric modulation of RORγt and PPARγ.

Parts of this chapter have been published as: Leijten-van de Gevel, I. A.*, Meijer, F. A.*, de Vries, R. M. J. M.* & Brunsveld, L. Allosteric small molecule modulators of nuclear receptors. *Mol. Cell. Endocrinol.* 485, 20–34 (2019).

* These authors contributed equally

Introduction

Structural organization of nuclear receptors

The nuclear receptor (NR) superfamily consists of 48 members that are structurally related but have functions in all kinds of physiological processes and, in connection with that, diseases. Their key role in these processes makes them a very attractive drug target.[1,2] NRs have a conserved domain organization starting at the N-terminus with the highly variable N-terminal domain (NTD). For most NRs this domain contains a ligand-independent activation function (AF1). The NTD is intrinsically disordered (ID), but the interaction with binding partners can induce folding which can enhance transcriptional activity.[3] The NTD is followed by the DNA binding domain (DBD) which uses its two zinc fingers to recognize specific hormone response elements (HREs). The affinity for specific HREs is dependent on the NR subtype and NR homo- or heterodimerization, or in some cases monomeric binding to extended HREs.[4,5] The DBD is connected to the ligand binding domain (LBD) via a hinge region that typically contains a nuclear localization signal and can undergo posttranslational modifications.[6] The LBD is a highly conserved domain typically built up out of 12 helices which are organized in an antiparallel, globular arrangement.[7] The classical "mouse-trap" model states that when an agonistic ligand binds in the ligand binding pocket (LBP), helix 12 (H12) covers the pocket and creates a surface suitable for coactivator binding.[8] Nowadays, this model is under debate and an alternative "dynamic stabilization" model is evoked.[9] This concept states that the LBD in its apo form is in a partially molten state and can adopt a wide range of conformations. Agonist binding stabilizes the fold of H12 and the surface elements required for coactivator binding in the active conformation.[10] Inverse agonists, on the other hand, can increase corepressor recruitment which represses transcription in constitutively active NRs.[11] Antagonists do not cause cofactor recruitment, but do prevent agonist binding and therefore passively repress transcription.[11] C-terminal to the LBD, certain NRs have an additional F-domain that has a variable length and has functions ranging from interacting with other proteins to stabilizing the ligand bound conformations of the LBD.[12]

Inter-domain allosteric regulation of nuclear receptor activity

Up until a few years ago, NR structural information was only available for certain separate domains. This did give a lot of information on ligand- and DNA binding as well as on dimerization of separate LBDs or DBDs, but left a demand for information

on the implications of inter-domain communication.[10] Since 2008, multi-domain structures obtained via different scattering techniques started appearing. These structures provided more insight into the interplay between the different NR domains. In particular, it became clear that the different domains within a NR act and communicate via modulatory, allosteric mechanisms. Allostery, in general, is the process where binding of an interaction partner, e.g. ligand or protein, at one site of a protein results in a functional change at another, topographically distinct, site. This means that there is communication over a distance between the binding site, 'input', and the site of the biological response, 'output', via a conformational change in the protein structure.[13,14] Different endogenic types of allosteric regulatory mechanisms have been described for NRs as conceptually summarized in Figure 1.

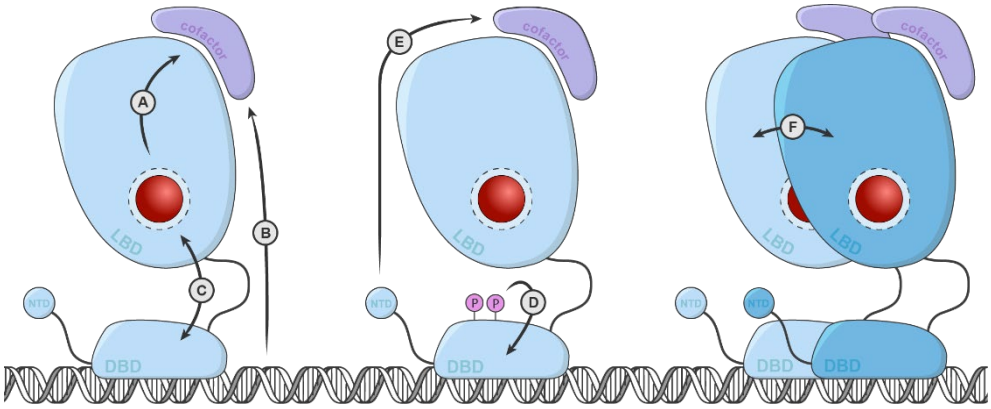

Figure 1 | Conceptual modes of endogenous NR allosteric regulation. (*A*) From the Ligand Binding Pocket to the cofactor binding site (*B*) From the DNA to the cofactor binding site (*C*) Between the DNA Binding Domain and the Ligand Binding Domain (*D*) Via post-translational modifications within and over NR domains (*E*) From the N-terminal domain to the cofactor binding site (*F*) Between NR dimerization partners.

First of all, and most obvious, the majority of NR ligands bind to the LBP, which causes a conformational change in the LBD and as a result regulates cofactor recruitment elsewhere on the LBD (Figure 1*A*).[15] Besides this prime NR allosteric mechanism, other and frequently more subtle allosteric mechanisms can be found in endogenous NR regulation.

The interplay of the specific HRE with the cofactor binding site of a NR is an example of such an allosteric mechanism via inter-domain communication (Figure 1*B*).[16–18] Several studies have been performed to obtain a better understanding of the

allosteric communication between the DBD and cofactor binding site.[19–21] In these studies, isothermal titration calorimetry (ITC) and hydrogen/deuterium exchange (HDX) techniques were used, showing an enhancement of cofactor recruitment upon binding of the receptor complex to its HRE. The LBD and DBD can also allosterically influence each-others ligand affinity, as exemplified by Helsen *et al.* (2012) (Figure 1*C*).[22] When residues from the LBD-DBD surface, known to correlate with pathologies, were mutated, mutations on one domain led to altered ligand/DNA binding of the other domain.[22]

Another example of allosteric mechanisms in NR regulation is the mediation of activity via post-translational modifications (PTMs). PTMs can be present at one site of the protein and can have various effects, including modifying cofactor interactions, changing cellular localization, regulating protein stability and influencing DNA binding at a different site (Figure 1*D*).[23] The most intensively studied PTMs on NRs are phosphorylation, acetylation, ubiquitinylation and SUMOylation. Examples of these are known for almost all NRs and their functioning, including allosteric modes, has been reviewed elsewhere.[24–26]

The NR NTD has also been described to be involved in allosteric communication (Figure 1*E*). Even though there is poor conservation in NTD sequence, in the mineralocorticoid receptor (MR), glucocorticoid receptor (GR) and progesterone receptor (PR) an increase in helical content is observed in reaction to TATA box binding protein (TBP) binding to the NTD, indicating a common mechanism of regulation.[27–29]

Homodimerization or heterodimerization with the retinoid X receptor (RXR) is a common phenomenon for regulation of NRs (Figure 1*F*). These processes, similar to the binding of other protein partners, change the structural plasticity, and thereby the behavior of a NR.[30,31] This, in turn, can allosterically affect the recruitment and binding of ligands. Although most heterodimers are formed with RXR, “atypical” heterodimers present a novel class of physical complexes which might constitute an uncharted space to target nuclear receptor actions.[32]

The above summary acts to illustrate that NR regulation involves several allosteric mechanisms. For a more detailed review on this subject the reader could consider an extensive review by Fernandez.[33] Despite these various endogenous allosteric mechanisms, the number of actual endogenic molecules known to act via allosteric pockets on the NR is extremely limited. In this chapter, allosteric processes in NR

modulation using small molecules will be discussed as well as assays available to find these molecules. Allosteric NR modulation by synthetic small molecules is a relatively new area of research, in contrast to the classic targeting of the orthosteric LBP.[34,35] While extremely successful, targeting NRs via the orthosteric LBP also brings along certain limitations and challenges.[36] Selectivity issues can arise due to a high degree of similarity in the LBP between certain NRs, which can lead to side effects. Furthermore, mutations can occur in the LBP upon prolonged drug-treatment, which can lead to drug resistance or even agonist/antagonist switching.[36–38] Allosteric modulation of NRs with small molecules, via targeting binding sites beyond the orthosteric pocket, could therefore be a valuable alternative way of targeting NRs that could potentially overcome some of the described shortcomings of orthosteric ligands.

Small molecule allosteric modulation in drug discovery

Allosteric small molecule modulators and their potential in drug discovery

Most receptor classes possess endogenous ligands that bind to a defined site, typically termed the orthosteric binding site. Most drugs on the market are similarly targeting these orthosteric pockets and are in essence thus competing with the endogenous ligands.[34,36,39] Allosteric ligands bind to sites on proteins that do not overlap with the orthosteric site and are therefore potentially resistant to orthosteric competition.[40] For multiple receptor classes, such as GPCRs and ligand-gated ion channels, but also for enzymes, a significant number of allosteric modulators have already been identified with considerable success.[41–46] Especially for GPCRs and proteins kinases, multiple allosteric ligands have been identified with some being approved by the FDA, such as Sensipar and Gleevec, and multiple drugs are undergoing clinical trials.[44,47,48] Within the last two decades, an increasing number of connected publications can be observed, demonstrating the growth in interest and development of allosteric modulators (Figure 2). NRs have similarly seen an increase in attention regarding the identification of allosteric ligands, but here the number of publications is still lagging strongly behind those for other receptor classes.

The rapid increase in the attention for allosteric modulators can be explained by several key advantages such ligands have in comparison with orthosteric ligands. First, allosteric sites show greater structural diversity compared to the more conserved orthosteric sites. This could thus lead to a higher degree of selectivity for

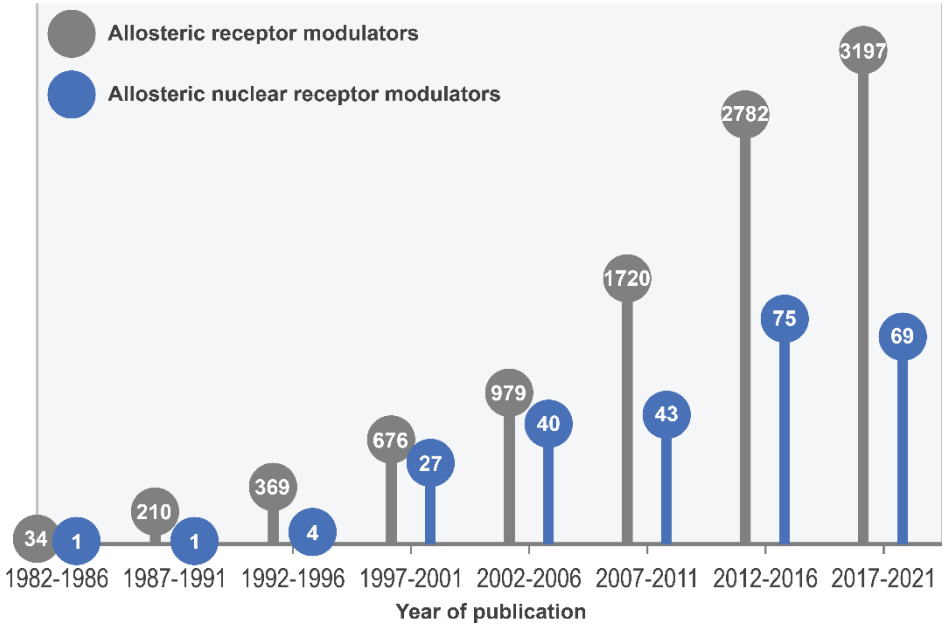

Figure 2 | Results of a SciFinder search showing the number of publications on 'allosteric receptor modulators' (shown in grey) between 1982 and 2021. The subset of these publications focusing on 'allosteric ligands for nuclear receptors' is shown in blue.

closely related proteins.[37,49] Second, as mentioned earlier, allosteric compounds are typically not in competition with the receptor's endogenous ligand. Therefore, allosteric modulators could eventually be used at lower concentrations resulting in reduced side effects. Furthermore, in the case of drug-resistant mutations in the orthosteric binding site, allosteric ligands can pose a promising alternative entry. In addition, since the binding of the allosteric ligand can potentially modulate the binding affinity and efficacy of the orthosteric ligand, a pathway is provided to fine-tune the physiological response of both. Despite these favorable characteristics, the challenge of discovering allosteric drugs is a highly relevant current limitation, since allosteric sites are often not identified or lack specific assay formats for targeted ligand screening.[49] At present, the majority of potential drug molecules are identified using high-throughput screening (HTS), for which the binding affinity of the ligand is often a hallmark to define the quality of the hit. The orthosteric site can, however, be expected to be dominant in this aspect, limiting the identification of ligands with allosteric binding modes.

The different modes-of-action of allosteric modulators described in literature, as well as the different assay techniques developed for the identification of such

allosteric ligands, can serve as inspiration for allosteric targeting of NRs. A compact summary of these concepts, illustrated with selected highlights, as described for other receptor classes is therefore discussed below.

Mechanisms of action of allosteric receptor modulators

The mechanisms by which allosteric modulators exert their function has been investigated in molecular detail, especially using crystal- and solution-based structural data. Allosteric modulators can induce an altered physiological response in multiple ways because their binding changes the preference of populating certain conformations by the protein of interest, alone or in consort with an endogenous ligand for the orthosteric site (Figure 3). The section below is geared mostly to membrane proteins and specifically GPCRs as the studies of these proteins serve as important illustrative examples for the much less investigated small molecule NR allosteric modulation.

The majority of the allosteric ligands present in literature bind to pockets in an area surrounding the canonical binding site. This, in turn, influences the binding affinity and efficacy of the orthosteric ligand (Figure 3*A*).[44] Nevertheless, an allosteric molecule does not have to be in close proximity of the orthosteric site to alter the binding kinetics of the endogenous ligand. This arises from the fact that allosterically induced conformational shifts can be at one part of the protein, but can also change the conformation of the entire protein.[50,51]

Allosteric ligands can also alter the dimerization behavior of a protein (Figure 3*B*). For receptor tyrosine kinases, examples are present for both inhibiting dimerization by binding of a monoclonal antibody to the dimerization interface and enhancing dimerization by covalent attachment of a small molecule.[52,53]

ID protein domains have also come to the forefront for allosteric regulation with small molecules (Figure 3*C*). The absence of a defined secondary structure in these domains makes them devoid of a classical binding pocket.[54,55] Nevertheless, small molecules and macromolecules have been shown to be capable of binding to these regions and of subsequently inducing a defined secondary structure.[56,57]

Bitopic ligands, also known as dualsteric ligands, are allosteric modulators in which the orthosteric and allosteric pharmacophore are covalently linked, allowing them to bind to both pockets simultaneously (Figure 3*D*). Apart from ensuring a stronger binding of the bitopic ligand to the receptor, the additional allosteric

pharmacophore can lead to an improved selectivity and a nuance in receptor activation.[58–60]

Certain receptor proteins contain allosteric pockets featuring a reactive group that can be addressed with a covalent ligand (Figure 3*E*). From a therapeutic point-of-view, such reactive groups are especially relevant when they represent mutated residues correlated to disease development. When compounds make use of a mutated residue, the natural protein is not affected.[61]

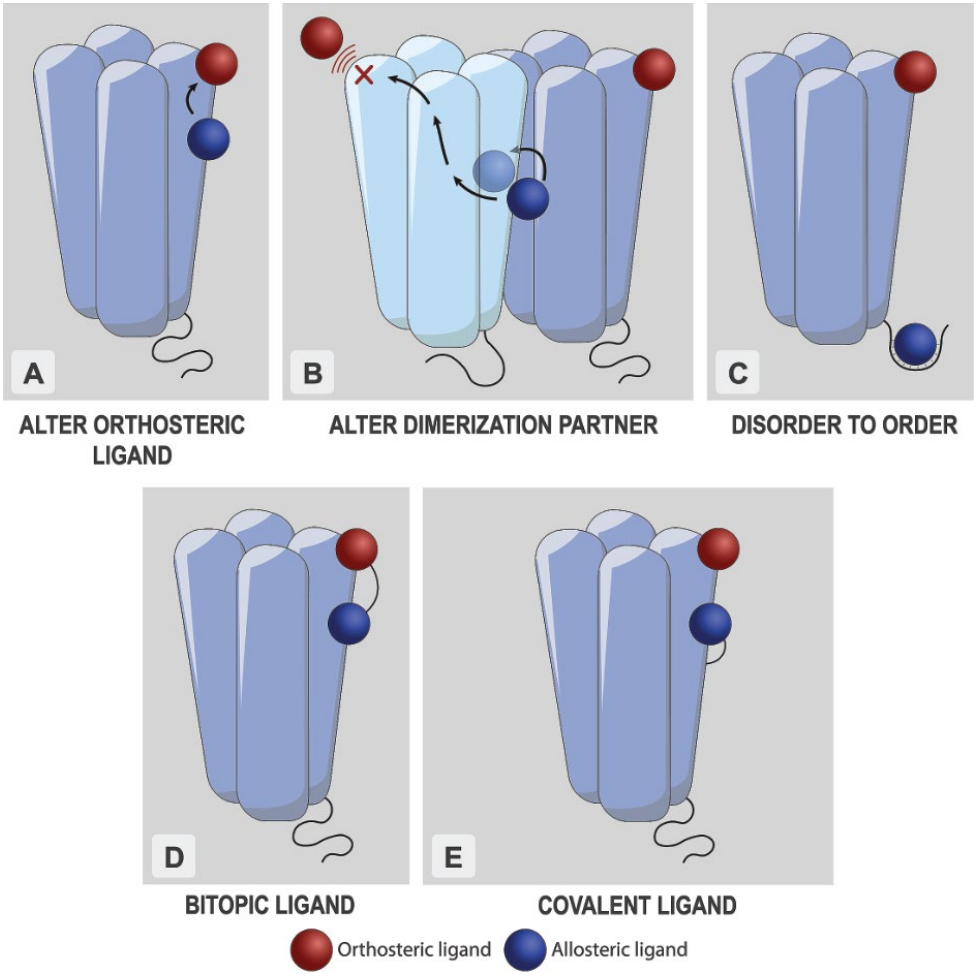

Figure 3 | Schematic representation of five different modes of allosteric modulation of receptor activity. (*A*) Allosteric compounds can change orthosteric ligand binding. (*B*) Via allosteric binding, dimerization behavior can be altered. (*C*) Binding of an allosteric ligand can induce structure in a disordered region. (*D*) A bitopic ligand links an orthosteric and an allosteric binding site. (*E*) Allosteric ligands can be covalently attached.

Techniques for the identification of allosteric ligands

The increase in focus on the modulation of proteins by allosteric ligands comes with a concurrent demand for novel screening techniques that both aid in the identification of allosteric pockets and in the discovery of small molecules specifically targeting these pockets. Some of the most promising techniques and examples, including computational approaches, fragment soaking, tethering and phage display, are shortly summarized mentioned here to act as a potential framework to be translated to NRs.

Crystal structures of ligand-bound proteins provide high-resolution information about the binding mode of the ligand. The resulting static picture can be further refined with techniques providing dynamic information.[62] Over the last decades, numerous computational methods have been developed to provide a better understanding of the dynamic behavior of the protein, which is of high relevance for the identification of allosteric sites.[63–68] The computer-aided drug design allows to help understand how allosteric modulators exert their function.[69]

Fragment-based drug discovery is achieving a strong impact for discovering allosteric binding sites, for example via X-ray crystallography based fragment soaking approaches.[70] Typically, cocktails of 5-10 fragments are soaked into a crystal of the protein of interest.[71] When one or more fragments bind to the protein the additional electron density directly reveals the location of the fragment's binding pocket and the structure of the fragment.

Tethering is not only a technique applied to discover covalent drug binding or orthosteric drugs, but it could also be considered as a technique to identify ligands for allosteric pockets. Different tethering strategies have been developed, of which for example disulfide tethering is well-known. This technique involves the formation of a reversible disulfide bond via the linking of a thiol-containing fragment to a, potentially genetically introduced, cysteine residue in a protein.[72–74] At equilibrium, the mixture will consist predominantly of the protein bound to the fragment with the highest binding affinity. By use of the covalent bond formation between the fragment and the protein, the affinity of the fragment for the target protein is amplified, which can be useful for detection at lower concentrations. The direction of the ligands to a specific site makes the approach particularly useful in case of a known allosteric site for which novel allosteric ligands should be identified.

Phage display methods have been used occasionally in the search for allosteric receptor modulators. The technique involves the expression of a random library of peptides on the coat proteins of bacteriophages.[75] By physically linking the peptide and its genetic material, novel ligands with desired properties can be easily identified via this approach.[76] The unbiased nature of the phage display technique provides potential for the identification of allosteric modulators for targets of which specific allosteric pockets have not yet been identified.

Nuclear Receptor allosteric modulators

NRs, like other receptors, have been targeted on allosteric sites. At the moment, the most studied allosteric modulators include those that target the AF-2 cofactor binding site, the DBD or DNA response elements, modulate the receptor dimerization, modulate PTMs or target alternative sites in the LBD. These different classes will be discussed briefly, with the main focus on the alternative pockets in the LBD. In the context of this thesis, allosteric compounds are considered as compounds that bind at a different site than the orthosteric site and lead to stabilization or inducement of other NR conformations, and not only inhibit, for example, DNA or coactivator binding (to the DBD or AF-2 site).

Approaches for allosteric modulation of NRs on and beyond the Ligand Binding Domain

NRs are typically activated by the binding of agonistic ligands, resulting in the recruitment of specific cofactors leading to a certain biological response via enhanced gene transcription. One type of alternative NR modulation is, therefore, via the direct inhibition of cofactor binding at the AF-2 site (Figure 4*A*).[77,78] Many types of AF-2 site inhibitors have been described, such as constrained peptides, peptide mimetics and small molecule inhibitors, all typically mimicking the helical LXXLL cofactor binding motif.[39]

NR homo- and heterodimerization also provide entries for allosteric modulation via small molecules (Figure 4*B*). Through its ability to form heterodimeric assemblies, RXR can modulate and activate multiple NR partners such as peroxisome proliferator-activated receptor (PPAR), liver X receptor (LXR) and Nurr1. The type of RXR ligand can have a substantial effect on the dimerization behavior of RXR and therefore on the transactivation to its dimer partner.[79–81]

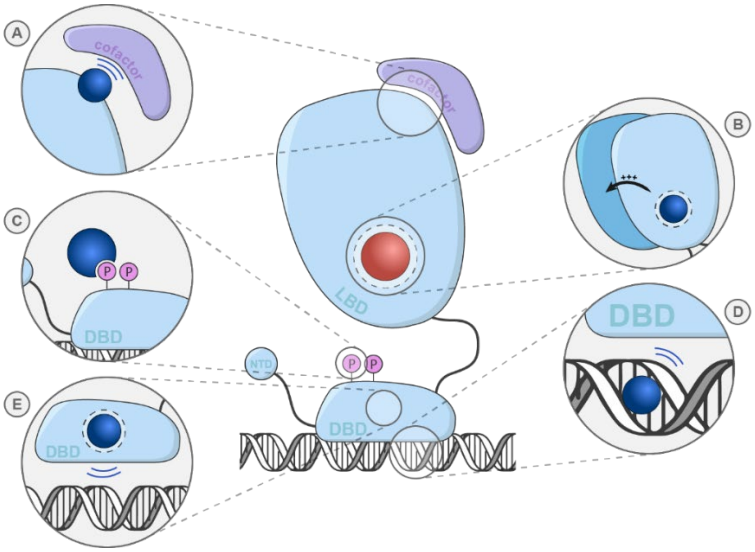

Figure 4 | Different modes of actions for small molecule-based allosteric NR modulation outside of the ligand binding domain. (*A*) Via binding to the cofactor binding site. (*B*) Via compounds modulating the NR dimerization. (*C*) Via the recognition of post-translational modifications. (*D*) Via modulation of the DNA response element. (*E*) Via binding to the DNA binding domain.

Several ligands are known that allosterically modulate NRs by acting at or via PTMs (Figure 4*C*). For PPARγ, for example, phosphorylation of Ser-273 was found to increase insulin sensitivity by upregulating a specific set of target genes without fully activating the receptor.[82] When compounds with minimal agonistic activity bind the PPARγ LBP, there is inhibition of Ser-273 phosphorylation without causing PPARγ activation associated side-effects.[83]

Interactions between the NR DBD and the DNA are crucial for the expression of the NR target genes. Targeting the DBD is, therefore, another potential strategy for NR modulation. The first option is the blocking of specific HREs at the DNA, inhibiting the binding of the NR DBD (Figure 4*D*).[84–86] The second strategy is via ligands that target the zinc fingers of the DBD (Figure 4*E*). Zinc fingers play an important role in stabilizing the DBD, meaning that disrupting these zinc fingers results in a destabilization of the DBD leading to a reduction of DNA binding.[36,74,87]

Allosteric pockets on and in the NR LBD

Most effort is dedicated to compounds that bind to allosteric sites within the LBD, which we have categorized into three sub-groups, depending on their binding location (Figure 5). The first group, targeting expanded orthosteric sites, binds (part of) the orthosteric pocket and subsequently extends from there into additional pockets that are unique for a certain NR. The compounds in the second group, the dual site binders, bind the LBD in a two to one stoichiometry where typically one of the two ligands binds in the LBP and the second ligand binds a surface exposed site elsewhere on the LBD. The third group of compounds addresses pockets fully outside of the orthosteric LBP, which we will term alternative pockets.

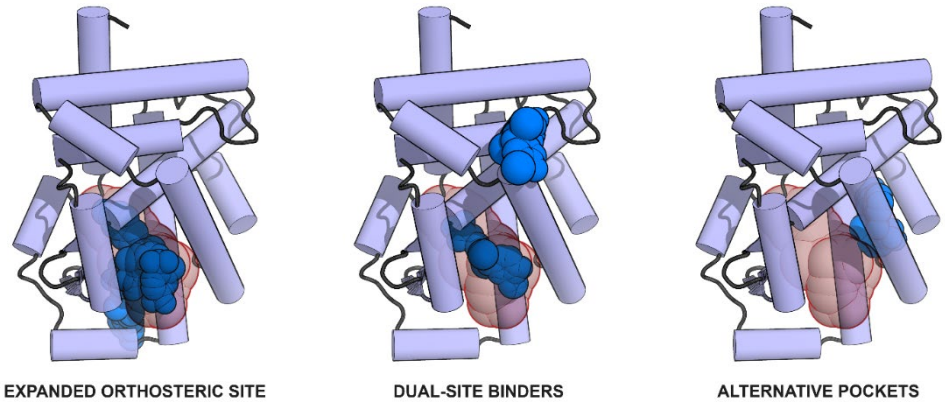

Figure 5 | Three conceptual modes of allosteric binding sites in the NR LBD. The expanded orthosteric site binders address the classical LBP, but also extend into novel pockets, unique for a specific NR. The dual-site binders bind twice to the LBD, typically one time in the LBP and a second time to an allosteric site. The alternative pockets modulators bind exclusively to an allosteric pocket. The orthosteric pocket is indicated in red.

Expanded orthosteric site

The size and plasticity of the orthosteric pocket greatly varies between different NRs, ranging from barely existing to as big as 1600 Å^3.[88] There has been structural evidence that ligands, especially fatty acid analogs, can bind to the orthosteric LBP of various NRs with a different binding mode. Therefore, NRs can recognize the same ligand but binding can lead to another biological response.[89,90] As an example for a case where ligands take it one step further by binding to the orthosteric LBP and extending out to neighboring pockets connected to the classical LBP the allosteric pocket of PPARγ is discussed in more detail.

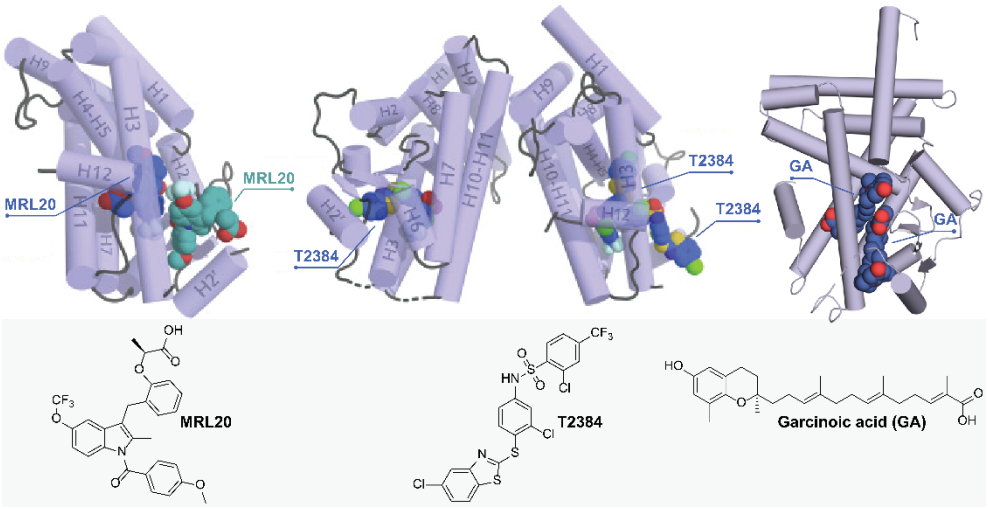

Figure 6. Overview of allosteric ligands binding to the expanded orthosteric site of PPARγ and their corresponding crystal structures. *Left*, PPARγ with MRL-20 (blue) (PDB: 2Q59). The second MRL-20 (in teal) is positioned at the predicted binding site. *Middle*, PPARγ with T2384 (PDB: 3K8S). *Right*, PPARγ with garcinoic acid (PDB: 7AWD).

PPARγ is a NR that is well-known for having one of the largest orthosteric binding-pockets. The PPARγ pocket is composed of three sub-pockets which have a combined volume of >1200 Å^3.[91] PPARγ plays an important role in energy homeostasis and inflammation and therefore modulating its activity can be beneficial in e.g. obesity and diabetes.[92] Hughes *et al*. discovered that at high concentrations the agonist MRL-20 still increased the interaction between PPARγ and coactivator when the orthosteric site was blocked using a small covalent modifier.[93] Using NMR and TR-FRET they confirmed that MRL-20 binds with high affinity to the orthosteric site and with lower affinity in an adjacent pocket, in both cases causing agonistic behavior.[93] The agonistic behavior of the first binding site is caused by direct stabilization of H12 and the AF-2 surface, whereas the second binding site likely stabilizes H3 which facilitates interactions with the loop between H11 and H12 and with that causes stabilization of the co-activator binding region.[93] Covalent modifiers with different sizes and chemical properties were used to define the binding site of MRL-20 more precisely (Figure 6, *Left*).[91] Another example where one compound is able to bind two connected sites at the same time in the PPARγ LBD is the flexible ligand T2384.[94] In the crystal structure, T2384 is both observed in a U-shape in the canonical LBP and in a S-shape in the canonical LBP in combination with an extra molecule in the alternate site (Figure 6, *Middle*).[94] By

making mutant proteins that lack one of the two binding sites, it was elucidated that the combined antagonist/agonist behavior that is observed for this compound in the native protein is caused by an agonistic effect of binding in the orthosteric pocket and an antagonistic effect of binding in the connected allosteric pocket.[94] These binding-modes were confirmed with NMR where it was concluded that both the U and S compound-conformation in the orthosteric pocket exist when adding one equivalent of the compound and the alternate binding site gets populated when adding more than one equivalent.[95] The vitamin E mimetic garcinoic acid (GA) can also bind twice in the extended orthosteric pocket of PPARγ leading to the protein adopting a fully active conformation (Figure 6, *Right*).[96] By doing so, an unanticipated co-factor recruitment profile is observed compared to that of canonical agonists.[96] In addition to the instances where one compound binds to both the orthosteric and a connected alternate site, there are also a couple of examples where a synthetic ligand and a naturally occurring lipid together occupy the two pockets of PPARγ.[97,98]

Dual site binding

In addition to the canonical LBP, ligands were also found that can bind both to the orthosteric site and to another, surface exposed, site on the LBD (Figure 5, *Middle*). Although the function of the binding to these secondary binding sites is frequently not fully understood yet, some of these ligands were shown to have the capacity to modulate the NRs in a non-traditional way. For the scope of this chapter, examples were not included here.[99]

Alternative pockets in the LBD

The two previously mentioned classes of LBD allosteric sites are either an expansion of the orthosteric site or a secondary binding site for an orthosteric ligand (dual site binding). The third class deals with allosteric pockets on the LBD fully independent from the orthosteric pocket in terms of the type of ligand or spatial overlap. Such allosteric sites are known and structurally described for retinoic acid related orphan receptor γ t (RORγt), RXR, and androgen receptor (AR).[100–102] In this chapter, only RORγt will be discussed.

RORγt

RORγt is a key regulator protein for the development of T cells into Th17 cells, which results in tissue inflammation by the excretion of pro-inflammatory cytokines such

as IL-17a.[103–105] Inhibition of RORγt has, therefore, been found to be a promising strategy in the treatment of autoimmune diseases by diminishing the inflammatory response.[106–108] Many synthetic small molecule inverse agonists for RORγt have been identified in literature, most of them targeting the orthosteric LBP.[109–114] However, a few years ago a novel acyl- indazole series of RORγt modulators was disclosed by the company Merck/MSD containing a different chemotype in comparison with the already known modulators.[115] Scheepstra *et al.* identified that these ligands were binding at an alternative binding pocket in the LBD of RORγt.[101]

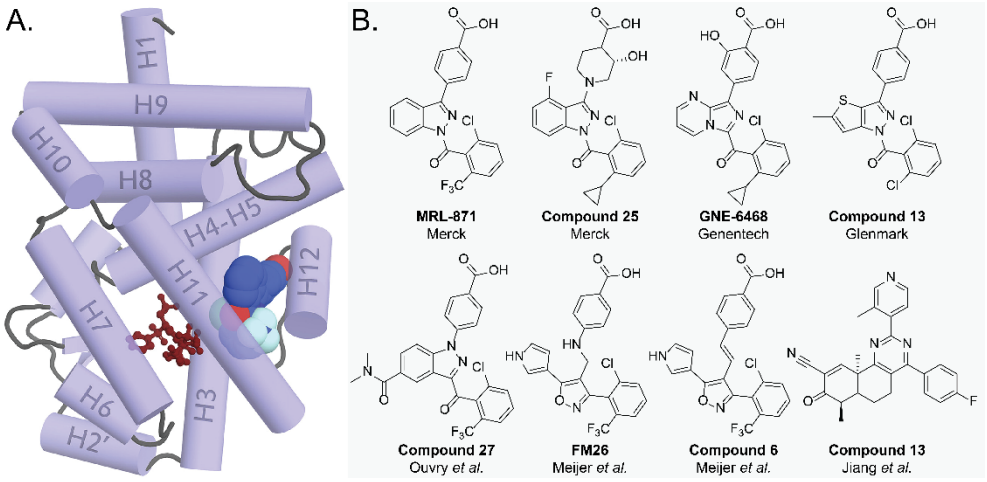

Figure 7. Overview of NRs targeted via alternative allosteric pockets. (*A*) RORγt with MRL-871 (overlay with the protein with T0901317 (PDB: 4YPQ & 4NB6)). The orthosteric ligand is shown in red and the allosteric ligands in blue. (*B*) A selection of reported RORγt allosteric ligands is shown.

For four of these acyl-indazole ligands (MRL-871, MRL-299, MRL-367, MRL-673), a high-resolution crystal structure has been elucidated, in which it can be clearly observed that these modulators bind in an allosteric binding site, distal to the orthosteric binding pocket, at the position where H12 is normally located in its agonistic conformation. This allosteric binding site is shown illustratively for MRL-871 in Figure 7*A*. The allosteric pocket is formed by H4, H5, H11 and the repositioned H12, which has a unique conformation by folding back over the ligand. In this conformation, the recruitment of coactivators to the AF-2 is prevented. Via this binding mode, the allosteric ligands are functionally acting as inverse agonists with a similar effect as regular orthosteric inhibitors, but in contrast, not in competition with the orthosteric ligands.[116–120] The acyl-indazole ligands interact

with the allosteric pocket mainly via hydrophobic interactions and additionally via H-bonding between the carboxylic acid moiety of the ligand and the Gln-329 side chain (H3) as well as the main chain amide of Ala-497 and Phe-498 (H12) of the protein. In addition to structural studies, the allosteric modulators were also tested in time-resolved fluorescence coactivator recruitment (TR-FRET) assays and cellular assays, which showed IC_{50} values in the nanomolar range. This means that these compounds can be considered as NR allosteric compounds with a potency that reaches clinical demands.

With the discovery of these RORγt allosteric ligands, follow-up research on these compounds has been performed by many companies and research groups.[121–125] Merck improved the affinity and pharmacokinetic profile of MRL-871 leading to compound 25 (Figure 7*B*) Genentech performed an extensive SAR study around the MRL series of compounds, varying the indazole core and also making changes to the carboxylic acid and 3-acylarene moiety.[121] They specifically attempted to improve the selectivity for RORγt over other NRs, since a remarkable cross-reactivity with PPARγ was observed for the MRL derivatives.[101] From this study, GNE-0946 and GNE-6468 (Figure 7*B*) were identified as highly potent compounds in both biochemical and cellular assays, with improved selectivity and physiochemical properties. Glenmark Pharmaceuticals performed a scaffold hopping approach with MRL-871 as a starting point, resulting in compound 13 with a thiophenopyrazole core (Figure 7*B*) as one of the best hits.[123,126,127] The compounds were tested in biochemical TR-FRET assays, where one of the compounds showed an IC_{50} value of less than 50 nM. Ouvry *et al.* mainly focused on improving the metabolic stability of MRL by replacing the heterocyclic amide linkage, since related compounds have shown in vivo instability due to hydrolytic cleavage.[125] For this purpose, different linkers were incorporated on a reverse indazole scaffold, which was derived from one of the MRL analogs, and the library was screened in a RORγt/Gal4 cell-based assay. Incorporation of an ether linker, compound 27 (Figure 7*B*), resulted in the most potent ligand. Furthermore, the ligand was also tested in phototoxicity assays where it turned out to have a phototoxic irritancy factor above the toxic level, which could not be improved by some further structural changes. Interestingly, the crystal structure of RORγt with compound 27 was elucidated which revealed binding to the same allosteric pocket as MRL-871 in a similar orientation.[125] Meijer et al. explored an alternative isoxazole core where the initial lead compound was FM26 (Figure 7*B*).[128] This was then optimized leading to discovery of compounds with an increased potency,

pharmacokinetic properties, and a good selectivity profile such as compound 6 (Figure 7*B*).[129] Also, recently, a novel series of cysteine-dependent, allosteric inverse agonists for RORγt was discovered.[130] Site-directed mutagenesis and molecular dynamics support a mechanism of action for these compounds through specific binding to Cys-476 on H11. Compound 13 of this series (Figure 7*B*) is orally available and active in a murine model of rheumatoid arthritis supporting the development of compounds of this class for therapeutic purposes.[130]

Conclusion & perspective

NRs are a promising target in pathology because of their regulating role within the human genome. The primary focus of NR targeting has classically been via the orthosteric LBP. Small-molecule modulators binding to this part of the protein have yielded great successes, nevertheless, issues such as cross-reactivity, selectivity, and drug resistance remain major challenges. In recent years, allosteric modulation of protein receptors has gained attention, with drugs with allosteric modes of action on the market for GPCRs and kinases, and multiple drugs undergoing clinical trials. The first allosteric ligands for NRs were shown to have low binding affinities towards their target. But, recently, nanomolar potent allosteric site modulators have been discovered for several NRs, bringing allosteric targeting of NRs also to the center of attention.

The LBD is presently the most promising NR domain for allosteric targeting due to the high affinities and the functional effects of the allosteric compounds that have been found. In addition, there is considerable structural information available for this domain, making *de novo* drug synthesis, computational guided studies, and medicinal chemistry more straightforward. Nevertheless, the scarcity of full-length structures and the absence thereof in the presence of allosteric ligands, still limits a concise delineation of the allosteric effects on the multi-domain protein level for these new kinds of compounds.

Allosteric modulation via nuclear receptor dimerization, mainly via the LBD, has delivered interesting entries for drug development that could be further investigated. To date, the mechanism by which the activation of specific dimers is controlled is still rather poorly understood. The structural diversity of the amino acid residues present at the dimerization interface between NRs is significant. Therefore, the possibility arises to generate synthetic ligands that can selectively bind to the dimerization interface to either stabilize or inhibit specific homo- and

heterodimer formation. These synthetic ligands can serve as interesting approaches to target specific pathways, but also to fundamentally understand the importance of the protein dimers.

Although most success in NR allosteric targeting has been on the LBD, other strategies such as allosteric modulation via PTMs also show high potential and have already yielded some successes. The intrinsically disordered nature of the NTD of NRs together with the fact that this domain contains multiple sites for PTMs makes this domain of NRs of particular interest for allosteric modulation via addressing the PTMs.[131,132] Allosteric modulators which either enhance or abolish these PTMs selectively, can lead to an improved understanding on the modulatory role of these PTMs and can potentially be interesting for drug discovery.

Reflecting on the allosteric mechanisms found for other receptor classes, it becomes clear that NRs possibly also harbor analogous sites with the potential to be similarly allosterically modulated. To date, the vast majority of these approaches, such as bitopic ligands and covalent attaching, have remained unexplored for NRs while the potential for drug discovery can be substantial. Allosteric sites that are in close proximity of the canonical LBP can be targeted by bitopic ligands to more accurately force a desired biological response. Additionally, for NRs with an expanded orthosteric site, the orthosteric ligand can be combined with pharmacophores that occupy directly neighboring pockets. This will ultimately potentially result in a modulation of efficacy, enhanced affinity, and selectivity of the ligand for the specific NR. These type of ligands can, therefore, reduce the cross-reactivity of ligands to other NRs, which remains a serious problem in NR research.[133] Also covalently attachment of molecules is an interesting approach to target NRs. Covalent modulators have the potential to more selectively target NRs using a lower dose, and perhaps also specifically target NR mutants.

A major challenge for the field is the actual discovery of such allosteric ligands, which is in part due to the high potency of orthosteric ligands, biasing screening campaigns. Several entries could be explored in order to identify allosteric modulators more easily. (1) By blocking the orthosteric site with a transcriptionally active or silent covalent modulator, NRs can subsequently only be modulated using an allosteric ligand, which can then be detected by conventional screening assays. (2) By (temporary) covalent tethering of compounds at a specific, allosteric site of the protein. (3) By exploiting the orthosteric ligand as entry for generation of bitopic ligands for both expanded LBPs and pockets that are in close proximity. (4) Besides

the above-mentioned specific techniques and targets, also more diverse and directed screening methods, such as those based on computational approaches, fragment-based screening, and phage display could be further optimized or developed towards allosteric site targeting.

NRs have been shown to harbor multiple allosteric sites that can potentially be used for drug discovery. A number of promising examples of small molecule allosteric NR targeting concepts have recently been reported, illustrating the high potential of this concept. Inspiration for novel modes of allosteric NR modulation can be found in other receptor classes or, alternatively, via novel chemical concepts such as tethering, bitopic ligands and fragment-based screening. The future for allosteric small molecule modulators of Nuclear Receptors is highly promising.

Aim and outline of this thesis

The previous section has placed allosteric modulation of NRs in perspective and outlined the possibilities to use this strategy in drug discovery. While a lot of effort is put into the development of new allosteric ligands, in this thesis a step back is taken, and the focus is put on the pockets themselves instead of the compounds binding them. The aim of this thesis is to understand existing (allosteric) pockets and investigate new ones using protein engineering and assay development as the main tools.

In **Chapter 2** the allosteric pocket as found in RORγt was studied in detail. The prerequisites to form this pocket in terms of crucial residues were elucidated using extensive mutagenic studies. Two unique characteristics of RORγt, a Gln-487 residue and a prolonged helix 11 prime proved crucial for allosteric compound binding. With that this chapter proves the uniqueness of this pocket in RORγt and corroborates the importance and feasibility of developing compounds that bind this pocket for the treatment of autoimmune diseases.

Chapter 3 aimed to artificially create an allosteric pocket, like the one found in RORγt, in RORα and RORβ. Inhibiting these receptors using allosteric inverse agonists could aid in the understanding of the functions of these receptors without requiring for example knock-out animals. Additionally, RORα inhibition could yield the same opportunities in autoimmunity as RORγt but without the associated risks of thymic apoptosis and inhibiting RORβ could be beneficial for some mental conditions. Mutagenesis was used to extensively increase the similarity of these

receptors to RORγt in the allosteric region. However, even very drastic alterations did not yield high affinity binding to RORγt inverse agonists. While unfortunate, this further underlines the uniqueness of the allosteric pocket in RORγt.

In **Chapter 4** the off-target activity of RORγt allosteric inverse agonist MRL-871 towards PPARγ was investigated. The binding of MRL-871 to PPARγ was already found in the initial paper describing this compound. However, the binding mode and exact effects were unknown and, as described in the previous section, PPARγ has a large, extended binding pocket with multiple arms. In this chapter the exact binding location and implications of binding of MRL-871 in the extended PPARγ ligand binding pocket (Figure 5, *Left*) were elucidated using protein crystallography and biochemical assays.

Chapter 5 describes a novel assay that can, amongst others, be used to study binding of allosteric ligands to NRs. Many assays look indirectly at downstream effects or are dependent on fluorescent labels or expensive equipment. This assay presents a novel way to look at compound-induced thermal stabilization and enables the fit of association constants directly. To do so protein in absence and presence of a fixed amount of compound is subjected to a heat challenge. High speed centrifugation is used to separate folded from unfolded protein after which the amount of protein in the supernatant is quantified using Bradford reagent. The chapter describes the realization and optimization of this assay as well as some first applications.

Finally, in **Chapter 6**, the work presented in this thesis is put into perspective. This chapter furthermore presents opportunities for future research.

References

1. Zhao, L., Zhou, S. & Gustafsson, J.-Å. Nuclear Receptors: Recent Drug Discovery for Cancer Therapies. *Endocr. Rev.* **40**, 1207–1249 (2019).
2. Santos, R. *et al.* A comprehensive map of molecular drug targets. *Nat. Rev. Drug Discov.* **16**, 19–34 (2017).
3. Kumar, R. & Litwack, G. Structural and functional relationships of the steroid hormone receptors' N-terminal transactivation domain. *Steroids* **74**, 877–883 (2009).
4. Helsen, C. *et al.* Structural basis for nuclear hormone receptor DNA binding. *Mol. Cell. Endocrinol.* **348**, 411–417 (2012).
5. Penvose, A., Keenan, J. L., Bray, D., Ramlall, V. & Siggers, T. Comprehensive study of nuclear receptor DNA binding provides a revised framework for understanding receptor specificity. *Nat. Commun.* **10**, 2514 (2019).

6. Haelens, A., Tanner, T., Denayer, S., Callewaert, L. & Claessens, F. The hinge region regulates DNA binding, nuclear translocation, and transactivation of the androgen receptor. *Cancer Res.* **67**, 4514–23 (2007).
7. Bourguet, W., Ruff, M., Chambon, P., Gronemeyer, H. & Moras, D. Crystal structure of the ligand-binding domain of the human nuclear receptor RXR-α. *Nature* **375**, 377–382 (1995).
8. Renaud, J.-P. *et al.* Crystal structure of the RAR-γ ligand-binding domain bound to all-trans retinoic acid. *Nature* **378**, 681–689 (1995).
9. Pissios, P., Tzameli, I., Kushner, P. J. & Moore, D. D. Dynamic Stabilization of Nuclear Receptor Ligand Binding Domains by Hormone or Corepressor Binding. *Mol. Cell* **6**, 245–253 (2000).
10. Rastinejad, F., Huang, P., Chandra, V. & Khorasanizadeh, S. Understanding nuclear receptor form and function using structural biology. *J. Mol. Endocrinol.* **51**, T1–T21 (2013).
11. Kojetin, D. J. & Burris, T. P. Small molecule modulation of nuclear receptor conformational dynamics: implications for function and drug discovery. *Mol. Pharmacol.* **83**, 1–8 (2013).
12. Patel, S. R. & Skafar, D. F. Modulation of nuclear receptor activity by the F domain. *Mol. Cell. Endocrinol.* **418**, 298–305 (2015).
13. Changeux, J. P. & Christopoulos, A. Allosteric Modulation as a Unifying Mechanism for Receptor Function and Regulation. *Cell* **166**, 1084–1102 (2016).
14. Wodak, S. J. *et al.* Allostery in Its Many Disguises: From Theory to Applications. *Structure* **27**, 566–578 (2019).
15. Hilser, V. J. & Thompson, E. B. Structural dynamics, intrinsic disorder, and allostery in nuclear receptors as transcription factors. *J. Biol. Chem.* **286**, 39675–82 (2011).
16. Hall, J. M., McDonnell, D. P. & Korach, K. S. Allosteric Regulation of Estrogen Receptor Structure, Function, and Coactivator Recruitment by Different Estrogen Response Elements. *Mol. Endocrinol.* **16**, 469–486 (2002).
17. Meijsing, S. H. *et al.* DNA Binding Site Sequence Directs Glucocorticoid Receptor Structure and Activity. *Science* **324**, 407–410 (2009).
18. Frank, F., Okafor, C. D. & Ortlund, E. A. The first crystal structure of a DNA-free nuclear receptor DNA binding domain sheds light on DNA-driven allostery in the glucocorticoid receptor. *Sci. Rep.* **8**, 13497 (2018).
19. Putcha, B.-D. K. & Fernandez, E. J. Direct interdomain interactions can mediate allosterism in the thyroid receptor. *J. Biol. Chem.* **284**, 22517–22524 (2009).
20. Zhang, J. *et al.* DNA binding alters coactivator interaction surfaces of the intact VDR-RXR complex. *Nat. Struct. Mol. Biol.* **18**, 556–563 (2011).
21. de Vera, I. M. S. *et al.* Synergistic Regulation of Coregulator/Nuclear Receptor Interaction by Ligand and DNA. *Structure* **25**, 1506-1518.e4 (2017).
22. Helsen, C. *et al.* Evidence for DNA-binding domain--ligand-binding domain communications in the androgen receptor. *Mol. Cell. Biol.* **32**, 3033–43 (2012).
23. Becares Salles, N., Gage, M. C. & Pineda-Torra, I. Post-translational modifications of lipid-activated nuclear receptors: Focus on metabolism. *Endocrinology* **158**, en.2016-1577 (2016).
24. Faus, H. & Haendler, B. Post-translational modifications of steroid receptors. *Biomed. Pharmacother.* **60**, 520–528 (2006).

25. Anbalagan, M., Huderson, B., Murphy, L. & Rowan, B. G. Post-translational modifications of nuclear receptors and human disease. *Nucl. Recept. Signal.* **10**, e001 (2012).
26. Brunmeir, R., Xu, F., Brunmeir, R. & Xu, F. Functional Regulation of PPARs through Post-Translational Modifications. *Int. J. Mol. Sci.* **19**, 1738 (2018).
27. Fischer, K., Kelly, S. M., Watt, K., Price, N. C. & McEwan, I. J. Conformation of the Mineralocorticoid Receptor N-terminal Domain: Evidence for Induced and Stable Structure. *Mol. Endocrinol.* **24**, 1935–1948 (2010).
28. Khan, S. H., Ling, J. & Kumar, R. TBP Binding-Induced Folding of the Glucocorticoid Receptor AF1 Domain Facilitates Its Interaction with Steroid Receptor Coactivator-1. *PLoS ONE* **6**, e21939 (2011).
29. Kumar, R. *et al.* Regulation of the structurally dynamic N-terminal domain of progesterone receptor by protein-induced folding. *J. Biol. Chem.* **288**, 30285–99 (2013).
30. Jin, L. & Li, Y. Structural and functional insights into nuclear receptor signaling. *Adv. Drug Deliv. Rev.* **62**, 1218–26 (2010).
31. Wang, N., Zou, Q., Xu, J., Zhang, J. & Liu, J. Ligand binding and heterodimerization with retinoid X receptor α (RXRα) induce farnesoid X receptor (FXR) conformational changes affecting coactivator binding. *J. Biol. Chem.* **293**, 18180–18191 (2018).
32. De Bosscher, K., Desmet, S. J., Clarisse, D., Estébanez-Perpiña, E. & Brunsveld, L. Nuclear receptor crosstalk — defining the mechanisms for therapeutic innovation. *Nat. Rev. Endocrinol.* **16**, 363–377 (2020).
33. Fernandez, E. J. Allosteric pathways in nuclear receptors — Potential targets for drug design. *Pharmacol. Ther.* **183**, 152–159 (2018).
34. Moore, T. W., Mayne, C. G. & Katzenellenbogen, J. a. Minireview: Not picking pockets: nuclear receptor alternate-site modulators (NRAMs). *Mol. Endocrinol. Baltim. Md* **24**, 683–95 (2010).
35. Zhang, C. *et al.* Allosteric binding on nuclear receptors: Insights on screening of non-competitive endocrine-disrupting chemicals. *Environ. Int.* **159**, 107009 (2022).
36. Caboni, L. & Lloyd, D. G. Beyond the ligand-binding pocket: targeting alternate sites in nuclear receptors. *Med. Res. Rev.* **33**, 1081–1118 (2013).
37. Lu, S., Li, S. & Zhang, J. Harnessing allostery: a novel approach to drug discovery. *Med. Res. Rev.* **34**, 1242–1285 (2014).
38. Liu, H., Han, R., Li, J., Liu, H. & Zheng, L. Molecular mechanism of R-bicalutamide switching from androgen receptor antagonist to agonist induced by amino acid mutations using molecular dynamics simulations and free energy calculation. *J. Comput. Aided Mol. Des.* **30**, 1189–1200 (2016).
39. Tice, C. M. & Zheng, Y. J. Non-canonical modulators of nuclear receptors. *Bioorg. Med. Chem. Lett.* **26**, 4157–4164 (2016).
40. van Westen, G. J. P., Gaulton, A. & Overington, J. P. Chemical, Target, and Bioactive Properties of Allosteric Modulation. *PLoS Comput. Biol.* **10**, (2014).
41. Taly, A., Hénin, J., Changeux, J.-P. & Cecchini, M. Allosteric regulation of pentameric ligand-gated ion channels: an emerging mechanistic perspective. *Channels Austin Tex* **8**, 350–60 (2014).
42. Gentry, P. R., Sexton, P. M. & Christopoulos, A. Novel Allosteric Modulators of G Protein-coupled Receptors. *J. Biol. Chem.* **290**, 19478–88 (2015).

43. Foster, D. J. & Conn, P. J. Allosteric Modulation of GPCRs: New Insights and Potential Utility for Treatment of Schizophrenia and Other CNS Disorders. *Neuron* **94**, 431–446 (2017).
44. Changeux, J.-P. & Christopoulos, A. Allosteric modulation as a unifying mechanism for receptor function and regulation. *Diabetes Obes. Metab.* **19**, 4–21 (2017).
45. Thal, D. M., Glukhova, A., Sexton, P. M. & Christopoulos, A. Structural insights into G-protein-coupled receptor allostery. *Nature* **559**, 45–53 (2018).
46. Guarnera, E. & Berezovsky, I. N. Allosteric drugs and mutations: chances, challenges, and necessity. *Curr. Opin. Struct. Biol.* **62**, 149–157 (2020).
47. Block, G. A. *et al.* Cinacalcet for Secondary Hyperparathyroidism in Patients Receiving Hemodialysis. *N. Engl. J. Med.* **350**, 1516–1525 (2004).
48. Buchdunger, E. *et al.* Inhibition of the Abl protein-tyrosine kinase in vitro and in vivo by a 2-phenylaminopyrimidine derivative. *Cancer Res.* **56**, 100–4 (1996).
49. Nussinov, R. & Tsai, C.-J. Allostery in Disease and in Drug Discovery. *Cell* **153**, 293–305 (2013).
50. Oikonomakos, N. G., Skamnaki, V. T., Tsitsanou, K. E., Gavalas, N. G. & Johnson, L. N. A new allosteric site in glycogen phosphorylase b as a target for drug interactions. *Struct. Lond. Engl. 1993* **8**, 575–84 (2000).
51. Pargellis, C. *et al.* Inhibition of p38 MAP kinase by utilizing a novel allosteric binding site. *Nat. Struct. Biol.* **9**, 268–272 (2002).
52. Cho, H.-S. *et al.* Structure of the extracellular region of HER2 alone and in complex with the Herceptin Fab. *Nature* **421**, 756–760 (2003).
53. Zheng, J. *et al.* β-Glucocerebrosidase Modulators Promote Dimerization of β-Glucocerebrosidase and Reveal an Allosteric Binding Site. *J. Am. Chem. Soc.* **140**, 5914–5924 (2018).
54. Dunker, A. K. *et al.* Protein disorder and the evolution of molecular recognition: theory, predictions and observations. *Pac. Symp. Biocomput. Pac. Symp. Biocomput.* 473–84 (1998).
55. Wright, P. E. & Dyson, H. J. Intrinsically disordered proteins in cellular signalling and regulation. *Nat. Rev. Mol. Cell Biol.* **16**, 18–29 (2015).
56. Motlagh, H. N., Li, J., Thompson, E. B. & Hilser, V. J. Interplay between allostery and intrinsic disorder in an ensemble. *Biochem. Soc. Trans.* **40**, 975–80 (2012).
57. Motlagh, H. N., Wrabl, J. O., Li, J. & Hilser, V. J. The ensemble nature of allostery. *Nature* **508**, 331–339 (2014).
58. Catterall, W. A. *et al.* Voltage-gated ion channels and gating modifier toxins. *Toxicon* **49**, 124–141 (2007).
59. Lane, J. R., Sexton, P. M. & Christopoulos, A. Bridging the gap: bitopic ligands of G-protein-coupled receptors. *Trends Pharmacol. Sci.* **34**, 59–66 (2013).
60. Mohr, K. *et al.* Rational design of dualsteric GPCR ligands: quests and promise. *Br. J. Pharmacol.* **159**, 997–1008 (2010).
61. Ostrem, J. M., Peters, U., Sos, M. L., Wells, J. A. & Shokat, K. M. K-Ras(G12C) inhibitors allosterically control GTP affinity and effector interactions. *Nature* **503**, 548–551 (2013).
62. Carvalho, A. L., Trincão, J. & Romão, M. J. X-Ray Crystallography in Drug Discovery. in *Methods in molecular biology (Clifton, N.J.)* vol. 572 31–56 (2010).

63. Huang, W. *et al.* Allosite: A method for predicting allosteric sites. *Bioinformatics* **29**, 2357–2359 (2013).
64. Huang, W. *et al.* ASBench: Benchmarking sets for allosteric discovery. *Bioinformatics* **31**, 2598–2600 (2015).
65. Lu, S., Ji, M., Ni, D. & Zhang, J. Discovery of hidden allosteric sites as novel targets for allosteric drug design. *Drug Discov. Today* **23**, 359–365 (2018).
66. Greener, J. G. & Sternberg, M. J. Structure-based prediction of protein allostery. *Curr. Opin. Struct. Biol.* **50**, 1–8 (2018).
67. Huang, M. *et al.* AlloFinder: a strategy for allosteric modulator discovery and allosterome analyses. *Nucleic Acids Res.* **46**, W451–W458 (2018).
68. Ni, D. *et al.* Along the allostery stream: Recent advances in computational methods for allosteric drug discovery. *WIREs Comput. Mol. Sci.* e1585 (2021) doi:10.1002/wcms.1585.
69. Macalino, S. J. Y., Gosu, V., Hong, S. & Choi, S. Role of computer-aided drug design in modern drug discovery. *Arch. Pharm. Res.* **38**, 1686–1701 (2015).
70. Kuo, L. C. Preface. in *Fragment-Based Drug Design* (ed. Kuo, L. C. B. T.-M. in E.) vol. 493 xxi–xxii (Academic Press, 2011).
71. Bauman, J. D. *et al.* Crystallographic Fragment Screening. **56**, 2738–2746 (2014).
72. Erlanson, D. A., Wells, J. A. & Braisted, A. C. Tethering: Fragment-Based Drug Discovery. *Annu. Rev. Biophys. Biomol. Struct.* **33**, 199–223 (2004).
73. Hardy, J. A. A link means a lot: disulfide tethering in structure-based drug design. *Comput. Struct. Approaches Drug Discov. Ligand-Protein Interact.* 318–347 (2008).
74. Sijbesma, E. *et al.* Fluorescence Anisotropy-Based Tethering for Discovery of Protein–Protein Interaction Stabilizers. *ACS Chem. Biol.* **15**, 3143–3148 (2020).
75. Pande, J., Szewczyk, M. M. & Grover, A. K. Phage display: Concept, innovations, applications and future. *Biotechnol. Adv.* **28**, 849–858 (2010).
76. Tipps, M. E., Lawshe, J. E., Ellington, A. D. & Mihic, S. J. Identification of novel specific allosteric modulators of the glycine receptor using phage display. *J. Biol. Chem.* **285**, 22840–22845 (2010).
77. Wang, Y. *et al.* A second binding site for hydroxytamoxifen within the coactivator-binding groove of estrogen receptor beta. *Proc. Natl. Acad. Sci.* **103**, 9908–9911 (2006).
78. Fischer, A. & Smieško, M. Allosteric Binding Sites On Nuclear Receptors: Focus On Drug Efficacy and Selectivity. *Int. J. Mol. Sci.* **21**, 534 (2020).
79. Scheepstra, M. *et al.* Ligand Dependent Switch from RXR Homo- to RXR-NURR1 Heterodimerization. *ACS Chem. Neurosci.* **8**, 2065–2077 (2017).
80. McFarland, K. *et al.* Low Dose Bexarotene Treatment Rescues Dopamine Neurons and Restores Behavioral Function in Models of Parkinson's Disease. *ACS Chem. Neurosci.* **4**, 1430–1438 (2013).
81. Giner, X. C., Cotnoir-White, D., Mader, S. & Lévesque, D. Selective ligand activity at Nur/retinoid X receptor complexes revealed by dimer-specific bioluminescence resonance energy transfer-based sensors. *FASEB J.* **29**, 4256–4267 (2015).
82. Choi, J. H. *et al.* Anti-diabetic drugs inhibit obesity-linked phosphorylation of PPARγ by Cdk5. *Nature* **466**, 451–456 (2010).
83. Choi, J. H. *et al.* Antidiabetic actions of a non-agonist PPARγ ligand blocking Cdk5-mediated phosphorylation. *Nature* **477**, 477–481 (2011).

84. Gearhart, M. D. *et al.* Inhibition of DNA Binding by Human Estrogen-Related Receptor 2 and Estrogen Receptor α with Minor Groove Binding Polyamides. *Biochemistry* **44**, 4196–4203 (2005).
85. Nickols, N. G. & Dervan, P. B. Suppression of androgen receptor-mediated gene expression by a sequence-specific DNA-binding polyamide. *Proc. Natl. Acad. Sci. U. S. A.* **104**, 10418–10423 (2007).
86. Veras Ribeiro Filho, H. *et al.* Modulation of nuclear receptor function: Targeting the protein-DNA interface. *Mol. Cell. Endocrinol.* **484**, 1–14 (2019).
87. Whittal, R. M. *et al.* Preferential Oxidation of Zinc Finger 2 in Estrogen Receptor DNA-binding Domain Prevents Dimerization and, Hence, DNA Binding. *Biochemistry* **39**, 8406–8417 (2000).
88. Gallastegui, N., Mackinnon, J. A. G., Fletterick, R. J. & Estébanez-Perpiñá, E. Advances in our structural understanding of orphan nuclear receptors. *Trends Biochem. Sci.* **40**, 25–35 (2015).
89. Egea, P. F., Mitschler, A. & Moras, D. Molecular recognition of agonist ligands by RXRs. *Mol. Endocrinol. Baltim. Md* **16**, 987–97 (2002).
90. Itoh, T. *et al.* Structural basis for the activation of PPARgamma by oxidized fatty acids. *Nat. Struct. Mol. Biol.* **15**, 924–31 (2008).
91. Brust, R. *et al.* Modification of the Orthosteric PPARγ Covalent Antagonist Scaffold Yields an Improved Dual-Site Allosteric Inhibitor. *ACS Chem. Biol.* **12**, 969–978 (2017).
92. Varga, T., Czimmerer, Z. & Nagy, L. PPARs are a unique set of fatty acid regulated transcription factors controlling both lipid metabolism and inflammation. *Biochim. Biophys. Acta* **1812**, 1007–22 (2011).
93. Hughes, T. S. *et al.* An alternate binding site for PPARγ ligands. *Nat. Commun.* **5**, 3571 (2014).
94. Li, Y. *et al.* T2384, a novel antidiabetic agent with unique peroxisome proliferator-activated receptor gamma binding properties. *J. Biol. Chem.* **283**, 9168–76 (2008).
95. Hughes, T. S. *et al.* Probing the Complex Binding Modes of the PPARγ Partial Agonist 2-Chloro- *N* -(3-chloro-4-((5-chlorobenzo[*d*]thiazol-2-yl)thio)phenyl)-4-(trifluoromethyl)benzenesulfonamide (T2384) to Orthosteric and Allosteric Sites with NMR Spectroscopy. *J. Med. Chem.* **59**, 10335–10341 (2016).
96. Willems, S. *et al.* Endogenous vitamin E metabolites mediate allosteric PPARγ activation with unprecedented co-regulatory interactions. *Cell Chem. Biol.* **28**, 1489-1500.e8 (2021).
97. Jang, J. Y. *et al.* Structural basis for differential activities of enantiomeric PPARγ agonists: Binding of S35 to the alternate site. *Biochim. Biophys. Acta BBA - Proteins Proteomics* **1865**, 674–681 (2017).
98. Shang, J. *et al.* Cooperative cobinding of synthetic and natural ligands to the nuclear receptor PPARγ. *eLife* **7**, (2018).
99. Meijer, F. A., Leijten-van de Gevel, I. A., de Vries, R. M. J. M. & Brunsveld, L. Allosteric small molecule modulators of nuclear receptors. *Mol. Cell. Endocrinol.* **485**, 20–34 (2019).
100. Chen, L. *et al.* Sulindac-derived RXRalpha modulators inhibit cancer cell growth by binding to a novel site. *Chem. Biol.* **21**, 596–607 (2014).
101. Scheepstra, M. *et al.* Identification of an allosteric binding site for RORγt inhibition. *Nat. Commun.* **6**, 8833 (2015).

102. Biron, E. & Bédard, F. Recent progress in the development of protein-protein interaction inhibitors targeting androgen receptor-coactivator binding in prostate cancer. *J. Steroid Biochem. Mol. Biol.* **161**, 36–44 (2016).
103. Ivanov, I. I. *et al.* The Orphan Nuclear Receptor ROR??t Directs the Differentiation Program of Proinflammatory IL-17+ T Helper Cells. *Cell* **126**, 1121–1133 (2006).
104. Korn, T., Bettelli, E., Oukka, M. & Kuchroo, V. K. IL-17 and Th17 Cells. *Annu. Rev. Immunol.* **27**, 485–517 (2009).
105. Yang, X. O. *et al.* T Helper 17 Lineage Differentiation Is Programmed by Orphan Nuclear Receptors ROR? and ROR? *Immunity* **28**, 29–39 (2008).
106. Isono, F., Fujita-Sato, S. & Ito, S. Inhibiting ROR??t/Th17 axis for autoimmune disorders. *Drug Discov. Today* **19**, 1205–1211 (2014).
107. Bronner, S. M., Zbieg, J. R. & Crawford, J. J. RORγ antagonists and inverse agonists: a patent review. *Expert Opin. Ther. Pat.* **27**, 101–112 (2017).
108. Gege, C. Retinoic acid-related orphan receptor gamma t (RORγt) inverse agonists/antagonists for the treatment of inflammatory diseases – where are we presently? *Expert Opin. Drug Discov.* **16**, 1517–1535 (2021).
109. Kamenecka, T. M., Lyda, B., Chang, M. R. & Griffin, P. R. Synthetic modulators of the retinoic acid receptor-related orphan receptors. *MedChemComm* **4**, 764–776 (2013).
110. Fauber, B. P. & Magnuson, S. Modulators of the nuclear receptor retinoic acid receptor-related orphan receptor-gamma (RORgamma or RORc). *J. Med. Chem.* **57**, 5871–5892 (2014).
111. Pandya, V. B., Kumar, S., Sachchidanand, Sharma, R. & Desai, R. C. Combating Autoimmune Diseases with Retinoic Acid Receptor-Related Orphan Receptor-γ (RORγ or RORc) Inhibitors: Hits and Misses. *J. Med. Chem.* **61**, 10976–10995 (2018).
112. Duan, J. J.-W. *et al.* Structure-based Discovery of Phenyl (3-Phenylpyrrolidin-3-yl)sulfones as Selective, Orally Active RORγt Inverse Agonists. *ACS Med. Chem. Lett.* (2019) doi:10.1021/acsmedchemlett.9b00010.
113. Sun, N., Guo, H. & Wang, Y. Retinoic acid receptor-related orphan receptor gamma-t (RORγt) inhibitors in clinical development for the treatment of autoimmune diseases: a patent review (2016-present). *Expert Opin. Ther. Pat.* **29**, 663–674 (2019).
114. Saenz, S. A. *et al.* Small molecule allosteric inhibitors of RORγt block Th17-dependent inflammation and associated gene expression in vivo. *PLOS ONE* **16**, e0248034 (2021).
115. Karstens, W. F. J. et al. RORgammaT Inhibitors. *PCT Int Appl* (2012).
116. Li, X. *et al.* Structural studies unravel the active conformation of apo RORγt nuclear receptor and a common inverse agonism of two diverse classes of RORγt inhibitors. *J. Biol. Chem.* **292**, 11618–11630 (2017).
117. Kallen, J. *et al.* Structural States of RORγt: X-ray Elucidation of Molecular Mechanisms and Binding Interactions for Natural and Synthetic Compounds. *ChemMedChem* **12**, 1014–1021 (2017).
118. Noguchi, M. *et al.* Ternary crystal structure of human RORγ ligand-binding-domain, an inhibitor and corepressor peptide provides a new insight into corepressor interaction. *Sci. Rep.* **8**, 17374 (2018).
119. Yuan, C. *et al.* Molecular dynamics simulations on RORγt: insights into its functional agonism and inverse agonism. *Acta Pharmacol. Sin.* **40**, 1480–1489 (2019).
120. Huang, M., Bolin, S., Miller, H. & Ng, H. L. RORγ Structural Plasticity and Druggability. *Int. J. Mol. Sci.* **21**, 5329 (2020).

121. Fauber, B. P. *et al.* Discovery of imidazo[1,5-a]pyridines and -pyrimidines as potent and selective RORc inverse agonists. *Bioorg. Med. Chem. Lett.* **25**, 2907–2912 (2015).
122. Zhang, H. *et al.* Discovery of N-(Indazol-3-yl)piperidine-4-carboxylic Acids as RORγt Allosteric Inhibitors for Autoimmune Diseases. *ACS Med. Chem. Lett.* **11**, 114–119 (2020).
123. Chaudari, S. S. et al. Bicyclic Heterocyclic Compounds as ROR gamma Modulators.
124. Shaikh, N. S. *et al.* Discovery and pharmacological evaluation of indole derivatives as potent and selective RORγt inverse agonist for multiple autoimmune conditions. *Bioorg. Med. Chem. Lett.* **29**, 2208–2217 (2019).
125. Ouvry, G. *et al.* Discovery of phenoxyindazoles and phenylthioindazoles as RORγ inverse agonists. *Bioorg. Med. Chem. Lett.* **26**, 5802–5808 (2016).
126. Gege, C. Retinoid-related orphan receptor γ t modulators: comparison of Glenmark's me-too patent application (WO2015008234) with the originator application from Merck Sharp and Dohme (WO2012106995). *Expert Opin. Ther. Pat.* **25**, 1215–1221 (2015).
127. de Vries, R. M. J. M., Meijer, F. A., Doveston, R. G. & Brunsveld, L. Elucidation of an allosteric mode-of-action for a thienopyrazole RORγt inverse agonist. *ChemMedChem* (2020) doi:10.1002/cmdc.202000044.
128. Meijer, F. *et al.* Ligand-Based Design of Allosteric Retinoic Acid Receptor-Related Orphan Receptor γt (RORγt) Inverse Agonists. *J. Med. Chem.* acs.jmedchem.9b01372-acs.jmedchem.9b01372 (2019) doi:10.1021/acs.jmedchem.9b01372.
129. Meijer, F. A. *et al.* Structure–Activity Relationship Studies of Trisubstituted Isoxazoles as Selective Allosteric Ligands for the Retinoic-Acid-Receptor-Related Orphan Receptor γt. *J. Med. Chem.* **64**, 9238–9258 (2021).
130. Jiang, X. *et al.* A novel series of cysteine-dependent, allosteric inverse agonists of the nuclear receptor RORγt. *Bioorg. Med. Chem. Lett.* **30**, 126967–126967 (2020).
131. Simons, S. S., Edwards, D. P., Kumar, R. & Kumar, R. Minireview: dynamic structures of nuclear hormone receptors: new promises and challenges. *Mol. Endocrinol. Baltim. Md* **28**, 173–82 (2014).
132. Hill, K. K., Roemer, S. C., Churchill, M. E. A. & Edwards, D. P. Structural and functional analysis of domains of the progesterone receptor. *Mol. Cell. Endocrinol.* **348**, 418–429 (2012).
133. Moras, D. & Gronemeyer, H. The nuclear receptor ligand-binding domain: structure and function. *Curr. Opin. Cell Biol.* **10**, 384–391 (1998).

Chapter 2

Delineation of the Molecular Determinants of the Unique Allosteric Binding Site of RORγt

Abstract

Nuclear receptors (NRs) are high interest targets in drug discovery due to their involvement in numerous biological processes and diseases. The classic way to target NRs is via their, hydrophobic, orthosteric pocket. While successful, this comes with challenges including side effects due to lack of selectivity. Allosteric modulation of NR activity constitutes a promising novel pharmacological strategy. The retinoic acid receptor-related orphan receptor-γt (RORγt) is a constitutively active NR that positively regulates the expression of interleukin-17 (IL-17) in T helper 17 (Th17) cells. Inhibiting this process is an upcoming strategy for treating autoimmune diseases. Recently, an allosteric binding pocket in the C-terminal region of the ligand binding domain (LBD) of RORγt was discovered, amenable to small molecule drug discovery. Compounds that bind this pocket induce a reorientation of helix 12 thus preventing coactivator recruitment. Inverse agonists binding this site with high affinity are actively being pursued. To elucidate the pocket formation mechanism, verify the uniqueness of this pocket and underline the relevance of clinically targeting this site, here the key-characteristics of the RORγt allosteric region were identified and compared to other NRs. Mutations in the LBD were evaluated regarding, coactivator, orthosteric and allosteric ligand binding. Two molecular elements unique to RORγt, the length of helix 11' and a glutamine at the 487 position, are shown to be crucial for formation of the allosteric pocket. This unique combination of elements for RORγt implies high potential regarding the subtype selective targeting of this NR, for more selective treatment of autoimmune diseases.

This chapter has been published as: Leijten-van de Gevel, I. A. & Brunsveld, L. Delineation of the molecular determinants of the unique allosteric binding site of the orphan nuclear receptor RORγt. *J. Biol. Chem.* 295, 9183–9191 (2020).

Introduction

The nuclear receptor (NR) superfamily in humans consists of 48 transcription factors that are essential for various physiological processes and the dysregulation of these proteins occurs in many diseases.[1] Within this family, there is a high level of homology between the members that all have a similar domain structure. The ligand binding domain (LBD) of NRs integrates endogenous and exogenous signaling into a transcriptional output and binds to ligands via a three-layer antiparallel alpha-helical sandwich where the middle layer of helices is absent in the lower half of the domain, thus creating a cavity.[2,3] Because of the hydrophobic character of this cavity, most NRs interact with lipid soluble ligands[3] that can alter the conformational equilibrium of this domain with concomitant modulation of cofactor recruitment and changes in target gene expression.[4] While highly successful, targeting of this, orthosteric, binding site by drugs comes with challenges in selectivity, side effects, disease related mutations and resistance occurrence.[5–7] Next to developing orthosteric partial (ant)agonists[8,9], allosteric modulation of NR activity has been brought forward as novel pharmacological strategy, potentially overcoming some of the challenges connected to orthosteric ligand targeting.[10–12] Several examples of NR allosteric binding sites have been reported, in part overlapping with the orthosteric binding site.[13–15]

An intriguing allosteric site, highly promising for small molecule targeting, was identified for the retinoic acid receptor-related orphan receptor-γt (RORγt).[16] RORγt is a constitutively active orphan NR[17] that positively regulates the expression of interleukin-17 (IL-17) in Th17 cells.[18–20] Direct inhibition of IL-17 in autoimmune diseases using monoclonal antibodies has already been proven to be effective in psoriasis with three FDA approved drugs in the clinic[21–23] and with other clinical applications further emerging.[24] Small molecule inhibition of RORγt is similarly of high interest and inhibitory inverse agonists, also of the orthosteric type, are therefore intensely pursued.[25,26]

Ligands that bind to the allosteric pocket in the C-terminal region of the LBD of RORγt also act as inverse agonists[16,27–30], and appear to do so highly NR isoform selectively. They inhibit cofactor binding by inducing a reorientation of RORγt helix 12 (H12) incompatible with accommodating the classical LXXLL coactivator motif (Figure S1). Upon allosteric ligand binding, the helix 11 prime (H11'), the alpha helical linker that connects helix 11 (H11) and H12 and a unique feature of the ROR family, unfolds and allows reorientation of H12. Together, this generates a cavity

between helices 3 (H3), 4 (H4), H11, H11' and H12. The resulting RORγt conformation antagonizes cofactor binding in a manner different from "classical" orthogonal targeting, which results in destabilizing H12 folding.[31] A variety of compounds targeting this allosteric pocket have recently been published[16,27–30] and effects thereof on autoimmune models studied.[32] Notwithstanding, the mechanism underlying the formation of the allosteric pocket in RORγt, the prerequisites thereof and the NR isoform specificity are poorly understood. Delineation of the molecular determinants of this RORγt allosteric binding site is crucial for addressing these issues and for underlining the developmental potential of targeting this site.

In this chapter, we performed structure and sequence alignments, to identify unique elements and key-differences between RORγt and other NRs in the allosteric region. Crucial amino acids within the allosteric site and those connecting distant helices in the allosteric fold were evaluated. The role of these specific RORγt elements were subsequently studied in the context of their response to both orthosteric and allosteric ligands to obtain a comprehensive understanding of their role in the formation of the allosteric pocket and implications for drug development and NR selectivity.

Results

Identification of unique RORγt elements aligned with allosteric pocket formation

An in-depth structure analysis and multiple sequence alignments were executed to identify amino acids crucial for RORγt allosteric pocket formation. Residues within 4Å of the allosteric ligand MRL-871 in the RORγt crystal structure (PDB 4YPQ)[16] were examined and considered for mutational studies (Figure 1, Figure 2 bold letters). Residues pointing out of the allosteric pocket and not engaged in obvious interactions between secondary structure elements were excluded (Leu-324, Val-480, Leu-483, Phe-498 and Tyr-502). The Dali server[33] was used for structural alignment of the RORγt LBD (PDB 3KYT)[34] against the full PDB.[33,34] The list of resulting structures was checked for human NRs, and all 39 of the other human NRs for which a LBD crystal structure is available could be identified (for RORβ the structure of the 98% similar protein derived from Rattus norvegicus was used). For each NR the structure with the highest similarity score, compared to the RORγt structure, was chosen and a multiple sequence alignment based on the structural

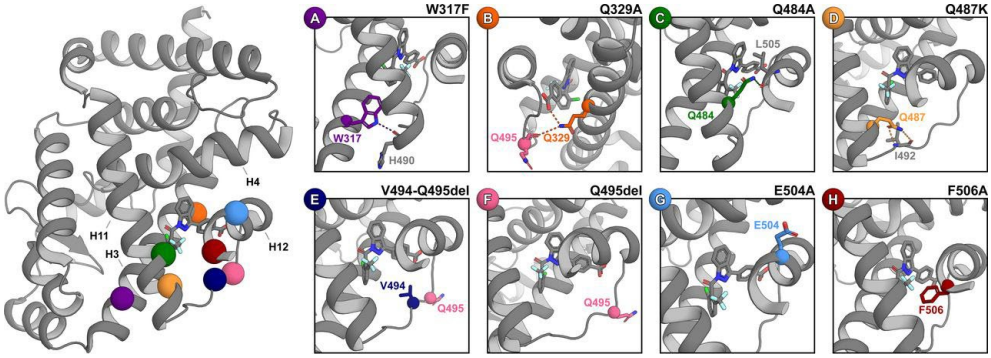

Figure 1 | Selected residues for in-depth evaluation within 4 Å of the allosteric compound MRL-871. *Left*, Overview of the full LBD, with the alpha carbons of the selected residues shown as colored spheres. *Right*, Close-up of respective mutations of W317 (*A*), Q329 (*B*), Q484 (*C*), Q487 (*D*), V494-Q495 (*E*), Q495 (*F*), E504 (*G*), and F506 (*H*).

information was made. The eight NRs for which no structural information about their LBDs was available were added to the alignment afterwards using the MAFFT online service[35], which was also used to create a phylogenetic tree based on the sequence similarities (Figure 2).[35,36] The alignment was used to determine level of conservation of the amino acids in the allosteric pocket (Figure S2). Amino acids of RORγt that were over 30% conserved within the NR superfamily (Thr-325, Leu-353 and Lys-354) and Ile-328 and Leu-505, that have a similarly sized hydrophobic residue at this position in most NRs, were not mutated. Alanines in the allosteric pocket were also not considered for mutations (Ala-321, Ala-496, and Ala-497). Resultingly, residues Trp-317, Gln-329, Gln-484, Gln-487, Glu-E504 and Phe-506 as well as the unique H11' Val-494-Gln-495 stretch were identified for in detail analysis (Figure 1).

The tryptophan at position 317 in RORγt makes a hydrogen bond to His-490 in H11' in the allosteric fold (Figure 1A). This tryptophan is uniquely present in the ROR, Retinoic acid receptor (RAR) and Rev-erb, family while 77% of NRs do not have a hydrogen bond donor at this position. Since the most abundant residue at this position is a phenylalanine, a W317F construct was designed to elucidate the role of the hydrogen bond in forming the allosteric pocket. Gln-329 appears to fulfill a dual role within the allosteric pocket by connecting H3 and H11' and by making a hydrogen bond to the carboxylic acid of the allosteric ligand (Figure 1B). Deleting these hydrogen bonds was hypothesized to correspond to a loss of affinity for allosteric ligands. In order to test this, and because this position has highly variable amino acids in other NRs, a Q329A mutation was introduced. Gln-484 makes a

hydrogen bond to H12 in both the agonistic (Thr-508) and allosteric (Leu-505) fold (Figure 1C) potentially aiding in the stability of both folds. Interestingly, this amino acid is not conserved within the ROR family. In order to elucidate its role in allosteric pocket formation, a Q484A mutation was made. Gln-487 forms two hydrogen bonds to the backbone around Ile-492 in the unfolded H11', which seems to help to correctly position this loop over the allosteric pocket (Figure 1D). The same

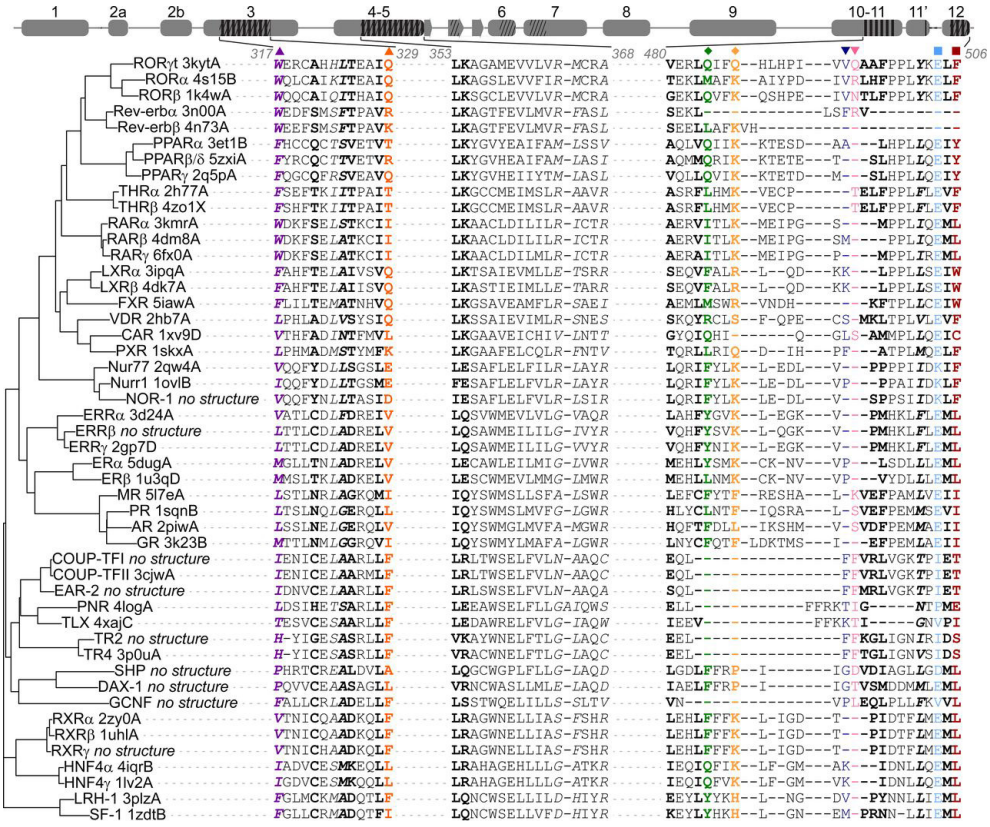

Figure 2 | Multiple-sequence alignment of the human NR LBDs based on structural alignment. On the *left* a phylogenetic tree is shown, based on the sequence.[33,35,36] On the *top*, a 2D outline of the RORγt LBD is given with helices numbered according to convention. *Boldface stripes and letters* indicate regions within 4 Å of the allosteric compound (PDB entry 4YPQ). *Cursive stripes and letters* indicate regions within 4 Å of the orthosteric compound (PDB entry 3KYT) (note the overlap between both binding sites in H3, H4–5, and H12). Crystal structures that were used for the structural alignment are indicated with their 4-digit PDB code. NRs for which no LBD crystal structures were available are indicated. Residues chosen for mutagenesis are highlighted in different colors, and their connected colored symbol for easy identification in subsequent studies is listed.

glutamine residue is only present in the Pregnane X receptor (PXR), while 50% of NRs, including RORα and RORβ, have a lysine at this position that would not be able to make both hydrogen bonds. To evaluate the specific role of this glutamine in comparison to the other NRs a Q487K mutation was made. Phe-506 makes a π-π stacking interaction with the allosteric ligand[37], which might be a prerequisite for binding (Figure 1H), therefore a F506A mutation was made. A final feature, which might be key in forming the allosteric pocket, is the length of H11'. In the ROR family, there are 10 residues between H11 and H12, while in all other NRs, this region has a length of a maximum of 8 residues. The crucial nature of the length of H11' for correctly positioning H12 was investigated using two RORγt constructs featuring a single (Q495del) or double (V494-Q495del) deletion (Figure 1E-F). The deleted residues were selected in such a way that no specific side-chain interactions would be lost. A final control construct was made that should be able to bind to compounds in the same way as the wildtype protein, but without the ability to bind to a coactivator sequence. The E504A mutation removes one side of the charge clamp[38], necessary for coactivator binding (Figure 1G).

Coactivator affinity is only affected by Helix 12 mutations

A Fluorescence Anisotropy (FA) assay was employed to determine the unliganded coactivator affinity of the different RORγt constructs as a means to establish correct folding and basal level towards ligand response. The wildtype RORγt LBD showed an affinity to the FITC-labeled SRC1b2 coactivator peptide of 14.5 ± 4.53 μM (Table 1, Figure S3). The Q487K and Q495del constructs demonstrated coactivator

Protein	**K_d (μm) SCR1b2**
Wild type	14.5 ± 4.5
W317F	78.6 ± 10.4
Q329A	34.3 ± 11.7
Q484A	4.87 ± 3.69
Q487K	9.65 ± 0.95
E504A	200 ± 36
F506A	365 ± 292
Q495del	12.2 ± 5.3
V494-Q495del	33.7 ± 9.1

Table 1 | Kd values of the wild-type and mutated proteins toward FITC-labeled SRC1b2 peptide Values shown are means ± S.D. from five independently executed and fitted experiments.

affinities in the same range with K_d values of respectively 9.65 ± 0.95 µM and 12.2 ± 5.3 µM. The Q484A construct bound somewhat stronger to the coactivator peptide than the wildtype protein with a K_d value of 4.87 ± 3.69 µM, indicating a high basal affinity. Q329A and V494-Q495del showed a slightly decreased intrinsic affinity compared to the wildtype protein with K_d values of respectively 34.3 ± 11.7 µM and 33.7 ± 9.1 µM. The RORγt W317F construct bound much even weaker and had a K_d value of only 78.6 ± 10.4 µM. The FA signal of the E504A and F506A constructs only increased at very high protein concentrations, and the K_d values at 200 ± 36 µM and 365 ± 292 µM respectively reveal their loss of coactivator affinity. Together, these data indicate that, except for the mutations in H12, the other constructs feature intrinsic coactivator affinities that allow subsequent evaluation of inverse agonist binding.

Ligand binding in the RORγt orthosteric pocket is not affected by mutations in the RORγt allosteric pocket

The functionality of the different RORγt LBDs in response to ligands, was evaluated using a known orthosteric agonist and inverse agonist. For this, respectively 20α-Hydroxycholesterol and ursolic acid (UA) were chosen (Figure S1) as their binding mode is well known and constricted to the classical, orthosteric binding pocket

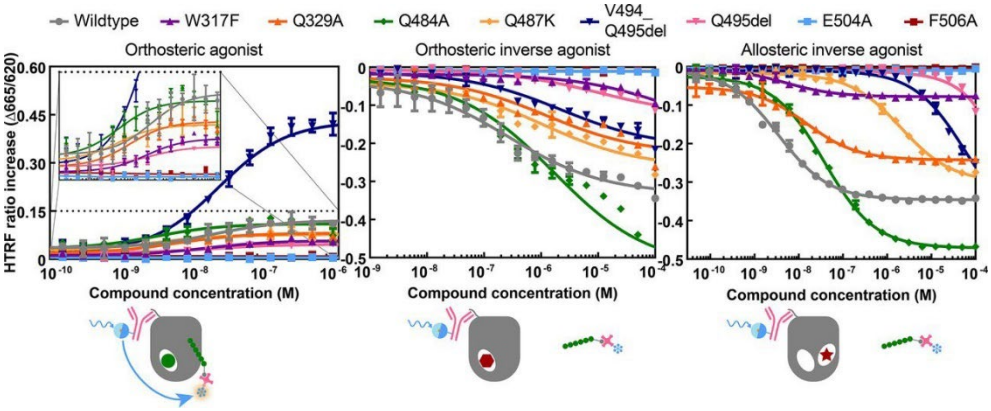

Figure 3 | Representative HTRF binding curves of the WT and mutated proteins. Dose-response curves from the HTRF coactivator recruitment assay at fixed protein (20 nM) and SRC1b2 (100 nM) concentrations are shown. *Left*, 20a-hydroxycholesterol titration; *middle*, ursolic acid titration; *right*, MRL-871 titration. Bottom, schematic representation of the assay. Mean ± S.D. from one experiment performed in duplicate is shown with the corresponding fit.

(PDB entry 5K3M).[34] A homogeneous time-resolved FRET (HTRF) assay and Differential Scanning Fluorimetry (DSF) were utilized for this. In HTRF, the RORγt LBDs were labeled using a terbium labeled His6-tag binding antibody which functions as a fluorescent donor. Biotinylated SRC1b2 coactivator peptide with streptavidin D2 was used as the fluorescent acceptor. Upon increasing the 20α-Hydroxycholesterol concentration, an increase in FRET ratio is anticipated, while addition of UA will decrease this ratio. In Figure 3 (left and middle) it is shown that this holds true for all constructs except the H12 E504A and F506A proteins, which have no affinity for the coactivator peptide. EC_{50} or IC_{50} values were found in the same range for the wildtype and mutated RORγt LBDs for these compounds (Table S1). The difference in maximum HTRF ratio increase that is obtained for the V494-Q495 construct by 20α- Hydroxycholesterol might be related to a different positioning of H12 by the shorter H11'. The differences in HTRF ratio decrease caused by UA are caused by differences in starting levels without ligand (Figure S4). All HTRF ratios go down to the level that is also reached in the absence of protein. To orthogonally validate the orthosteric ligand binding effects in a coactivator

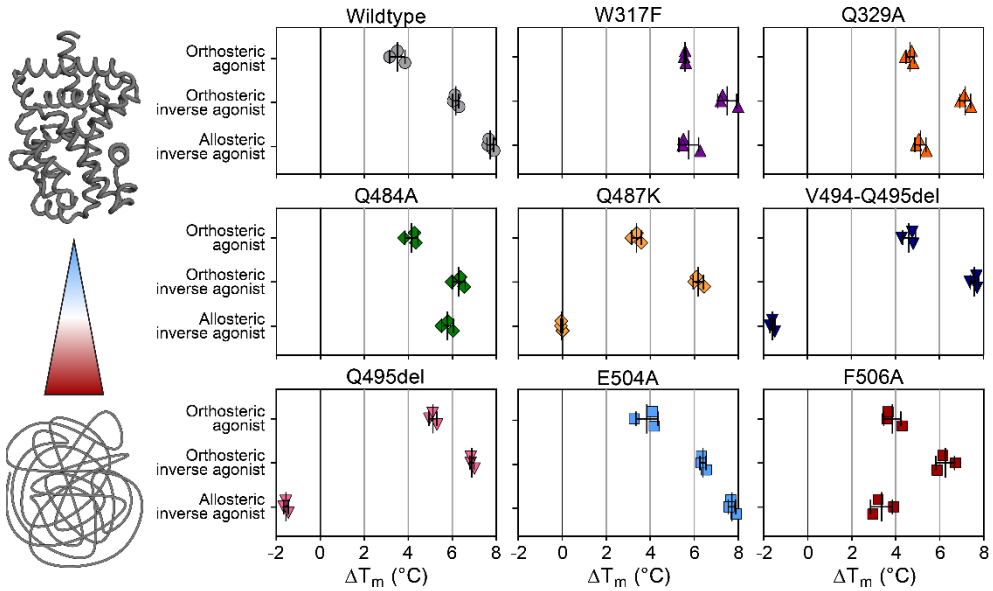

Figure 4 | Average ΔT_m values of ligand effects on the RORγt protein constructs in DSF. T_m of protein (5 mM) is determined in the absence and presence of different ligands (10 mM). The T_m without ligand is subtracted from that with ligand, yielding the ΔT_m. *Left*, schematic of the assay; graphs, data per protein. *Right*, graphs show the average ΔT_m per experiment and mean ± S.D. from 3 experiments performed in duplicate.

independent manner, DSF studies were also performed with these compounds on all the protein constructs (Figure 4, Figure S5, Table S2). All proteins are stabilized both by binding to the orthosteric inverse agonist UA, by an average 6.7 ± 0.6 °C, and by binding the orthosteric agonist 20α-Hydroxycholesterol (4.3 ± 0.8 °C). The data also clearly allow concluding that even though the E504A and F506A constructs are not able to efficiently bind to a coactivator, they are still capable of binding to the orthosteric ligands, as they show strong stabilization upon addition of these compounds. Together, these findings show that all protein constructs have a functioning orthosteric pocket, which is not affected by the mutations around the allosteric pocket.

Helix 11' and Gln-487 are crucial for formation of the RORγt allosteric pocket and allosteric ligand response

The response of the different RORγt to an allosteric inverse agonist was also evaluated using HTRF and DSF assays. In HTRF, the allosteric inverse agonist MRL-871 inhibited the coactivator binding of wildtype RORγt with an IC_{50} of 4.90 ± 1.98 nM (Figure 3, *right*, Table S1). Three RORγt constructs matched this nanomolar inhibitory activity, being W317F with an IC_{50} of 3.09 ± 1.97 nM and Q329A and Q484A with IC_{50} values of respectively 13.1 ± 4.6 nM and 28.5 ± 11.5 nM. RORγt Q487K interacted over 500 times weaker with the allosteric ligand than the wildtype RORγt LBD with an IC_{50} of 2.75 ± 0.65 µM. The two deletion constructs hardly showed binding to the allosteric compound with IC_{50} values of only ~50-100 µM. Again, the difference in bottom plateaus is caused by the difference in starting levels, due to the varying coactivator affinity (Figure S4).

The findings regarding coactivator recruitment were reflected in the DSF studies (Figure 4, Figure S5 and Table S2). The wildtype RORγt LBD and E504A, which could not be measured in HTRF due to its lack of coactivator binding, both showed an increase in melting temperature (T_m) of 7.7 ± 0.2 °C in the presence of the allosteric inverse agonist. The W317F, Q329A, Q484A and F506A constructs were also stabilized upon allosteric ligand binding, albeit somewhat weaker, by respectively 5.8 ± 0.5 °C, 5.1 ± 0.2 °C, 5.8 ± 0.3 °C and 3.4 ± 0.5 °C. Interestingly, Q487K had the exact same melting temperature in the absence and presence of MRL-871, meaning that this protein was not stabilized upon the addition of the allosteric ligand. The deletion constructs even showed a decrease in the T_m upon MRL-871 treatment of -1.6 ± 0.1 °C for both the single and double deletion. When plotting the ΔT_m's determined in the DSF assay against the IC_{50} values from the HTRF (Figure S6) a

strong correlation can be observed, pointing to correlated mechanisms of allosteric pocket modulation observed via the two different assay formats.

Discussion

The most N-terminal amino acid evaluated (Trp-317) reveals an important contribution towards protein activity and stability. The W317F mutation leads to a lower intrinsic coactivator affinity of RORγt (Table 1, Figure S3) and lowers the protein stability (Figure S7) as compared to the wildtype protein. Crystal structure analysis reveals that in the apo[39] and agonist bound[34] state Trp-317 does not only contribute to a hydrophobic network, as extensively investigated by Sun et al. (2018)[40], but that the indole nitrogen also serves as a hydrogen bond donor towards the backbone amide of L391 in H7-8. These characteristics illustrate why the W317F protein is less stable and active. The allosteric inverse agonist has similar effects on W317F as on the wildtype protein in terms of inverse agonism and conferring protein stability (Figures 3-4). Together, this shows that the hydrogen bond between Trp-317 and His-490, and Trp-317 more in general, is not of relevance for the formation of the allosteric pocket.

The construct with the Q329A mutation is binding slightly less strong to the FITC-labeled SRC1b2 peptide and is about 1 °C less thermal stable than the wildtype RORγt (Table 1, Figure S7). In the HTRF the IC_{50} value for the allosteric inverse agonist was in the same range as for the wildtype protein (Figure 3) and the DSF results also report a strong thermal stabilization of the construct upon addition of the allosteric ligand (Figure 4). Yuan et al. conducted molecular dynamics simulations on RORγt bound to MRL-871 and reported that the hydrogen-bonding interaction between Gln-329 and the ligand, as observed in the crystal structure, is only present during 1.5% of their simulation time.[41] These simulations thus corroborate the experimental findings from this study that the Gln-329 is not crucial for binding of the MRL-871 allosteric ligand. Analogously, the Gln-329 can be considered to not be a crucial determinant for forming the RORγt allosteric pocket.

The mutation of the RORγt Gln-484 to an alanine slightly increases the affinity of the LBD towards the coactivator peptide. In the crystal structure of the agonist liganded and apo RORγt, the Gln-484 sidechain appears to make a hydrogen bond to Thr-508 in H12, but closer inspection into the actual electron densities reveals that the orientation of this sidechain is unclear. In contrast, in the crystal structure of RORγt LBD bound to the allosteric inverse agonist, the electron density of the

sidechain of Gln-484, which makes a hydrogen bond with Ser-507, is highly defined. The Q484A constructs is indeed somewhat less susceptible to allosteric inverse agonist binding than the wildtype protein, with the IC_{50} value in the HTRF assay being ~6 times weaker. A similar effect is seen upon titration of allosteric compound FM26 (Figure S8).[30] Concomitantly, MRL-871 still induces a strong stabilization of the thermal stability of the protein, but to a lesser extent than observed for the wildtype protein. These results thus highlight that, while not crucial, Gln-484 contributes to formation of the allosteric pocket, most probably via hydrogen bonding towards H12.

The Gln-487 revealed itself to be highly crucial for the formation of the allosteric pocket. In the assays designed to validate the classical orthosteric regulation of the RORγt LBD, the Q487K construct showed very similar behavior as the wildtype protein. The thermal stability of the apo Q487K construct is even a bit higher than that of the wildtype and orthosteric ligand binding, both of the agonist and inverse agonist type, leads to similar coactivator recruitment and inhibition effects. These observations are in line with the design expectations, since the singular hydrogen bond that Gln-487 makes with Ser-508 in H12 in the agonistic fold, can most probably be made with the lysine mutation as well. In striking contrast to the absence of effects on the orthosteric pocket, the Q487K construct featured very pronounced differences, as compared to the wildtype RORγt, with regards to its allosteric pocket. In the HTRF assay the IC_{50} value for MRL-871 inhibition of the Q487K construct is weakened with a factor of 560 and the shift for allosteric compound FM26 appears to be even bigger (Figure S8).[30] In the DSF assay no thermal stabilization at all is observed upon dosing of the allosteric ligand. The glutamine at the 487 position is highly unique within the NR superfamily and only shared with PXR, which is otherwise only 28% identical. Half of all NRs, including RORα and RORβ, have a lysine at this position. These results and observations are highly relevant as this implies that on the one hand the allosteric pocket formation might be uniquely attributable to RORγt via this glutamine and that on the other hand selective ligand targeting of RORγt might be ideally suited via this allosteric pocket.

The two RORγt constructs with a single or double amino acid deletion in the H11' allowed evaluating the importance of this longer linker between H11 and H12, unique to the ROR family. The results from the FA assay showed that shortening of the H11' did not affect the capacity of RORγt to bind to a coactivator peptide (Table

1, Figure S3). Furthermore, the orthosteric ligands, both of agonistic and of inverse agonistic nature, induced coactivator binding and thermal stability effects in line with those for the wildtype protein. In very outspoken contrast to the above, the addition of the allosteric inverse agonist showed a completely different profile on the two H11' deletion constructs as compared to the wildtype protein. In the HTRF assay, MRL-871 only inhibited both proteins at high micromolar concentrations and in DSF the allosteric ligand even destabilizes these proteins. The crystal structure of RORγt bound to MRL-871 reveals that with the formation of the allosteric pocket H11' extends to form a loop which allows H12 to be positioned overlapping with the site where coactivators can normally bind (Figure S1). Shortening of this loop leads to constructs that cannot span this distance anymore, thus preventing H12 to form the allosteric pocket. This finding leads to conclude that NRs that do not have this H11' might not be able to form a similar allosteric pocket.

The E504A construct was designed as a control protein with both the orthosteric and allosteric pocket functioning, but without the ability to efficiently bind coactivator protein or peptide.[38] The experimental results confirm this behavior, with the FA data reporting coactivator binding only at very high protein concentrations (Table 1, Figure S3), while the DSF data report thermal stability and ligand response as a virtual copy of the wildtype protein (Figure 4).

In the conformation the RORγt LBD adopts upon allosteric inverse agonist binding, Phe-506 is pointing directly into the allosteric pocket and is involved in a π-π stacking interaction with the MRL-871 ligand.[16,41] In the apo or agonist-bound state, Phe-506 is involved in aromatic interactions with His-479 and Glu-502 providing an anchoring force to stabilize H12 in the active conformation even in the absence of ligand.[39] The F506A construct indeed shows diminished coactivator peptide binding to a similar extend as for the E504A construct (Table 1, Figure S3), illustrating the importance of the aromatic cluster in the active, agonistic, conformation. The orthosteric ligands do still bind just as good as to the wildtype protein as evidence by the thermal stabilization data (Figure 4). The absence of coactivator binding makes evaluation of MRL-871 in related assays not possible. The DSF assay reveals that the F506A construct is still able to bind and be stabilized by the allosteric inverse agonist, albeit to a lesser extent than the wildtype protein. This implies that the π-π stacking interaction between Phe-506 and MRL-871 is relevant, but not essential for allosteric compound binding. A similar observation was recently made upon structural comparison of different RORγt allosteric ligands.[37] Other NR

superfamily members contain various medium sized hydrophobic or aromatic residues at this position. Since even the F506A mutation retains affinity towards the allosteric compound, this specific amino acid is deemed not crucial for the formation of the allosteric pocket, but potentially modulatory towards allosteric ligand biding.

In conclusion, the molecular determinants of the RORγt allosteric pocket were evaluated in detail by selectively introduced mutations to the RORγt LBD. All RORγt proteins were still responsive towards orthosteric agonists and inverse agonists, demonstrating their overall functionality. From the set of proteins studied, two molecular elements came forward to be crucial for the formation of the allosteric pocket of RORγt. The combination of a Gln-487 and a long H11' are unique within the NR realm for RORγt. Whereas other amino acids that delineate the allosteric pocket can be replaced for those with other side chains, modifications to these two elements are detrimental. The results of this study thus strongly bring forward that the allosteric pocket as present in RORγt and receptive to MRL-871 and other ligands[16,27–30,37], is highly unique to RORγt within the NR superfamily. This implies that RORγt would possibly be the only NR capable of forming this specific type of allosteric pocket, which is also supported by a commercially available panel of cell-based NR reporter assays against which an MRL-871 analog was tested.[16] This uniqueness testifies to the potential of achieving high NR-subtype selectivity via drugging of this allosteric RORγt pocket for applications in Th17-mediated autoimmune diseases.

Experimental section

Site-directed mutagenesis

Point mutations (W317F, Q329A, Q484A, Q487K, E504A and F506A) were introduced using the QuikChange Lightning Multi Site-Directed Mutagenesis Kit (Agilent) in accordance with the protocols described in the kit manual. The parental DNA for this was a pET15b vector containing the RORγt LBD (residues 265-518) with an N-terminal His6-tag. Single primers designed to hybridize with the parental DNA containing 1-3 mismatches were utilized for this.

The primers for the deletion constructs, Q495del and V494_Q495del, were prepared via the method described by Liu and Naismith (43). In short, primers with overlap on the 5' end (pp) were designed in such a way that the deletion was in the pp region while the 3' ends (no) could hybridize to the DNA efficiently. For the PCR reaction, 0.2 ng/µL parental DNA was combined with 1 µM of both primers and 1X Phusion polymerase in HF buffer (Thermo

Scientific). The reaction started with denaturation (1 min, 98 °C) followed by 18 amplification steps. Each of these steps started with denaturation (10 s, 98 °C), followed by annealing (1 min, T_m no -5 °C) and extension (2:30 min, 72 °C). The method ended with a final annealing (1 min, T_m pp -5 °C) and extension (30 min, 72 °C) step.

For all mutagenesis reactions, the parental DNA was digested using DpnI followed by transformation into XL10-Gold Ultracompetent Cells (Agilent) by heat shock. Small cultures were initiated, using single colonies in 5 mL LB medium supplemented with ampicillin (100 µg/mL), overnight at 37 °C 250 rpm. DNA was isolated using the QIAprep® Spin Miniprep Kit (Qiagen) in accordance with the supplied protocol. The mutations were confirmed by sequencing using T7 promoter and T7 terminator primers (BaseClear).

Expression and Purification of the RORγt constructs

A pET15b vector containing the RORγt LBD (residues 265-518) with an N-terminal His6-tag was transformed into BL21(DE3) competent Escheria Coli (Novagen) by heat shock. A pre-culture was initiated, using a single colony in 8 mL LB medium supplemented with ampicillin (100 µg/mL), overnight at 37 °C 250 rpm. This culture was transferred to 500 mL TB medium with ampicillin (100 µg/mL), MgCl2 (0.5 mM), and antifoam (0.05 %), and incubated at 37 °C until OD600 nm = 1.0 was reached Isopropyl β-D-thiogalactoside (IPTG) (0.5 mM) was then added to induce expression, and the culture was incubated at 18 °C 150 rpm for 16 h. The bacteria were harvested using centrifugation (10,000 *g, 4 °C, 10 m) and dissolved in lysis buffer (50 mM Tris pH 8.0, 300 mM NaCl, 20 mM imidazole, 10 v/v% glycerol, 1mM tris(2-carboxyethyl)phosphine (TCEP)). The cells were lysed using a homogenizer (Avestin Emulsiflex C3) at 15,000 psi with additional cOmplete™, EDTA-free Protease Inhibitor Cocktail (1 tablet/50 mL buffer) and benzonase (1:10,000 v/v). The cell lysate was cleared by centrifugation (40,000 *g, 4 °C, 30 m) and purified via Ni2+ affinity column chromatography (QIAGEN, nickel-nitrilotriacetic acid (Ni-NTA) Superflow Cartridge). Elution fractions containing the protein of interest were afterwards dialyzed against a storage buffer (20 mM Tris pH 8.0, 150 mM NaCl, 10 v/v% glycerol, 5 mM DTT) overnight and, subsequently, stored at -80 °C until usage. Molecular weight and purity were assessed using Quadrupole Time-of-Flight LC/MS and SDS-page. This procedure was repeated for the mutated constructs.

RORγt-LBD SRC-1 coactivator protein titration Fluorescence Anisotropy (FA) assay

FA assays were performed in 10 µL volumes in triplicate in buffer containing 150 mM NaCl, 10 mM HEPES, 5 mM DTT, 10 mM CHAPS and 0.1 m/v % BSA. 10 nM FITC labelled SRC1b2 (Table S3) was present and His6-RORγt LBD was titrated to the peptide in round bottom, non-binding, black, 384-well plates (Corning #4511). The plates were measured in an Infinite F500 plate reader (Tecan) (excitation = 485 nm; emission = 535 nm). The data were then analyzed using GraphPad Prism software, where the curve-fitting was done via:

$$y = \frac{B_{max} * x}{K_d + x} + Background$$

Where Bmax is the maximum specific binding, constrained to a maximum value of 350, K_d is the equilibrium binding constant and Background is the amount of nonspecific binding with no added protein. Background was assumed to be constant between constructs within each experiment. The reported K_d values are the mean ± S.D. from five individually fitted independent experiments performed in singlicate.

RORγt-LBD SRC-1 coactivator compound titration Homogeneous time-resolved FRET (HTRF) assay

HTRF assays were performed in 10 µL volumes in triplicate in buffer containing 150 mM NaCl, 10 mM HEPES, 5 mM DTT, 10 mM CHAPS and 0.1 m/v % BSA. 20 nM His6-RORγt LBD, 100 nM biotin labelled SRC1b2 coactivator peptide (Table S3), 733 pM Terbium-labelled anti-His antibody (Cisbio, 61HISTLB) and 12.5 nM D2-labelled streptavidin (Cisbio, 610SADLB) were used. Compounds dissolved in DMSO were titrated to this mixture in round bottom, non-binding, white, 384-well plates (Corning #4513) keeping the DMSO concentration constant at 2%. After 30 min incubation at 4 °C, the plates were measured in an Infinite F500 plate reader (Tecan) (excitation = 340 nm; emission = 665 nm and 620 nm). The data were afterwards analyzed using GraphPad Prism software, where the curve-fitting was done via:

$$y = Bottom + \frac{Top - Bottom}{1 + (\frac{x^{Hillslope}}{IC_{50}{}^{Hillslope}})}$$

For inverse agonists UA and MRL-871 and via:

$$y = Bottom + \frac{x^{Hillslope} * (Top - Bottom)}{x^{Hillslope} + EC_{50}{}^{Hillslope}}$$

For agonist 20α-Hydroxycholesterol. The hillslope was assumed to be constant within samples with the same compound to aid in the fit of datasets where no plateau was reached. For the measurements with 20α-Hydroxycholesterol, data points at higher compound concentration than the top where the decrease in signal compared to the top was more than 10% were omitted for the fit. The reported EC_{50}/IC_{50} values are the mean ± S.D. from three individually fitted independent experiments performed in duplicate.

Differential Scanning Fluorimetry

Differential Scanning Fluorimetry (DSF) assays were performed using 40 µL samples containing 5 µM RORγt-LBD, 10 µM compound and 2.5X SYPRO® Orange (Sigma) in buffer containing 150 mM NaCl, 10 mM HEPES and 2% DMSO. The samples were heated from 30 °C to 64.5 °C at a rate of 0.3 °C per 15 s in a CFX96 Touch Real-Time PCR Detection System (Bio-Rad). Excitation (575/30 nm) and emission (630/40 nm) filters were used and the reported melting values were calculated as the local minimum between 35 °C and 60 °C in the negative derivative of the resulting melting curve. T_m and ΔT_m are determined as mean ± S.D. from 3 independent experiments performed in duplicate.

Supporting information

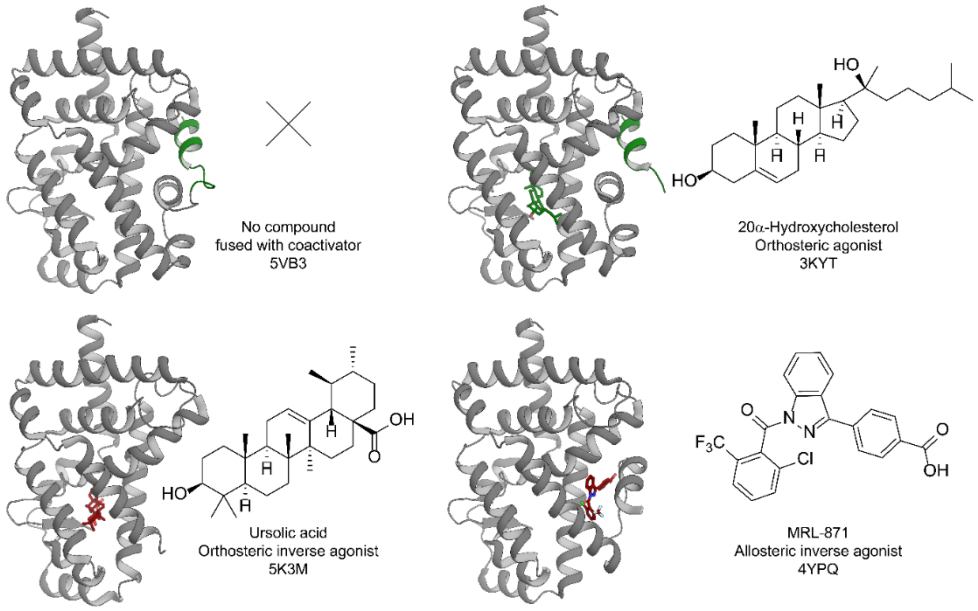

Supplementary figure 1 | RORγt LBD crystal structure in presence and absence of compounds. RORγt LBD is shown in gray, agonist and coactivator in green and inverse agonist in red. *Top left*: apo-structure of RORγt LBD fused with SRC2 coactivator peptide. *Top right*: 20α-Hydroxycholesterol (PDB: 3KYT). *Bottom left*: Ursolic acid (PDB: 5K3M), *Bottom right*: MRL-871 (PDB: 4YPQ)

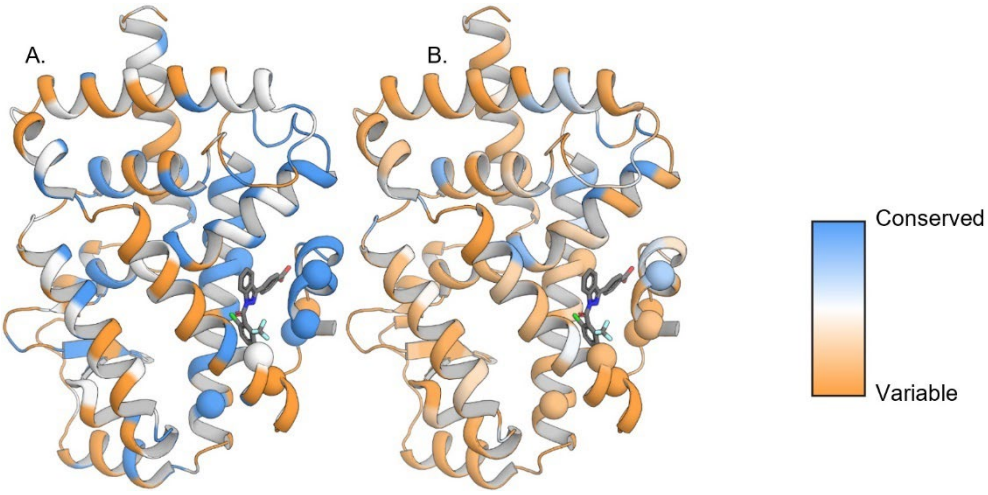

Supplementary figure 2 | Residue conservation within the ROR family and NR superfamily. Blue means conserved, orange means variable. Mutated residues are indicated with spheres at their C-alpha position. (*A*) Conservation of the residues present in RORγt over the human ROR family. (*B*) Conservation of residues present in RORγt over the human NR superfamily.

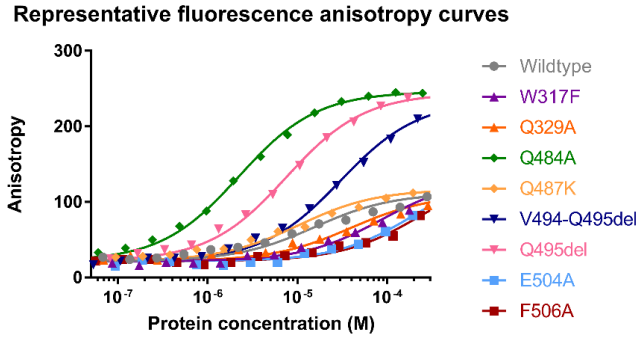

Supplementary figure 3 | Representative curves of a fluorescence anisotropy assay. The proteins are titrated towards a fixed concentration of FITC-labeled SRC1b2 peptide (10 nM). An increase in anisotropy indicates binding of the peptide to the protein.

Protein	EC_{50} 20α-Hydroxycholesterol (nM)	IC_{50} Ursolic Acid (nM)	IC_{50} MRL-871 (nM)	Fold decrease IC50 MRL
Wildtype	107.0 ± 59.5	181.1 ± 69.7	4.90 ± 1.98	
W317F	153.1 ± 65.0	1293 ± 2057	3.09 ± 1.97	0.6
Q329A	53.5 ± 18.2	260.8 ±189.0	13.1 ± 4.6	2.7
Q484A	39.1 ± 26.0	333.9 ± 315.3	28.5 ± 11.5	5.8
Q487K	64.3 ± 32.4	396.6 ± 356.0	$2.75*10^3 \pm 0.65*10^3$	561
E504A	ND*	67.12 **	ND*	ND*
F506A	ND*	ND*	ND*	ND*
Q495del	322.9 ± 72.4	$3.06*10^3 \pm 2.11*10^3$	$65.3*10^3$**	13312
V494_Q495del	265.5 ± 67.4	775.7 ± 865.4	$96.7*10^3 \pm 44.4*10^3$	19720

Supplementary table 1 | EC_{50}/IC_{50} values measured in HTRF with orthosteric and allosteric compounds. The reported EC_{50}/IC_{50} values are the mean ± S.D. from three individually fitted independent experiments performed in duplicate. * EC50/IC50 could not be determined because the change in signal caused by the compound was less than 10%. ** No standard deviation was determined because only one experiment could be fitted with confidence

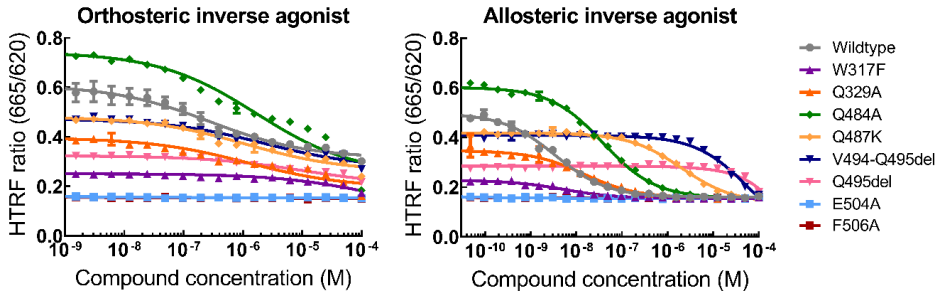

Supplementary figure 4 | Representative HTRF binding curves of the wildtype and mutated proteins. Dose-response curves from the HTRF coactivator recruitment assay at fixed protein (20 nM) and SRC1b2 (100 nM) concentrations. *Left*: Ursolic acid titration, *Right*: MRL-871 titration. No background subtraction. Mean ± S.D. of one experiment performed in duplicate is shown with corresponding fit.

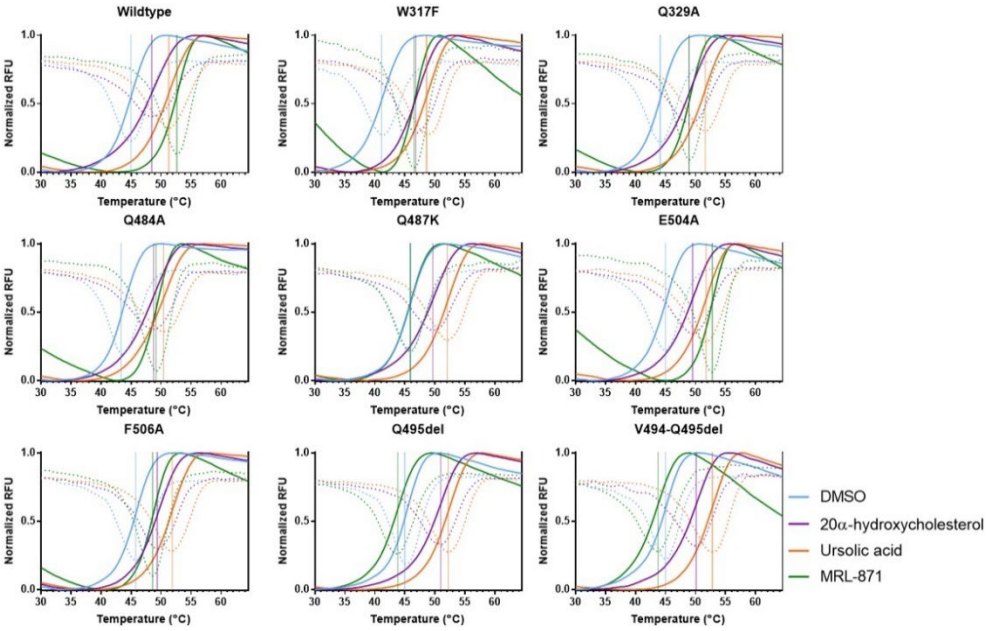

Supplementary figure 5 | Representative melting curves and derivatives from DSF. The normalized fluorescence as measured through excitation (575/30 nm) and emission (630/40 nm) filters is normalized per protein and indicated in solid curves. The negative derivative of these curves is indicated in dotted curves. The minimum of these curves is indicated with a solid vertical line, indicating the melting temperature under those specific conditions.

Protein	Tm vehicle (°C)	ΔTm 20α-Hydroxycholesterol (°C)	ΔTm Ursolic Acid (°C)	ΔTm MRL-871 (°C)
Wildtype	44.8 ± 0.3	3.5 ± 0.4	6.2 ± 0.1	7.7 ± 0.2
W317F	41.0 ± 0.1	5.6 ± 0.0	7.5 ± 0.4	5.8 ± 0.5
Q329A	44.0 ± 0.2	4.7 ± 0.2	7.2 ± 0.2	5.1 ± 0.2
Q484A	43.6 ± 0.3	4.1 ± 0.3	6.3 ± 0.3	5.8 ± 0.3
Q487K	45.7 ± 0.3	3.4 ± 0.2	6.2 ± 0.2	0.0 ± 0.0
E504A	45.0 ± 0.6	3.8 ± 0.5	6.4 ± 0.1	7.7 ± 0.2
F506A	45.3 ± 0.2	3.9 ± 0.4	6.3 ± 0.4	3.4 ± 0.5
Q495del	45.0 ± 0.3	5.1 ± 0.2	6.9 ± 0.1	-1.6 ± 0.1
V494_Q495del	44.7 ± 0.4	4.6 ± 0.3	7.6 ± 0.2	-1.6 ± 0.1
Average	44.4 ± 1.4	4.3 ± 0.8	6.7 ± 0.6	3.6 ± 3.8

Supplementary table 2 | Melting temperatures without compound and melting temperature increases caused by compound for the wildtype and mutated proteins. T_m vehicle shows the mean ± S.D. T_m without compound from 3 experiments performed in duplicate. ΔT_m is the mean ± S.D. difference with and without compound from 3 experiments performed in duplicate.

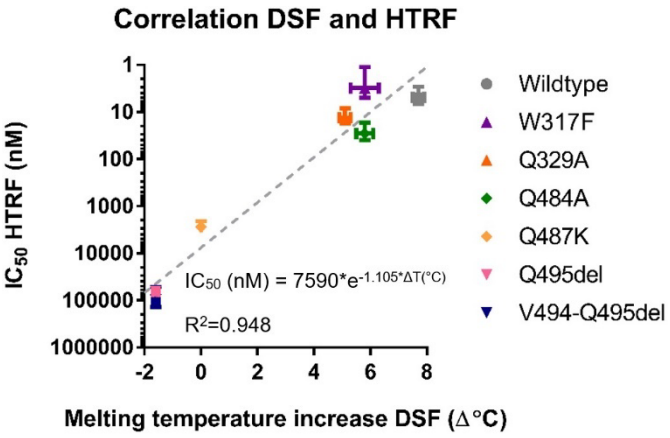

Supplementary figure 6 | Correlation between melting temperatures in DSF and IC50 values in HTRF in presence of MRL-871. A correlation can be observed between the melting temperature increase in DSF and the IC50 in HTRF caused by MRL-871. For the E504A and F506A constructs no correlation can be shown, because they don't show coactivator affinity and therefore their IC_{50} in HTRF towards MRL-871 cannot be determined.

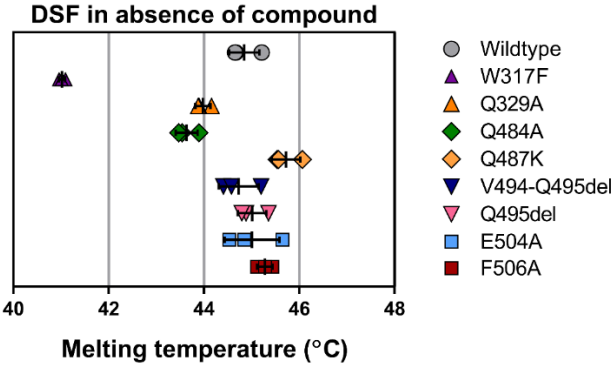

Supplementary figure 7 | Melting temperatures of the wildtype and mutated proteins in absence of compound. The melting temperatures are determined as the minimum of the negative derivative of the raw fluorescence plotted over an increase in temperature. Graph shows the average melting temperature per experiment and mean ± S.D. from 3 experiments performed in duplicate.

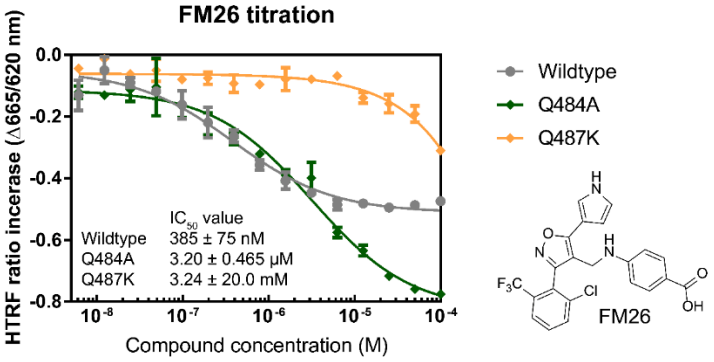

Supplementary figure 8 | HTRF binding curves of FM26 towards the wildtype, Q484A and Q487K proteins. *Left*: dose-response curves from the HTRF coactivator recruitment assay at fixed protein (20 nM) and SRC1b2 (100 nM) concentrations. Mean ± S.D. of one experiment performed in triplicate is shown with corresponding fit. *Right*: structure of FM26.

Name	Sequence
His6-RORγt LBD	MGSS*HHHHHH*SSGLVPRGSHMASLTEIEHLVQSVCKSYRETCQ LRLEDLLRQRSNIFSREEVTGYQRKSMWEM**W**ERCAHHLTEAI**Q** YVVEFAKRLSGFMELCQNDQIVLLKAGAMEVVLVRMCRAYNAD NRTVFFEGKYGGMELFRALGCSELISSIFDFSHSLSALHFSED EIALYTALVLINAHRPGLQEKRKVEQLQYNLELAFHHHLCKTH RQSILAKLPPKGKLRSLCSQHVERL**Q**IF**Q**HLHPIV**VQ**AAFPPL YK**E**L**F**STETESPVGLSK
FITC- SRC1b2	FITC-βA–SSLTERHKILHRLLQEGSPSD-NH2
Biotin- SRC1b2	Biotin-N-PSSHSSLTERHKILHRLLQEGSPSD-$CONH_2$

Supplementary table 3 | Sequences of protein and peptide used in this chapter. For the protein sequence the 6*His-tag is indicated in *italic* and the sites that are targeted by the mutagenesis are *bold*. Peptide sequences are based on box II of the Steroid Receptor Coactivator 1 using appropriate tags for assays.

Acknowledgments

Femke Meijer is acknowledged for providing FM26 and Rens de Vries for help with generating Figure 1.

References

1. Huang, P., Chandra, V. & Rastinejad, F. Structural Overview of the Nuclear Receptor Superfamily: Insights into Physiology and Therapeutics. *Annu. Rev. Physiol.* **72**, 247–272 (2010).
2. Bourguet, W., Ruff, M., Chambon, P., Gronemeyer, H. & Moras, D. Crystal structure of the ligand-binding domain of the human nuclear receptor RXR-α. *Nature* **375**, 377–382 (1995).
3. Jin, L. & Li, Y. *Structural and functional insights into nuclear receptor signaling. Advanced drug delivery reviews* vol. 62 1226 (NIH Public Access, 2010).
4. Rastinejad, F., Huang, P., Chandra, V. & Khorasanizadeh, S. Understanding nuclear receptor form and function using structural biology. *J. Mol. Endocrinol.* **51**, T1–T21 (2013).
5. Greschik, H., Flaig, R., Renaud, J. P. & Moras, D. Structural basis for the deactivation of the estrogen-related receptor γ by diethylstilbestrol or 4-hydroxytamoxifen and determinants of selectivity. *J. Biol. Chem.* **279**, 33639–33646 (2004).
6. Veldscholte, J. *et al.* A mutation in the ligand binding domain of the androgen receptor of human INCaP cells affects steroid binding characteristics and response to anti-androgens. *Biochem. Biophys. Res. Commun.* **173**, 534–540 (1990).
7. Liu, H. H., Han, R., Li, J., Liu, H. H. & Zheng, L. Molecular mechanism of R-bicalutamide switching from androgen receptor antagonist to agonist induced by amino acid mutations using molecular dynamics simulations and free energy calculation. *J. Comput. Aided Mol. Des.* **30**, 1189–1200 (2016).
8. Kojetin, D. J. & Burris, T. P. Small molecule modulation of nuclear receptor conformational dynamics: Implications for function and drug discovery. *Mol. Pharmacol.* **83**, 1–8 (2013).
9. Shang, J., Brust, R., Griffin, P. R., Kamenecka, T. M. & Kojetin, D. J. Quantitative structural assessment of graded receptor agonism. *Proc. Natl. Acad. Sci. U. S. A.* **116**, 22179–22188 (2019).
10. Tice, C. M. & Zheng, Y. J. *Non-canonical modulators of nuclear receptors*. *Bioorganic and Medicinal Chemistry Letters* vol. 26 4164 (Elsevier Ltd, 2016).
11. Fernandez, E. J. *Allosteric pathways in nuclear receptors — Potential targets for drug design*. *Pharmacology & Therapeutics* vol. 183 159 (2018).
12. Meijer, F. A., Leijten-van de Gevel, I. A., de Vries, R. M. J. M. & Brunsveld, L. Allosteric small molecule modulators of nuclear receptors. *Mol. Cell. Endocrinol.* **485**, 20–34 (2019).
13. Meyer, U., Costantino, G., Macchiarulo, A. & Pellicciari, R. Is Antagonism of E/Z-Guggulsterone at the Farnesoid X Receptor Mediated by a Noncanonical Binding Site? A Molecular Modeling Study. *J. Med. Chem.* **48**, 6948–6955 (2005).
14. Hughes, T. S. *et al.* An alternate binding site for PPARγ ligands. *Nat. Commun.* **5**, 1–13 (2014).

15. Chen, L. *et al.* Sulindac-derived RXRalpha modulators inhibit cancer cell growth by binding to a novel site. *Chem. Biol.* **21**, 596–607 (2014).
16. Scheepstra, M. *et al.* Identification of an allosteric binding site for RORγt inhibition. *Nat. Commun.* **6**, 8833–8833 (2015).
17. Zhang, Y., Luo, X. Y., Wu, D. H. & Xu, Y. ROR nuclear receptors: Structures, related diseases, and drug discovery. *Acta Pharmacol. Sin.* **36**, 71–87 (2015).
18. Ivanov, I. I. *et al.* The Orphan Nuclear Receptor RORγt Directs the Differentiation Program of Proinflammatory IL-17+ T Helper Cells. *Cell* **126**, 1121–1133 (2006).
19. Ichiyama, K. *et al.* Foxp3 inhibits RORgammat-mediated IL-17A mRNA transcription through direct interaction with RORgammat. *J. Biol. Chem.* **283**, 17003–8 (2008).
20. Manel, N., Unutmaz, D. & Littman, D. R. The differentiation of human TH-17 cells requires transforming growth factor-β and induction of the nuclear receptor RORγt. *Nat. Immunol.* **9**, 641–649 (2008).
21. Langley, R. G. *et al.* Secukinumab in Plaque Psoriasis — Results of Two Phase 3 Trials. *N. Engl. J. Med.* **371**, 326–338 (2014).
22. Lebwohl, M. *et al.* Phase 3 studies comparing brodalumab with ustekinumab in psoriasis. *N. Engl. J. Med.* **373**, 1318–1328 (2015).
23. Griffiths, C. E. M. *et al.* Comparison of ixekizumab with etanercept or placebo in moderate-to-severe psoriasis (UNCOVER-2 and UNCOVER-3): Results from two phase 3 randomised trials. *The Lancet* **386**, 541–551 (2015).
24. Miossec, P. & Kolls, J. K. Targeting IL-17 and T H 17 cells in chronic inflammation. *Nat. Rev. Drug Discov.* **11**, 763–776 (2012).
25. Pandya, V. B., Kumar, S., Sachchidanand, Sharma, R. & Desai, R. C. Combating Autoimmune Diseases with Retinoic Acid Receptor-Related Orphan Receptor-γ (RORγ or RORc) Inhibitors: Hits and Misses. *J. Med. Chem.* **61**, 10976–10995 (2018).
26. Kumar, N. *et al.* The Benzenesulfoamide T0901317 [N-(2,2,2-Trifluoroethyl)-N-[4-[2,2,2-trifluoro-1-hydroxy-1-(trifluoromethyl)ethyl]phenyl]-benzenesulfonamide] Is a Novel Retinoic Acid Receptor-Related Orphan Receptor-α/γ Inverse Agonist. *Mol. Pharmacol.* **77**, 228–236 (2010).
27. Chaudhari, S. S., Thomas, A., Dhone, S. V., Khairatkar-Joshi, N. & Bajpai, M. Bicyclic Heterocyclic Compounds as ROR gamma Modulators. (2015).
28. Fauber, B. P. *et al.* Discovery of imidazo[1,5-a]pyridines and -pyrimidines as potent and selective RORc inverse agonists. *Bioorg. Med. Chem. Lett.* **25**, 2907–2912 (2015).
29. Ouvry, G. *et al.* Discovery of phenoxyindazoles and phenylthioindazoles as RORγ inverse agonists. *Bioorg. Med. Chem. Lett.* **26**, 5802–5808 (2016).
30. Meijer, F. *et al.* Ligand-Based Design of Allosteric Retinoic Acid Receptor-Related Orphan Receptor γt (RORγt) Inverse Agonists. *J. Med. Chem.* acs.jmedchem.9b01372-acs.jmedchem.9b01372 (2019) doi:10.1021/acs.jmedchem.9b01372.
31. Fujita-Sato, S. *et al.* Structural basis of digoxin that antagonizes RORgamma t receptor activity and suppresses Th17 cell differentiation and interleukin (IL)-17 production. *J. Biol. Chem.* **286**, 31409–31417 (2011).
32. de Wit, J. *et al.* RORγt inhibitors suppress TH17 responses in inflammatory arthritis and inflammatory bowel disease. *J. Allergy Clin. Immunol.* **137**, 960–963 (2016).
33. Holm, L. & Rosenström, P. Dali server: conservation mapping in 3D. *Nucleic Acids Res.* **38**, W545–W549 (2010).

34. Jin, L. *et al.* Structural Basis for Hydroxycholesterols as Natural Ligands of Orphan Nuclear Receptor RORγ. *Mol. Endocrinol.* **24**, 923–929 (2010).
35. Katoh, K., Rozewicki, J. & Yamada, K. D. MAFFT online service: multiple sequence alignment, interactive sequence choice and visualization. *Brief. Bioinform.* **20**, 1160–1166 (2019).
36. Letunic, I. & Bork, P. Interactive Tree Of Life (iTOL) v4: recent updates and new developments. *Nucleic Acids Res.* **47**, W256–W259 (2019).
37. de Vries, R. M. J. M., Meijer, F. A., Doveston, R. G. & Brunsveld, L. Elucidation of an allosteric mode-of-action for a thienopyrazole RORγt inverse agonist. *ChemMedChem* (2020) doi:10.1002/cmdc.202000044.
38. Nolte, R. T. *et al.* Ligand binding and co-activator assembly of the peroxisome proliferator-activated receptor-gamma. *Nature* **395**, 137–143 (1998).
39. Li, X. *et al.* Structural studies unravel the active conformation of apo RORγt nuclear receptor and a common inverse agonism of two diverse classes of RORγt inhibitors. *J. Biol. Chem.* **292**, 11618–11630 (2017).
40. Sun, N. *et al.* Molecular Mechanism of Action of RORγt Agonists and Inverse Agonists: Insights from Molecular Dynamics Simulation. *Molecules* **23**, 3181–3181 (2018).
41. Yuan, C. *et al.* Molecular dynamics simulations on RORγt: insights into its functional agonism and inverse agonism. *Acta Pharmacol. Sin.* **40**, 1480–1489 (2019).

Chapter 3

Engineering an Allosteric Pocket in the Retinoic Acid Receptor-Related Orphan Receptors α and β

Abstract

The retinoic acid receptor related orphan receptor family consists of three members, RORα, RORβ and RORγ. RORγ(t) has been studied extensively as a target protein for drug development related to oncology and immunology. The other RORs, however, have been studied with a more limited set of molecular tool compounds available to investigate the function of or modulate these receptors. Recently, an allosteric pocket was discovered in the C-terminal region of the LBD of RORγt. This pocket presents an alternative method to target this receptor using inverse agonists. The individual members of the ROR family are closely related especially in their LBD domains. This raises the question whether an allosteric pocket similar to the one in RORγ might be present or possible to form in either of the other RORs. In this chapter, the possibility for RORα and RORβ to form an allosteric pocket, similar to the one found in RORγ, is investigated using mutagenesis and biochemical studies. Both bottom-up, going from specific to general, and top-down, moving from general to specific, approaches are used to systematically increase the similarity of the allosteric pocket region to RORγ. However, even 28 identical residues at the C-terminal end of the LBD of RORα were insufficient to induce allosteric pocket formation. These observations underline the uniqueness of the allosteric pocket for RORγ and the selectivity for RORγ that can be reached when targeting this pocket.

Introduction

The retinoic acid receptor related orphan receptor family consists of three members, RORα, RORβ and RORγ. RORγ(t) has been studied extensively as a target protein for drug development related to oncology and immunology. The other RORs, however, have been studied with a more limited set of molecular tool compounds available to investigate the function of or modulate these receptors.

RORα, together with RORγt, is responsible for T_H17 differentiation: deficiency of one of these receptors leads to reduced IL-17 expression while double deficiencies globally impairs T_H17 generation.[1] While most drug discovery efforts have been made towards RORγt inverse agonists, RORα targeting compounds might be useful as well in as therapeutic entry for inflammation or autoimmunity.[2–4] One motivation for RORα inhibition over RORγt would be that RORα inhibition does not carry the associated risks of thymic apoptosis that RORγt inverse agonists do have.[5] Besides its role in immune responses, RORα also has an important cardioprotective function.[6–8] The exact mechanism underlying this function still needs to be determined, but it seems that the role of RORα in regulating mitochondrial quality might be a part of this process.[9] RORα is sometimes described as a melatonin receptor, however it is debated if melatonin is a true ligand for RORα or that they are solely linked through alternative mechanisms.[7,10,11] Melatonin can regulate RORα indirectly via modulating the transcription or translation of RORα by binding to other receptors[12], altering RORα cofactor binding by inducing coactivator deacetylation[13], or by directly regulating REV-ERB which competes for the same recognition site as the RORs.[14] The competition between RORα and REV-ERBα is furthermore important for the maintenance of circadian clock function.[15–18] Most research on the functionalities of RORα is currently performed using “staggerer” mice which express a truncated and nonfunctional RORα.[19,20] Although a lot of information is gained using this approach, staggerer mice have impaired locomotor activity affecting their mobility and feeding behaviors, causing a search for alternative models.[21] Instead of using overexpression or knock-out, the use of specific and high affinity ligands could help gain information about the functionalities of RORα in different tissues.

The earlier research on localization and expression patterns of RORβ indicated the presence of this receptor in the central nervous system (CNS) and its importance in vision and the circadian rhythm.[22,23] In retinal cone photoreceptors, RORβ activates the opsin gene with short wavelength sensitivity, especially in synergy with the

retinal cone-rod homeobox factor.[24] Furthermore, RORβ knock-out replaces rods by primitive, nonfunctional cones, indicating RORβ might be crucial to commit photoreceptor precursors to rod differentiation.[25,26] In addition to influencing photoreceptor differentiation, RORβ also mediates differentiation of amacrine and horizontal interneurons that integrate visual information.[27] Together, this means the receptor plays an important role in both dim- and daylight vision and the transmission of this signal to the brain. Interestingly, RORβ knock-out does have some positive influences on emotional behavioral characteristics.[28] Mice lacking RORβ are less prone to anxiety-related and depression-like behaviors, indicating RORβ inhibition might be beneficial in some mental conditions including bi-polar disorder.[28,29] Furthermore, RORβ can regulate osteogenesis and may be targeted for age-associated bone loss.[30,31]

Recently, an allosteric pocket was discovered in the C-terminal region of the LBD of RORγt.[32] This pocket presents an alternative method to target this receptor using inverse agonists. The individual members of the ROR family are closely related (49.5 respectively 48.1% identical to RORγ for RORα and RORβ) especially in their LBD domains (53.6 respectively 50.6% identical to RORγ) (Figure 1).[33] This raises the question whether an allosteric pocket similar to the one in RORγ might be present or possible to form in either of the other RORs. Inhibiting RORα or RORβ using such a pocket could be useful to study the functions of these constitutively active receptors as well as provide starting points for drugs to aid in autoimmunity or mental health.

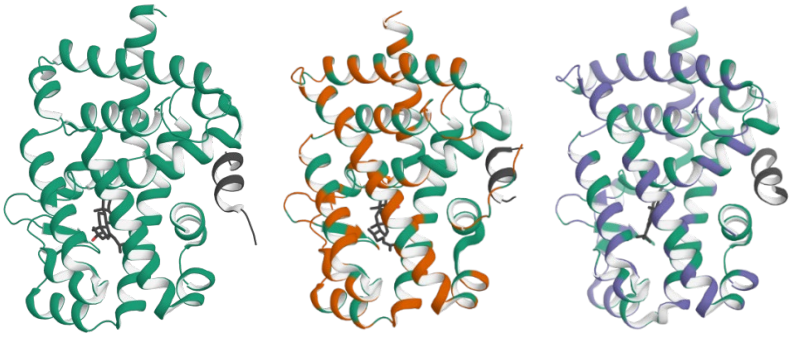

Figure 1 | Similarity between the members of the ROR family. For ease of comparison, all receptors are shown in their agonistic state. Compounds and coactivator peptides are displayed in gray. (*A*) RORγ LBD (green) bound to 20α-hydroxycholesterol (PDB: 3KYT). (*B*) RORα LBD (orange) bound to cholesterol, residues identical to RORγ are displayed green (PDB: 1N83). (*C*) RORβ LBD (purple) bound to all-trans retinoic acid, residues identical to RORγ are displayed green (PDB: 1NQ7).

In this chapter, the possibility for RORα and RORβ to form an allosteric pocket, similar to the one found in RORγ, is investigated using mutagenesis and biochemical studies. Both bottom-up, going from specific to general, and top-down, moving from general to specific, approaches are used to systematically increase the similarity of the allosteric pocket region to RORγ. However, even 28 identical residues at the C-terminal end of the LBD of RORα were insufficient to induce allosteric pocket formation. These observations underline the uniqueness of the allosteric pocket for RORγ and the selectivity for RORγ that can be reached when targeting this pocket.

Results and Discussion

Similarity of RORβ to RORγ is increased using a bottom-up approach

The goal of this chapter is to try to enforce the formation of an allosteric pocket in RORα and RORβ. For RORβ a bottom-up approach towards increasing the similarity to RORγ was explored (Figure 2, Table 1). This entails that residues of interest were cherry-picked based on rational investigations of the pocket. To identify the residues that might be important for allosteric pocket formation, the allosteric pocket of RORγ was studied in detail and compared to residues at the same location in RORβ. Scheepstra *et al.* (2015) present a two-dimensional plot showing the interactions between MRL-871 and the surrounding amino acids.[32] Of the amino acids shown in this image, only two, located in the H11', are different between RORγ and RORβ. In RORγ two alanines are present at the end of H11', just where flexibility might be important to make the close turn to H12. RORβ holds a threonine and a leucine at these positions of which the side chains might collide with the surrounding helices, or in the case of threonine disrupt the hydrophobic character of this part of the pocket. Based on this, the first mutant was designed to have these residues mutated to alanines (T440A, L441A), using site-directed mutagenesis, to imitate the H11' of RORγ.

The search area was extended to also consider residues within a larger distance from the compound. This way, two additional interesting amino acids were observed. Within the allosteric pocket of RORγ Ile-492 is located at the bottom with its sidechain directed into a hydrophobic area relatively close to the substituted phenyl ring of MRL-871. RORβ holds a glutamic acid residue at this position which might generate to much negative charge in this area. Therefore, in the second mutant an E436I mutation is included. Additional to this, a second mutation is

included in this construct. In Chapter 2, the importance of the glutamine residue at the end of H11 became apparent.[34] RORβ holds a lysine at this position which will be mutated to a glutamine (K431Q) in an attempt to create an allosteric pocket similar to RORγ. The third and final RORβ mutant, combines the previously mentioned mutations. In addition to this, one final residue, located at the top of the presumed allosteric pocket, is mutated to its RORγ equivalent. In RORγ an alanine is present here which corresponds with a cysteine in RORβ. To increase the similarity a C299A point mutation is made. All other residues within a 5Å radius of

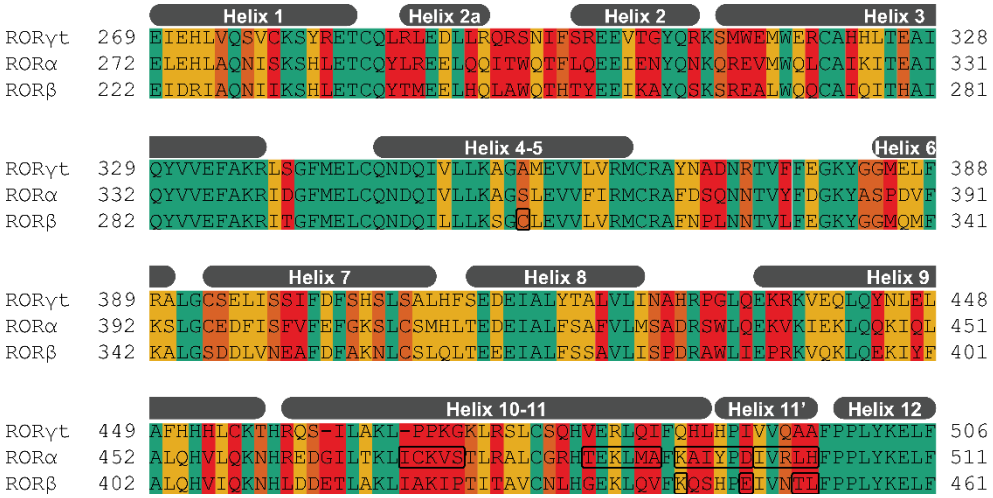

Figure 2 | Alignment of the protein sequences in the ROR LBD. *Top* RORγ, *middle* RORα and *bottom* RORβ. Residues highlighted in green are identical, yellow is highly similar, orange is moderately similar, and red is completely different from the RORγ equivalent.

Construct name	Mutations
RORα	none
RORα1	K492-D497 to RORγ
RORα2	K492-D497 + I498-H502 to RORγ
RORα3	K492-D497 + I498-H502 + I485-A490 to RORγ
RORα4	K492-D497 + I498-H502 + I485-A490 + I471-S475 to RORγ
RORβ	none
RORβ1	T440A, L441A
RORβ2	K431Q, E436I
RORβ3	C299A, K431Q, E436I, T440A, L441A

Table 1 | Overview of construct names with associated mutations

MRL-871 present similar chemical properties between RORβ and RORγ and are therefore assumed to be less important for allosteric pocket formation.

Similarity of RORα to RORγ is increased using a top-down approach

An alternative approach was chosen for the incorporation of the allosteric pocket of RORγ in RORα. Instead of rationally pinpointing crucial residues, the entire C-terminal section of RORγ is systematically inserted into RORα (Figure 2, Table 1). The first region that is entirely swapped stretches from the final residues of H11 to the first residues of H11'. Exchanging this series of amino acids at once to the corresponding ones of RORγ is done using the protocol of Liu and Naismith (2008).[35] The glutamine found to be crucial for allosteric pocket formation in RORγ is located in this region, being the reason for starting with mutating this site.[34] The second mutant adds the rest of H11' of RORγ to the construct. In the native construct, RORα has larger residues in this stretch than RORγ which could inhibit proper folding or point into the pocket inhibiting compound binding. The third mutant contains the same mutations as the first two, but also incorporates an additional section of H11. The residues in this stretch are less different between the two ROR isoforms, but nevertheless could play an unexpected role in allosteric pocket formation. The fourth and final mutant also alters the region in-between H10 and H11. While RORα and RORβ have a long and connected H10-H11 region, RORγ has two directly adjacent prolines and one fewer residue resulting in a kink between H10 and H11. It is hypothesized that this kink could make it possible to create a bend, needed for allosteric pocket formation.

Expression and purification of RORα needed optimization because of insolubility

Expression of both RORα and RORβ was first attempted using the same protocol normally used for RORγt. For RORβ, and all mutated constructs, this was successful and yielded large quantities of pure protein. For RORα, however, additional optimization was necessary. When attempting expression in *E. Coli* without optimization, almost all the protein ended up insoluble in inclusion bodies. This phenomenon in known for this protein and has previously been solved by doing expression in insect cells or refolding the protein.[36,37] Instead of using different cells or cumbersome refolding, we opted to utilize solubility tags to increase RORα yield. For this purpose, the expression of RORα with an N-terminal small ubiquitin modifying protein (SUMO), maltose binding protein (MBP), Glutathione S-transferase (GST) or Fasciola hepatica 8 (Fh8) tag was tested. After extensive

optimization, successful purification was done with a construct containing a N-terminal MBP for solubility and a C-terminal strep tag for purification. In short, the RORα constructs are expressed in BL21(DE3) *E. coli* in terrific broth and bacterial lysis is done using a homogenizer (Figure S1). For the first round of purification, strep-tactin chromatography is used eliminating possible truncated protein. Next, during overnight dialysis both the strep tag and the MBP are cleaved off using thrombin. Nickel chromatography is then used to separate His-RORα from the MBP and strep tag leading to pure protein.

Folding and stability of the RORα and RORβ constructs is similar to RORγ

To assess the fold and stability of the RORα and RORβ constructs, their folding was investigated using circular dichroism (CD), and their melting temperature (T_m) was measured using either a CD thermal shift assay (TSA) or a version of the Bradford-based thermal shift assay (BraTSA, see Chapter 5 for more detail).

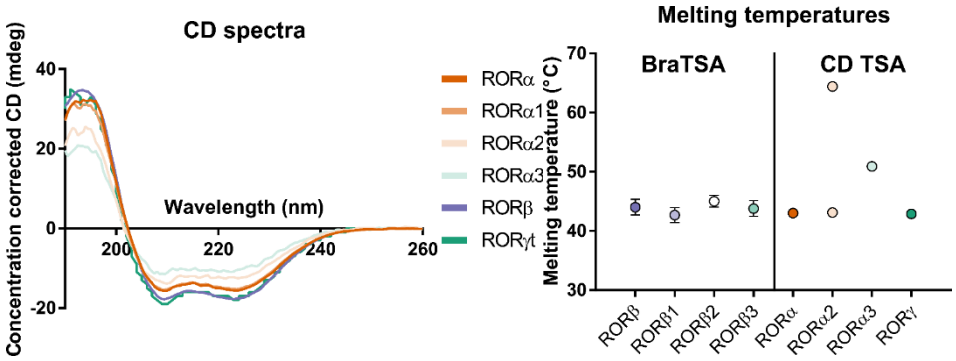

Figure 3 | Circular dichroism (CD) spectra and melting temperatures verify the integrity of the RORα and RORβ constructs. *Left*, CD spectra of a set of mutants. The signal is corrected for the amount of protein present in the sample. *Right*, melting temperatures of a set of mutants measured using either CD or a version of the Bradford-based thermal stability assay (BraTSA). For the melting temperatures measured using BraTSA mean ± S.D. from one experiment performed in triplicate is shown with the corresponding fit. For CD singlicate measurements are shown.

The CD spectra of all measured constructs display a similar pattern (Figure 3, *Left*). A peak around 193 nm is seen, followed by two negative bands at 208 and 222 nm. This pattern is typical for alpha-helices which are the main component of the ROR LBDs.[38] Therefore, this indicates that all measured constructs are correctly folded and are therefore expected to function appropriately.

To determine the T_m of NR LBDs, including RORγt, usually differential scanning fluorimetry (DSF) is used.[34] However, this was problematic for both RORα and RORβ. For all constructs, except the wildtype RORα, the initial fluorescence in this assay was very high, making it impossible to fit a melting curve (Figure S2). A reason for this could be that the outside of the protein is hydrophobic, causing dye binding and fluorescence. Therefore, it was decided to move to different techniques that do not depend on hydrophobic surfaces. For RORβ a preliminary version of the Bradford thermal stability assay (BraTSA) from chapter 5 was used. The RORβ constructs all have T_m values in the same ballpark. The wildtype construct has a T_m of 44.0 ± 1.3 °C. RORβ1 is slightly, but not significantly (*P*=0.3), destabilized to 42.7 ± 1.3 °C. RORβ2 melts at 45.0 ± 1.0 °C and RORβ3 at 43.8 ± 1.3 °C, both similar to the wildtype protein. This indicates that the mutations do not majorly affect the integrity of these proteins. For RORα CD was used to determine the T_m. This was done by monitoring the characteristic peak at 222 nm over a range of temperatures. Figure 3 shows that RORα has a similar T_m as RORγ (43.0 respectively 42.9 °C). Because this assay requires a lot of sample, not all mutants could be measured. RORα2 interestingly shows two clear transitions (Figure S3) meaning two distinct T_m values were fitted (43.1 and 64.4 °C). This seems to indicate that there may be two populations present for this mutant. RORα3 presents an elevated T_m of 50.9 using this assay. This could mean that the applied mutations cause stabilization, but it could also be an artifact caused by the lower protein concentration used in this sample compared to the other constructs (Figure S3).

Cofactor binding confirms the similarity increase of the mutants to RORγ

The integrity of the constructs is now confirmed, so the next step is to check if the constructs have affinity for coactivators. For this, two assay formats, fluorescence anisotropy (FA) and homogeneous time-resolved FRET (HTRF), are used (Figure 4).

For FA assays with RORγ, an SRC1b2 peptide is used often. Therefore, this peptide was tested against the RORα and RORβ constructs as well. RORα has a slightly higher affinity to the SRC1b2 peptide than RORγt (224 ± 36 nM respectively 515 ± 66 nM) while the affinity of RORα2 lies in between these constructs (379 ± 37 nM). This could be because the similarity in the cofactor binding region of RORα is altered towards RORγ, leading to behavior that has increased resemblance to RORγ. For the RORβ constructs this effect is even clearer. The wildtype proteins have the relatively highest (13.4 ± 1.1 μM for RORβ) and lowest (480 ± 285 μM for RORγ) affinities, while the mutants stepwise decrease their affinity with increasing

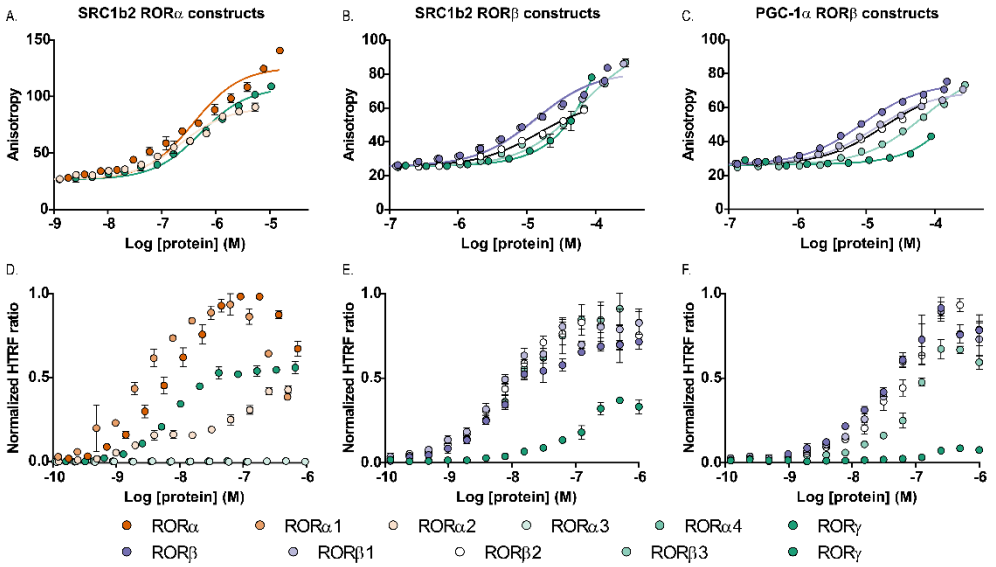

Figure 4 | Fluorescence anisotropy (FA) and homogeneous time-resolved FRET (HTRF) protein binding curves verify cofactor binding of the RORα and RORβ constructs. (*A-C*) FA cofactor interaction assay where protein is titrated to either SRC1b2 (*A, B*) or PGC-1α peptide (*C*). (*D-F*) HTRF assay where protein is titrated to either SRC1b2 (*D, E*) or PGC-1α peptide (*F*).

similarity to RORγ (13.8 ± 1.1 µM, 14.7 ± 2.4 µM and 61.9 µM for RORβ1, RORβ2 and RORβ3 respectively). PGC-1α is another cofactor that binds a lot of NRs. However, because of its low affinity to RORγ it is not used a lot in our lab. The RORβ constructs were titrated to this cofactor, leading to a very clear pattern. Wildtype RORβ binds with a K_d of 8.8 ± 0.5 µM, RORβ1 with 13.7 ± 0.9 µM, RORβ2 with 17.9 ± 1.8, and RORβ3 with 68.4 ±5.3 µM. RORγ binds too weak to quantify but has an even lower affinity. This is a significant reduction in binding affinity to PGC-1α with each additional mutation, illustrating very clearly that the mutants imitate RORγ behavior.

HTRF is less suitable to quantify the affinity between protein and cofactor, but can be used as an orthogonal technique to look at the interaction. Additionally, protein titrations give an indication about the usability of this assay for compound titrations. As with FP, in HTRF RORα shows a left-shifted binding curve compared to RORγ when titration protein towards SRC1b2 peptide. Because this assay uses lower protein concentrations, RORα1, RORα3 and RORα4 could be tested in this assay as well. Interestingly, RORα1 seems to bind SRC1b2 even stronger than the wildtype protein. RORα2 shows interesting behavior where at low concentrations

a similar curve to RORγt is seen, but upon increasing the concentration a plateau is seen after which a second binding event seems to take place. This effect was consistent upon several measurements and may confirm the hypothesis, indicated by the two melting temperatures (Figure 3), that two populations of this mutant are present. RORα3 and RORα4 seem unable to bind SRC1b2 under the provided conditions. This could mean these mutations are too disruptive to lead to a functioning protein. For RORβ, the SRC1b2 affinity seems barely effected by the mutations since the curves of all constructs roughly overlap. There is, however, a large difference between the affinity of the RORβ constructs and RORγt towards SRC1b2 where RORβ binds a lot stronger in this assay. For PGC-1α a more gradual change can be seen again where upon increasing similarity to RORγ the affinity decreases indicating the mutated residues are important in PGC-1α cofactor binding.

In conclusion, except for RORα2, 3 and 4, all mutants show cofactor binding behavior similar to, or in between, wildtype RORα, RORβ or RORγ, indicating proper functioning. RORα2 might exist in two populations leading to dual binding curves and melting temperatures. RORα3 and RORα4 seem too disruptively mutated to function.

Allosteric pocket formation

Proper stability, folding and cofactor interaction is confirmed for most constructs. This means the affinity of these proteins towards RORγt allosteric inverse agonists can be tested. A selection of inverse agonists with varying cores and substituents was chosen to increase the chance that one of these compounds would induce allosteric pocket formation in either RORα or RORβ (Figure 5).

For RORα, two variants of the HTRF assay were used to assess binding of allosteric compounds. In the classical set-up, ROR LBD and SRC1b2 peptide are present at fixed concentrations while compound is titrated (Figure 6, *Top*). RORγt has nanomolar affinity for MRL-871 (2.74 ± 0.15 nM), FM26 (47.0 ± 4.1 nM) and Glenmark's compound 13 (CPD13) (351 ± 27 nM). Wildtype RORα starts at a higher HTRF ratio because of its stronger affinity (*Figure 4D*). Protein cofactor interaction remains unaltered up till 10 μM and is only affected at very high concentrations of all compounds. This could mean that there is some binding at these concentrations, but it could be an artifact caused by the high amount of acid compound. The tested mutants bind too weakly to show a decrease in signal. In addition to the classical

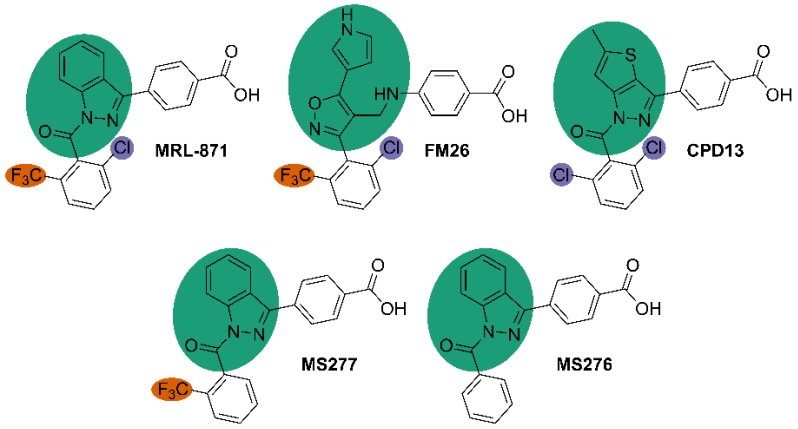

Figure 5 | RORγ allosteric inverse agonists. The core is highlighted in *green* while the substituents are indicated in *orange* (CF_3) and *purple* (Cl).

HTRF assay, an allosteric probe is used. This probe is based on MRL-871, but has a fluorescent label covalently attached. When this probe is titrated and binds, this leads to increased emission (Figure 6, *Bottom*). Because the probe has the attached fluorophore, the affinity is worse than MRL-871 as can be seen for the relatively late increase in HTRF ratio when RORγ is present. For the RORα constructs no increase in HTRF ratio is seen upon AlexaFluor-MRL titration. Only upon zooming in, it can be seen that there is a slight increase in HTRF ratio at very high compound concentrations for the mutants. Wildtype RORα stays at the baseline while RORα1 shows a small but clear increase. RORα2 does not seem to increase this interaction compared with RORα1, indicating that the end of H11' might be less important than be beginning. RORα3 behaves similar to RORα1 in this assay and RORα4 has the lowest increase of the mutants. This could mean that the kink in H10, that is artificially created in RORα4, is not crucial for allosteric pocket formation.

For RORβ a larger selection of compounds is used for compound titrations. MRL-871, the compound with the highest affinity for RORγ (8.49 ± 0.57 nM), only reduces the signal for the RORβ constructs very minorly at the highest measured concentration and does not enable fitting the data (IC_{50} > 100 µM). For FM26, a compound with an isoxazole core, the difference between RORγ and the RORβ constructs is somewhat smaller. RORγ binds this compound with an IC_{50} of 304 ± 33 nM. The RORβ constructs all bind with similar affinities: 54.9 ± 2.3 µM for the wildtype, 52.3 ± 2.5 µM for RORβ1, 31.3 ± 1.9 µM for RORβ2 and 63.9 ± 3.2 µM for RORβ3. This indicates that the mutations have little effect on binding of these

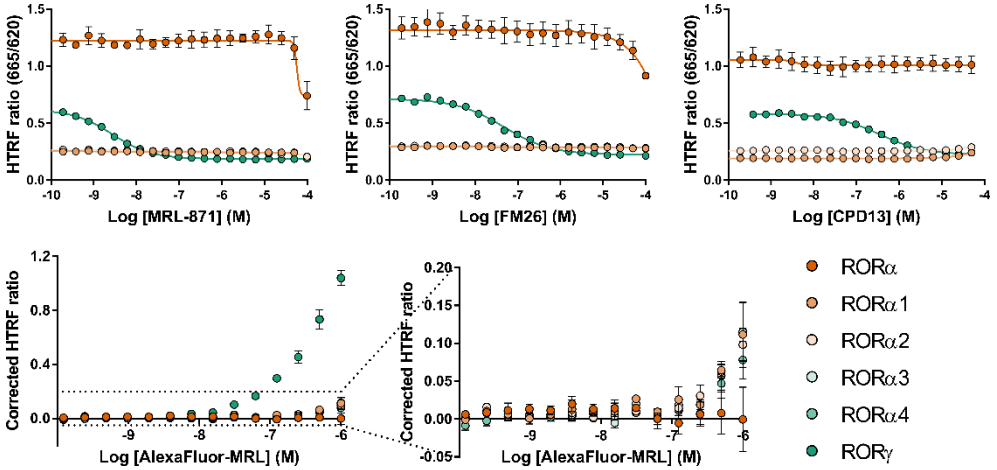

Figure 6 | HTRF curves for RORα constructs show no to low affinity for RORγ allosteric inverse agonists. *Top*, dose-response curves from the HTRF co-activator recruitment assay, using various RORγt inverse agonists, at fixed protein (25 nM) and SRC1b2 (100 nM) concentrations. Mean ± S.D. of one experiment performed in triplicate is shown. *Bottom*, AlexaFluor-MRL titration to fixed (25 nM) concentration of protein. The signal was corrected for the amount of fluorophore by subtracting data from a AlexaFluor-MRL titration in absence of protein. Mean ± S.D. of one experiment performed in triplicate is shown.

compounds except maybe the K431Q and E436I mutations of RORβ2. The affinity of RORγt for CPD13 is a little lower than the previous compounds (471 ± 68 nM). The RORβ constructs have a relatively similar affinity to this compound as to FM26 (71.2 ± 7.3 µM, 89.0 ± 9.4 µM, 65.9 ± 7.3 µM and 66.5 ± 10.0 µM for respectively wildtype RORβ, RORβ1, RORβ2 and RORβ3). Again RORβ2 has a slightly increased affinity compared to wildtype RORβ while RORβ2 does not lead to increased affinity underlining the importance of K431Q or E436I. In addition to the three compounds also used for RORα, two additional compounds are tested on the RORβ constructs. These constructs share the same core as MRL-871, but have less substituents on the benzene ring. Removal of these substituents leads to a strong and additive decrease in RORγt affinity for MS277 (145 ± 9 nM) and MS276 (12.7 ± 4.1 µM) compared to MRL-871. For the RORβ constructs, this decrease is not present and the compounds with less substituents even seem to bind a little better than MRL-871. MS277 binds with an IC_{50} of 100 ± 4 µM to wildtype RORβ, 89.5 ± 3.0 µM to RORβ1, 75.4 ± 2.6 µM to RORβ2 and 58.4 ± 1.6 µM to RORβ3. And MS276 binds with 113 ± 19 µM, 87.6 ± 17.7 µM, 69.4 ± 11.0 µM and 78.5 ± 13.9 µM to wildtype

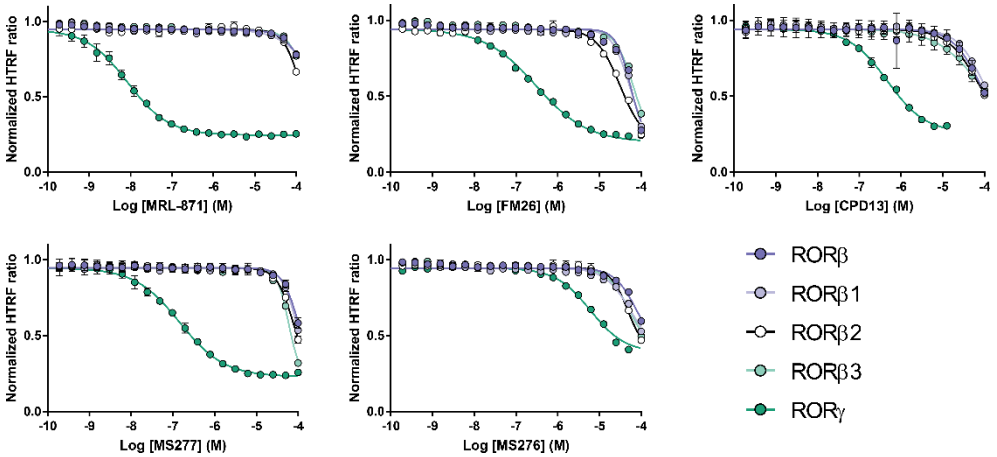

Figure 7 | HTRF curves for RORβ constructs show low affinity for RORγ allosteric inverse agonists. Dose-response curves from the HTRF co-activator recruitment assay, using various RORγt inverse agonists, at fixed protein (20 nM) and SRC1b2 (100 nM) concentrations. Mean ± S.D. of one experiment performed in triplicate is shown.

RORβ, RORβ1, RORβ2 and RORβ3 respectively. For MS277, the other of affinity to RORβ and its mutants bind is directly proportional to the increase in similarity to RORγ. For MS276 the same holds true, except that RORβ3 does not yield additional affinity compared to the other constructs. However, precaution needs to be taken with these conclusions since the differences are very small and might not be significant. The AlexaFluor-MRL probe is not tested for the RORβ constructs since the affinity for MRL-871 is already confirmed to be very low.

Conclusions

The RORα and RORβ constructs made in this chapter, did not bind existing RORγ inverse agonists with high affinity. This strongly underlines the uniqueness of the allosteric pocket of RORγt and the possibility to target this pocket therapeutically with high selectivity. However, in the limited structure activity relationship (SAR) study done in this chapter it appears that for certain compounds the relative selectivity for RORγt over RORα and RORβ is smaller. In our research this is especially true for compounds with fewer substituents on the benzene ring. For this reason, we would recommend to always check for the affinity of new compounds towards RORα and RORβ. This is a test that is easy to implement and is currently not routinely done.

Although the selectivity of allosteric inverse agonists for RORγt is very promising, it would still be interesting to find a pocket like this in RORα or RORβ as well. Based on our study it would be worthwhile testing or developing smaller compounds for these receptors. For instance, a compound based on FM26, but lacking the substituents on the benzene ring could be interesting to study. Furthermore, both bottom-up and top-down approaches had their own advantages and limitations. The small alterations done on RORβ appeared to have only small effects on the protein and pocket formation. By making only rational changes, less obvious important residues could be overlooked. The more drastic changes on RORα, however, did not only change its allosteric pocket formation, but also its expression efficiency and stability. This made it hard to study these mutants in all assays. For the future, a combination of these approaches could be wise. Instead of the additive mutations now done on RORα, I would recommend changing one region at a time. If changing a region has an effect, the mutations could be reversed systematically to find out which residues are responsible for this change in behavior. This way interesting residues can be pin-pointed without the need for rational design or the risks associated with changing large regions of a protein all at once.

In conclusion, the allosteric pocket present in RORγt seems to be unique for this NR, especially when using the compounds currently available. A more sophisticated approach would be advised to investigate the allosteric region of RORα and RORβ in the future.

Experimental section

Site-directed mutagenesis

Point mutations RORβ

Point mutations (C299A, K431Q, E436I, T440A and L441A) were introduced using the QuikChange Lightning Multi Site-Directed Mutagenesis Kit (Agilent) in accordance with the protocols described in the kit manual. The parental DNA for this was a pET15b vector containing the RORβ LBD (residues 207-451) with an N-terminal His6-tag (Table S#). For RORβ3, the mutated construct of RORβ2 was used as the basis instead. Single primers designed to hybridize with the parental DNA containing 1-3 mismatches were utilized for these mutations.

Swap mutations RORα

The primers for the swap constructs, (K492-D497, I498-H502, I485-A490 and I471-S475), were prepared via the method described by Liu and Naismith.[35] In short, primers with overlap on the 5' end (pp) were designed in such a way that the swap was in the pp region while the 3' ends (no) could hybridize to the DNA efficiently. For the PCR reaction, 0.2 ng/µL parental DNA was combined with 1 µM of both primers and 1X Phusion polymerase in HF buffer (Thermo Scientific). The parental DNA for this was a pET15b vector containing the RORα LBD (residues 272-523) with an N-terminal Maltose binding protein and His6-tag and a C-terminal Strep tag (Table S#). For RORα2-RORα4 the mutated constructs RORα1-RORα3 were used as parental DNA. Each reaction started with denaturation (1 min, 98 °C) followed by 18 amplification steps. Each of these steps started with denaturation (10 s, 98 °C), followed by annealing (1 min, T_m no -5 °C) and extension (2:30 min, 72 °C). The method ended with a final annealing (1 min, T_m pp -5 °C) and extension (30 min, 72 °C) step.

Transformation

For all mutagenesis reactions, the parental DNA was digested using DpnI followed by transformation into XL10-Gold Ultracompetent Cells (Agilent) by heat shock. Small cultures were initiated, using single colonies in 5 mL LB medium supplemented with ampicillin (100 µg/mL), overnight at 37 °C 250 rpm. DNA was isolated using the QIAprep® Spin Miniprep Kit (Qiagen) in accordance with the supplied protocol. The mutations were confirmed by sequencing using T7 promoter and T7 terminator primers (BaseClear).

Expression and Purification of the RORβ constructs

A pET15b vector containing the (mutated) RORβ LBD (residues 207-451) with an N-terminal His6-tag was transformed into BL21(DE3) competent Escheria Coli (Novagen) by heat shock. A pre-culture was initiated, using a single colony in 8 mL LB medium supplemented with ampicillin (100 µg/mL), overnight at 37 °C 250 rpm. This culture was transferred to TB medium with ampicillin (100 µg/mL), $MgSO_4$ (0.5 mM), and antifoam (0.05 %), and incubated at 37 °C, 160 rpm until OD600 nm = 1.0 was reached. Isopropyl β-D-thiogalactoside (IPTG) (0.5 mM) was then added to induce expression, and the culture was incubated at 15 °C 150 rpm overnight. The bacteria were harvested using centrifugation (10,000 *g, 4 °C, 10 m) and resuspended in lysis buffer (30 mM Tris (pH 7.0), 300 mM NaCl, 20 mM imidazole, 10 v/v% glycerol, 1mM tris(2-carboxyethyl)phosphine (TCEP)). The cells were lysed using a homogenizer (Avestin Emulsiflex C3) at 15,000 psi with additional phenylmethylsulfonyl fluoride (PMSF) (1:1000 v/v) and benzonase (1:10,000 v/v). The cell lysate was cleared by centrifugation (40,000 *g, 4 °C, 30 m) and purified via Ni^{2+} affinity column chromatography (QIAGEN, nickel-nitrilotriacetic acid (Ni-NTA) Superflow Cartridge). Elution fractions containing the protein of interest were afterwards dialyzed against a storage buffer (15 mM Tris (pH 7.0), 150 mM NaCl, 10 v/v% glycerol, 1 mM TCEP) overnight

and, subsequently, stored at -80 °C until usage. Molecular weight and purity were assessed using Quadrupole Time-of-Flight LC/MS and SDS-page.

Expression and Purification of the RORα constructs

A pET15b vector containing the (mutated) RORα LBD (residues 272-523) with an N-terminal Maltose binding protein and His6-tag and a C-terminal Strep tag (Table S#) was transformed into BL21(DE3) competent Escheria Coli (Novagen) by heat shock. A pre-culture was initiated, using a single colony in 8 mL LB medium supplemented with ampicillin (100 µg/mL), overnight at 37 °C 250 rpm. This culture was transferred to TB medium with ampicillin (100 µg/mL), $MgSO_4$ (0.5 mM), Glucose (0.2 wt%) and antifoam (0.05 %), and incubated at 37 °C, 150 rpm until OD_{600} nm = 1.0 was reached. Isopropyl β-D-thiogalactoside (IPTG) (0.5 mM) was then added to induce expression, and the culture was incubated at 18 °C 180 rpm overnight. The bacteria were harvested using centrifugation (10,000 *g, 4 °C, 10 m) and resuspended in lysis buffer (100 mM Tris (pH 8.0), 150 mM NaCl, 1mM EDTA). The cells were lysed using a homogenizer (Avestin Emulsiflex C3) at 15,000 psi after which the cell lysate was cleared by centrifugation (40,000 *g, 4 °C, 30 m). The first round of purification was done via Strep-Tactin chromatography where the supernatant was loaded onto a Strep-Tactin®XT Superflow® high capacity 5 mL cartridge. Elution was done using lysis buffer supplemented with 50 mM biotin. After this, the buffer was exchanged and the MBP and Strep tag were cleaved off using overnight dialysis (20 mM Tris (pH 8.0), 200 mM NaCl, 20 mM imidazole, 10% glycerol, 2.5 mM $CaCl_2$) where 1U thrombin/mg protein was added to the dialysis tubing. Subsequently the His-RORα LBD was purified via Ni^{2+} affinity column chromatography (QIAGEN, nickel-nitrilotriacetic acid (Ni-NTA) Superflow Cartridge). Elution fractions containing the protein of interest were afterwards dialyzed against a storage buffer (10 mM HEPES (pH 7.5), 150 mM NaCl) overnight and, subsequently, stored at -80 °C until usage. Molecular weight and purity were assessed using Quadrupole Time-of-Flight LC/MS and SDS-page.

Circular Dichroism

Buffer exchange (5 mM potassium phosphate (pH 7.4), 100 mM ammonium sulfate) was performed using MicroSpin™ G-25 columns and followed by centrifugation (12,500 *g, 4°C, 5 m). CD measurements were performed using a JASCO J-815. A UV quartz cuvette with a path length of 1 mm was filled with at least 90 µL of 0.10 mg/mL protein solution. CD, HT and Abs were measured from 260 to 180 nm at 4 °C with a data pitch of 0.5 nm, a standard sensitivity, D.I.T. of 2 s and 2.00 nm bandwidth at continuous scanning speed of 50 nm/min. 5 accumulations were made and measurements were baseline corrected.

For thermal denaturation, over a temperature ramp of 20-90°C at 0.6°C/min, CD, HT and Abs were measured at 208 and 222 nm, using a standard sensitivity, D.I.T. of 2 sec and 2.00

nm bandwidth. Data was analyzed using GraphPad Prism 7 software. Curves were fitted using a least squares fit for:

$$Y = Bottom + \frac{X^{Hillslope} * (Top - Bottom)}{X^{Hillslope} + EC_{50}{}^{Hillslope}}$$

Where $EC_{50} = T_M$.

DSF

See Chapter 2

Modified BraTSA using SDS page

3 µM protein in assay buffer (10 mM HEPES (pH 7.5), 150 mM NaCl) was aliquoted into 50 µL samples. The samples were subjected to a (38 -55 °C) range of temperatures in a C1000 Touch Thermo Cycler for 3 minutes followed by 25 °C for 3 minutes. 45µL of each sample was transferred to 1.5mL Eppendorf tubes and spinned at (15,000 *g, 4°C, 40 m) in a pre-cooled 5424R table-top microcentrifuge. 15µL of soluble protein fraction was obtained and mixed in a 1:1 ratio (v/v) with 2xSDS sample buffer solution (80mM Tris (pH 6.8), 2% SDS, 10% Glycerol, 0.0006% Bromophenol blue, 0.1M DTT, 0.05mg/mL BSA). Protein degradation was promoted using a 5 minute heating step at 95°C. 10µL of each denatured protein sample and 6µL Precision Plus TM All blue (or two color) Prestained Protein standards (10-250kDa) were added to a 15 well, 15µL, 4-20% Mini-PROTEAN® TGXTM Precast Protein gel. The gel was run at 150V for 55-65 minutes. SDS was washed away using dH2O for 30 minutes, the gel was stained using Bio-SafeTM Coomassie G250 stain (Bio-Rad) and de-stained in dH2O overnight. A gel image was made using the ImageQuant 350 of GE. Image analysis was performed using Image Studio Lite. Same sized rectangles were drawn around each protein band and signal intensity was calculated via the software using an average background correction of all borders with a 3 point band width. Protein intensities were divided by the BSA signal intensities of the same lane to correct for horizontal intensity variations in the gel or pipetting mistakes. Normalized intensities were plotted for the various temperatures and non-linear inhibition dose-response curves were plotted using the variable slope, four parameter algorithm of GraphPad:

$$Y = Bottom + \frac{X^{Hillslope} * (Top - Bottom)}{X^{Hillslope} + EC_{50}{}^{Hillslope}}$$

FP

See Chapter 2

HTRF

For the protein titrations assays were performed in 10 µL volumes in triplicate in buffer containing 150 mM NaCl, 10 mM HEPES, 5 mM DTT, 10 mM CHAPS, 2% DMSO and 0.1 m/v % BSA. 100 nM biotin labelled SRC1b2 coactivator peptide (Table S3), 733 pM Terbium-labelled anti-His antibody (Cisbio, 61HISTLB) and 41.6 nM respectively 25 nM D2-labelled streptavidin (Cisbio, 610SADLB) were used for the RORβ and RORα experiments. Proteins were titrated to this mixture in round bottom, non-binding, white, 384-well plates (Corning #4513). The plates were measured in an Infinite F500 plate reader (Tecan) (excitation = 340 nm; emission = 665 nm and 620 nm). HTRF ratio was determined by dividing the signal at 620 nm through that at 665 nm.

For the compound titrations see Chapter 2. For the RORα respectively RORβ constructs a protein concentration of 25 nM and 20 nM was used.

For the AlexaFluor-MRL titrations the compound titration protocol was followed, but biotin-SRC1b2 and streptavidin-d2 were excluded from the assay solution. Data was background corrected by subtracting the data where AlexaFluor-MRL was titrated in absence of protein.

Supplementary Information

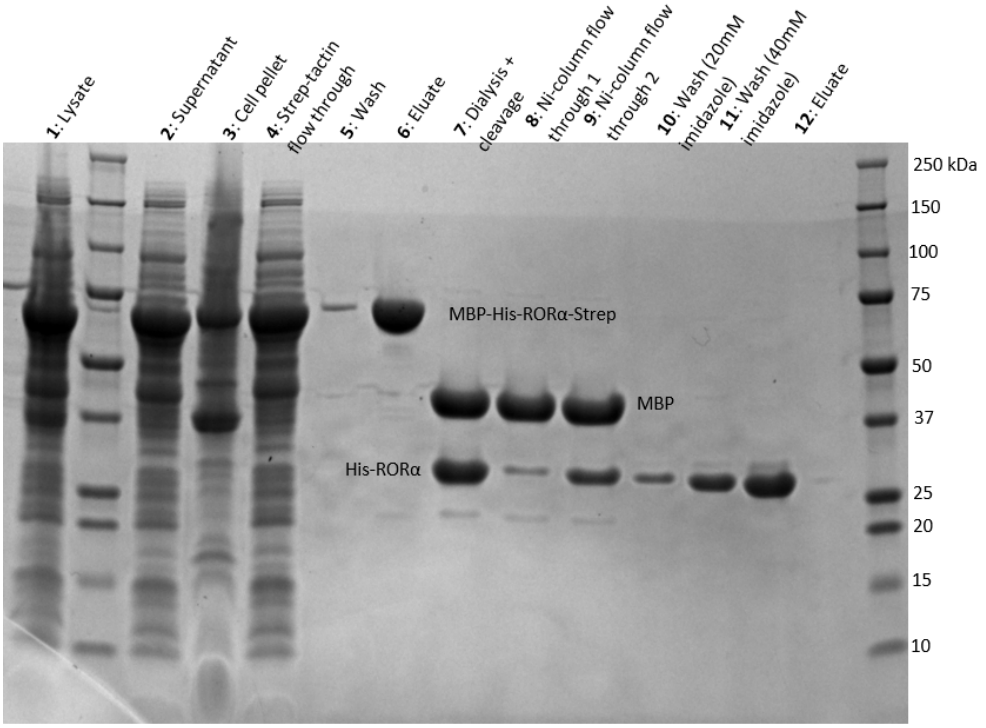

Figure S1 | SDS-page gel of the purification of the MBP-Thrombin-His-TEV-RORα-Thrombin-Strep construct. Lysate was separated into supernatant and cell pellet using high speed centrifugation. The eluate of the strep-tactin column yielded purified MBP-Thrombin-His-TEV-RORα-Thrombin-Strep. Dialyzation and cleavage of the thrombin sites leaded to cleaved MBP and His-TEV-RORα protein. These were successfully separated using Nickel chromatography leading to pure His-(TEV)-RORα constructs.

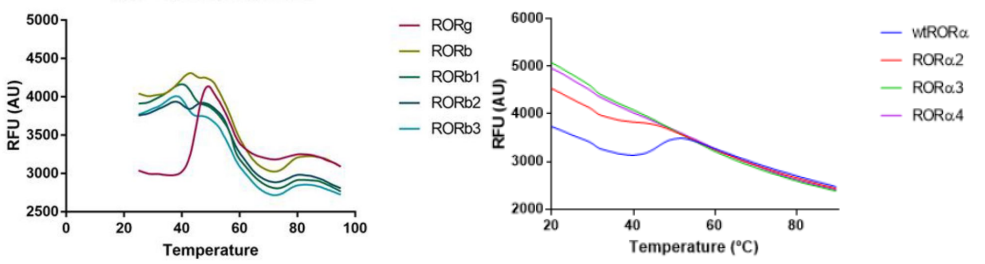

Figure S2 | RORα and RORβ constructs have high initial fluorescence in differential scanning fluorimetry (DSF). When attempting DSF on RORα and RORβ, all mutants and the RORβ wildtype protein have high initial fluorescence making it impossible to fit melting temperatures using this technique.

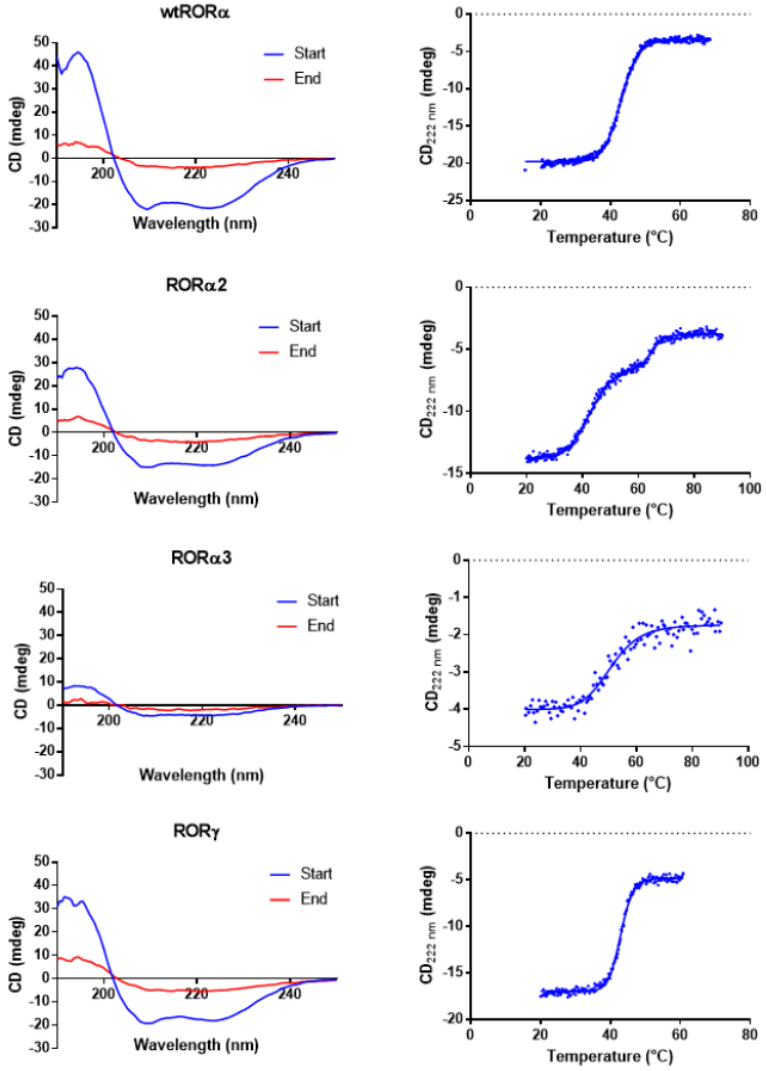

Figure S3 | Circular dichroism (CD) thermal stability experiments on RORα and RORγt. *Left*, full CD spectra before and after unfolding. *Right*, CD at 222 nm monitored over a range of temperatures enables fitting of unfolding curves.

Name	Sequence
His6-RORβ LBD	MGSS*HHHHHH*SSGLVPRGSHMITMTEIDRIAQNIIKSHLETCQ YTMEELHQLAWQTHTYEEIKAYQSKSREALWQQCAIQITHAIQ YVVEFAKRITGFMELCQNDQILLLKSG**C**LEVVLVRMCRAFNPL NNTVLFEGKYGGMQMFKALGSDDLVNEAFDFAKNLCSLQLTEE EIALFSSAVLISPDRAWLIEPRKVQKLQEKIYFALQHVIQKNH LDDETLAKLIAKIPTITAVCNLHGEKLQVF**K**QSHP**E**IVN**TL**FP PLYKELFN
MBP-His6-RORα-Strep LBD	MGKIEEGKLVIWINGDKGYNGLAEVGKKFEKDTGIKVTVEHPD KLEEKFPQVAATGDGPDIIFWAHDRFGGYAQSGLLAEITPDKA FQDKLYPFTWDAVRYNGKLIAYPIAVEALSLIYNKDLLPNPPK TWEEIPALDKELKAKGKSALMFNLQEPYFTWPLIAADGGYAFK YENGKYDIKDVGVDNAGAKAGLTFLVDLIKNKHMNADTDYSIA EAAFNKGETAMTINGPWAWSNIDTSKVNYGVTVLPTFKGQPSK PFVGVLSAGINAASPNKELAKEFLENYLLTDEGLEAVNKDKPL GAVALKSYEEELVKDPRIAATMENAQKGEIMPNIPQMSAFWYA VRTAVINAASGRQTVDEALKDAQTASGRQTVDEALKDAQTGGS GGS<u>LVPRGS</u>GSS*HHHHHH*SSG<u>ENLYFQG</u>GELEHLAQNISKSHL ETCQYLREELQQITWQTFLQEEIENYQNKQREVMWQLCAIKIT EAIQYVVEFAKRIDGFMELCQNDQIVLLKAGSLEVVFIRMCRA FDSQNNTVYFDGKYASPDVFKSLGCEDFISFVFEFGKSLCSMH LTEDEIALFSAFVLMSADRSWLQEKVKIEKLQQKIQLALQHVL QKNHREDGILTKL**ICKVS**TLRALCGRH**TEKLMA**F**KAIYPDIVR LH**FPPLYKELFTSEFEPAMQIDG<u>LVPRGS</u>GSAWSHPQFEK
FITC- SRC1b2	FITC-βA–SSLTERHKILHRLLQEGSPSD-NH2
Biotin- SRC1b2	Biotin-N-PSSHSSLTERHKILHRLLQEGSPSD-$CONH_2$
FITC-PGC-1α	FITC-EAEEPSLLKLLLAPANTQ-NH2
Biotin-PGC-1α	Biotin-GTPPPQEAEEPSLLKLLLAPANTQ-NH2

Supplementary table 1 | Sequences of protein and peptide used in this chapter. For the protein sequence the 6*His-tag is indicated in *italic*, cleavage sites are <u>underlined</u> and the sites that are targeted by the mutagenesis are **bold**.

Acknowledgments

Laureen de Bever and Twan Hopstaken performed the experimental work described in this chapter, for which they are gratefully acknowledged.

References

1. Yang, X. O. *et al.* T Helper 17 Lineage Differentiation Is Programmed by Orphan Nuclear Receptors RORα and RORγ. *Immunity* **28**, 29–39 (2008).
2. Park, J.-S. *et al.* Retinoic Acid Receptor-Related Receptor Alpha Ameliorates Autoimmune Arthritis via Inhibiting of Th17 Cells and Osteoclastogenesis. *Front. Immunol.* **10**, 2270 (2019).

3. Ho, C.-C. *et al.* Transcriptional Interactomic Inhibition of RORα Suppresses Th17-Related Inflammation. *J. Inflamm. Res.* **14**, 7091–7105 (2021).
4. Jetten, A. M., Beak, J. Y., Slominski, A. T. & Jensen, B. Retinoic Acid-Related Orphan Receptor (ROR) Inverse Agonists: Potential Therapeutic Strategies for Multiple Inflammatory Diseases? in *Nuclear Receptors: The Art and Science of Modulator Design and Discovery* (ed. Badr, M. Z.) 349–377 (Springer International Publishing, 2021). doi:10.1007/978-3-030-78315-0_14.
5. Wang, R. *et al.* Genetic and pharmacological inhibition of the nuclear receptor RORα regulates TH17 driven inflammatory disorders. *Nat. Commun.* **12**, 76 (2021).
6. He, B. *et al.* The nuclear melatonin receptor RORα is a novel endogenous defender against myocardial ischemia/reperfusion injury. *J. Pineal Res.* **60**, 313–326 (2016).
7. Xu, L. *et al.* Melatonin differentially regulates pathological and physiological cardiac hypertrophy: Crucial role of circadian nuclear receptor RORα signaling. *J. Pineal Res.* **67**, e12579 (2019).
8. Beak, J. Y. *et al.* The nuclear receptor RORα protects against angiotensin II-induced cardiac hypertrophy and heart failure. *Am. J. Physiol.-Heart Circ. Physiol.* **316**, H186–H200 (2019).
9. Beak, J. Y. *et al.* The nuclear receptor RORα preserves cardiomyocyte mitochondrial function by regulating caveolin-3-mediated mitophagy. *J. Biol. Chem.* **297**, (2021).
10. Zhao, Y. *et al.* Novel protective role of the circadian nuclear receptor retinoic acid-related orphan receptor-α in diabetic cardiomyopathy. *J. Pineal Res.* **62**, e12378 (2017).
11. Ma, H., Kang, J., Fan, W., He, H. & Huang, F. ROR: Nuclear Receptor for Melatonin or Not? *Molecules* **26**, 2693 (2021).
12. Han, D. *et al.* Activation of melatonin receptor 2 but not melatonin receptor 1 mediates melatonin-conferred cardioprotection against myocardial ischemia/reperfusion injury. *J. Pineal Res.* **67**, e12571 (2019).
13. Guo, P. *et al.* Melatonin Improves Mitochondrial Function by Promoting MT1/SIRT1/PGC-1 Alpha-Dependent Mitochondrial Biogenesis in Cadmium-Induced Hepatotoxicity In Vitro. *Toxicol. Sci.* **142**, 182–195 (2014).
14. Sánchez, D. I. *et al.* Melatonin modulates dysregulated circadian clocks in mice with diethylnitrosamine-induced hepatocellular carcinoma. *J. Pineal Res.* **65**, e12506 (2018).
15. Ueda, H. R. *et al.* A transcription factor response element for gene expression during circadian night. *Nature* **418**, 534–539 (2002).
16. Sato, T. K. *et al.* A Functional Genomics Strategy Reveals Rora as a Component of the Mammalian Circadian Clock. *Neuron* **43**, 527–537 (2004).
17. Akashi, M. & Takumi, T. The orphan nuclear receptor RORα regulates circadian transcription of the mammalian core-clock Bmal1. *Nat. Struct. Mol. Biol.* **12**, 441–448 (2005).
18. Solt, L. A., Kojetin, D. J. & Burris, T. P. The REV-ERBs and RORs: molecular links between circadian rhythms and lipid homeostasis. *Future Med. Chem.* **3**, 623–638 (2011).
19. Hamilton, B. A. *et al.* Disruption of the nuclear hormone receptor RORα in staggerer mice. *Nature* **379**, 736–739 (1996).

20. Dussault, I., Fawcett, D., Matthyssen, A., Bader, J.-A. & Giguère, V. Orphan nuclear receptor RORα-deficient mice display the cerebellar defects of staggerer. *Mech. Dev.* **70**, 147–153 (1998).
21. Billon, C., Sitaula, S. & Burris, T. P. Metabolic Characterization of a Novel RORα Knockout Mouse Model without Ataxia. *Front. Endocrinol.* **8**, 141 (2017).
22. Schaeren-Wierners, N., André, E., Kapfhammer, J. P. & Becker-André, M. The Expression Pattern of the Orphan Nuclear Receptor RORβ in the Developing and Adult Rat Nervous System Suggests a Role in the Processing of Sensory Information and in Circadian Rhythm. *Eur. J. Neurosci.* **9**, 2687–2701 (1997).
23. André, E. *et al.* Disruption of retinoid-related orphan receptor β changes circadian behavior, causes retinal degeneration and leads to vacillans phenotype in mice. *EMBO J.* **17**, 3867–3877 (1998).
24. Srinivas, M., Ng, L., Liu, H., Jia, L. & Forrest, D. Activation of the Blue Opsin Gene in Cone Photoreceptor Development by Retinoid-Related Orphan Receptor β. *Mol. Endocrinol.* **20**, 1728–1741 (2006).
25. Jia, L. *et al.* Retinoid-related orphan nuclear receptor RORβ is an early-acting factor in rod photoreceptor development. *Proc. Natl. Acad. Sci.* **106**, 17534–17539 (2009).
26. Fu, Y. *et al.* Feedback Induction of a Photoreceptor-specific Isoform of Retinoid-related Orphan Nuclear Receptor β by the Rod Transcription Factor NRL *. *J. Biol. Chem.* **289**, 32469–32480 (2014).
27. Liu, H. *et al.* An isoform of retinoid-related orphan receptor β directs differentiation of retinal amacrine and horizontal interneurons. *Nat. Commun.* **4**, 1813 (2013).
28. Masana, M. I., Sumaya, I. C., Becker-Andre, M. & Dubocovich, M. L. Behavioral characterization and modulation of circadian rhythms by light and melatonin in C3H/HeN mice homozygous for the RORβ knockout. *Am. J. Physiol.-Regul. Integr. Comp. Physiol.* **292**, R2357–R2367 (2007).
29. McGrath, C. L. *et al.* Evidence for genetic association of RORB with bipolar disorder. *BMC Psychiatry* **9**, 70 (2009).
30. Roforth, M. M., Liu, G., Khosla, S. & Monroe, D. G. Examination of nuclear receptor expression in osteoblasts reveals rorβ as an important regulator of osteogenesis. *J. Bone Miner. Res.* **27**, 891–901 (2012).
31. Roforth, M. M., Khosla, S. & Monroe, D. G. Identification of Rorβ targets in cultured osteoblasts and in human bone. *Biochem. Biophys. Res. Commun.* **440**, 768–773 (2013).
32. Scheepstra, M. *et al.* Identification of an allosteric binding site for RORγt inhibition. *Nat. Commun.* **6**, 8833–8833 (2015).
33. Altschul, S. F., Gish, W., Miller, W., Myers, E. W. & Lipman, D. J. Basic local alignment search tool. *J. Mol. Biol.* **215**, 403–410 (1990).
34. Leijten-van de Gevel, I. A. & Brunsveld, L. Delineation of the molecular determinants of the unique allosteric binding site of the orphan nuclear receptor RORγt. *J. Biol. Chem.* **295**, 9183–9191 (2020).
35. Liu, H. & Naismith, J. H. An efficient one-step site-directed deletion, insertion, single and multiple-site plasmid mutagenesis protocol. *BMC Biotechnol.* **8**, 91–91 (2008).
36. Kallen, J. A. *et al.* X-Ray Structure of the hRORα LBD at 1.63 Å: Structural and Functional Data that Cholesterol or a Cholesterol Derivative Is the Natural Ligand of RORα. *Structure* **10**, 1697–1707 (2002).

37. Lechtken, A., Zündorf, I., Dingermann, T., Firla, B. & Steinhilber, D. Overexpression, refolding, and purification of polyhistidine-tagged human retinoic acid related orphan receptor RORα4. *Protein Expr. Purif.* **49**, 114–120 (2006).
38. Greenfield, N. J. Using circular dichroism spectra to estimate protein secondary structure. *Nat. Protoc.* **1**, 2876–2890 (2006).

Chapter 4

Indazole MRL-871 Interacts with PPARγ via a Binding Mode that Induces Partial Agonism

Abstract

Peroxisome proliferator-activated receptor gamma (PPARγ) is a nuclear receptor that plays a central role in several metabolic processes. Targeting this receptor has been a successful strategy for inducing insulin-sensitizing effects in patients with type 2 diabetes. Current compounds that target PPARγ have side effects resulting from their full agonistic nature, arguing for the discovery of PPARγ partial agonists with novel chemotypes. In this chapter, we elucidated the binding mode of the prototypical indazole-compound MRL-871 to PPARγ using a combination of X-ray crystallography and biochemical assays. The binding location of this compound is located between PPARγ helices 3, 5, 7 and 11 where the compound is stabilizing the beta-sheet region with a hydrogen bond between its carboxylic acid moiety and PPARγ Ser370. This unique binding mode differs from that of the benzoyl 2-methyl indoles, as most similar PPARγ ligands reported. MRL-871 binds with high affinity to PPARγ but induces only limited coactivator stabilization, highlighting its partial agonistic characteristics. Affinity analysis of MRL-871 and related compounds towards retinoic acid receptor-related orphan receptor gamma t (RORγt) and PPARγ indicates the possibility for tuning of selectivity. Together this makes MRL-871 an interesting starting point for the development of novel PPARγ ligands.

This chapter has been submitted as: Leijten-van de Gevel, I. A., van Herk, K. H. N., de Vries, R. M. J. M., Ottenheym, N. J. & Brunsveld, L. Indazole MRL-871 Interacts with PPARγ via a Binding Mode that Induces Partial Agonism.

Introduction

The peroxisome proliferator-activated receptor gamma (PPARγ) is a member of the nuclear receptor (NR) superfamily and plays a major role in metabolic processes including adipogenesis, lipid metabolism and insulin sensitivity.[1] This makes PPARγ an interesting drug target for example for type 2 diabetes. Synthetic PPARγ agonists of the thiazolidinedione (TZD) class[2] have been used for their insulin-sensitizing effects in the clinic since the 1990s. However, these TZDs come with side effects mainly ascribed to their full agonistic nature, which could potentially affect the transcription of hundreds of genes.[3] As such, there is a need for conceptually novel PPARγ targeting drugs, potentially with a mode of action shifted towards partial agonism or selective PPARγ modulation that can uncouple insulin sensitizing actions from adverse effects.[1,4–7]

Bruning et al. discovered, through hydrogen/deuterium exchange experiments, that while full agonists stabilize helix 12, which directly leads to stabilization of the coactivator binding surface, certain partial agonists can instead stabilize the β-sheet region of the PPARγ LBD.[4] Choi et al. revealed that increased PPARγ phosphorylation at serine 273 (Ser245 in PPARγ1), which is adjacent to the β-sheet region, leads to dysregulation of genes involved in insulin sensitivity.[8] Molecules that do not display classical PPARγ agonism and stabilize the β-sheet, which "freezes" that region in a configuration less optimal for Cdk5 phosphorylation, have antidiabetic effects in obese mice.[8,9] These observations have directed the search towards PPARγ ligands with minimal coactivator recruitment activity, but tight interactions with the β-sheet region. A highly relevant feature of the PPARγ LBD in this respect is the presence of a so-called "alternate" binding site.[10] This site, first described by Hughes et al., partially overlaps with one of the arms of the orthosteric binding site, but extends towards a solvent exposed pocket formed by the Ω-loop (Figure 1A).[10] Typically, this alternate pocket gets occupied after ligand binding to the orthosteric pocket, either by the same compound, a different (endogenous) ligand or a covalent antagonist.[10,11]

The PPARγ LBD is relatively permissive towards ligands of diverse chemical structures, albeit typically with lower affinities.[5,12,13] As such, we were intrigued by an off-target PPARγ activity in a class of indazole-compounds that were discovered as novel allosteric modulators for the retinoic acid receptor related orphan receptor (ROR)γt.[14,15] Notwithstanding certain structural similarities with benzoyl 2-

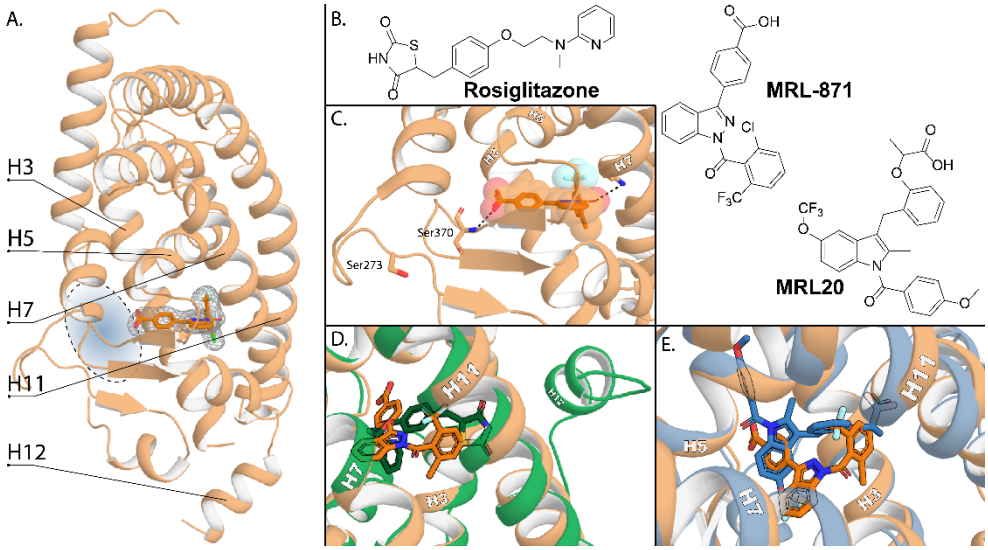

Figure 1 | Co-crystal structure of PPARγ (light orange) with MRL-871 (dark orange). (*A*) Overview of the binding location of MRL-871 in the full LBD of PPARγ. The electron density map around the compound is shown as an isomesh. The blue region with the dotted oval indicates the alternate site. (*B*) Molecular structures of MRL-871, Rosiglitazone and MRL20 (*C*) Close-up of the binding position. Hydrogen bonds are indicated as black dotted lines. (*D*) Overlay of the binding positions of MRL-871 (orange) and rosiglitazone (green, PDB: 2PRG). (*E*) Overlay of the binding positions of MRL-871 (orange) and MRL20 (blue, PDB: 2Q59).

methyl indole PPARγ ligands such as MRL20,[16] the significant molecular differences with archetypical PPARγ ligands brought forward the potential of a unique PPARγ binding mode for these indazoles. In this chapter, we elucidate the binding mode of the prototypical indazole-compound MRL-871 to PPARγ using a combination of X-ray crystallography and biochemical assays. MRL-871 addresses a unique set of interactions in the PPARγ ligand binding pocket, resulting in a PPARγ binding affinity stronger than the TZD rosiglitazone, but with a much weaker agonistic effect on coactivator recruitment.

Results and Discussion

Protein X-ray crystallography was utilized to obtain the co-crystal structure of PPARγ in complex with MRL-871. The crystal structure (Table S1, PDB: 6TDC) shows the complete LBD of PPARγ, with MRL-871 binding between helices 3, 5, 7, and 11 and the beta sheet region (Figure 1A). MRL-871 is wrapped around helix 3, stabilized by multiple hydrophobic interactions with helix 3 and helix 7. Its benzoic acid moiety is directed towards the β-sheet region, while the bis-*ortho*-substituted

phenyl ring is pointing in the opposite direction, mostly interacting with helix 3, but also with helices 5 and 7. In addition to these hydrophobic contacts, there are also relevant polar interactions (Figure 1C). The amide oxygen interacts with the amine of Lys395. The carboxylic acid partakes in a hydrogen bond with the backbone of Ser370. Proximity of ligands to Ser370 is known to correlate with stabilization of the beta sheet region and the helix 2-helix 2' loop.[8] Such a binding mode, where the ligand is not extending towards and interacting with helices 11 and 12, also called branch I, is usually associated with partial agonistic behavior.[6] Comparison of the binding modes of MRL-871 and full agonist rosiglitazone (Figure 1D), reveals this clear difference in the degree of protrusion towards helix 12. By extending in that direction, rosiglitazone stabilizes helix 12 favoring coactivator binding.[17] In contrast, MRL-871 is not interfacing with helix 12. Helix 12 is as such not stabilized in the active agonistic position, but points away from its own LBD to interact with the cofactor binding groove of a symmetry mate PPARγ (Figure S1). In solution the overall conformation of helix 12 is likely to be flexible, resulting in partial agonism (vide infra).[18] Figure 1E shows an overlay between the binding positions of MRL-871 and MRL20 (PDB 2Q59).[4] Despite structural similarities of these compounds (Figure 1B), their binding modes are profoundly distinct. MRL-871 is generally directed more towards helix 7, while MRL20 is extended alongside helix 3 and protrudes further into PPARγ branch I.

Biochemical studies were conducted to determine the functional implications of the interaction between MRL-871 and PPARγ. Rosiglitazone (Figure 1B) was used as a reference compound because of its well-studied agonistic binding mode. First, a thermal stabilization analysis was performed.[19–21] The ligand-induced stabilization was analyzed using differential scanning fluorimetry (DSF) for which the PPARγ LBD was incubated in the presence and absence of MRL-871 or rosiglitazone (Figure 2A).[22,23] Without compound, the PPARγ LBD had a melting temperature of 47.5 ± 0.7 °C. Four equivalents of rosiglitazone (14 μM) increased the melting temperature to 48.8 ± 1.0 °C (1.3 °C increase, P=0.01), while the same amount of MRL-871 increased the melting temperature to 50.2 ± 0.7 °C (2.7 °C increase, P<0.0001). The binding of MRL-871 thus has a significant stabilizing effect on PPARγ, stronger than the established drug compound. Of note; these data also reflect that MRL-871 has a strong affinity to PPARγ in the absence of coactivator.

A compound concentration dependent heat challenge assay was performed to obtain dissociation constants (K_D) for the ligand PPARγ interaction. After the heat

challenge folded and denatured protein were separated by means of centrifugation and the remaining soluble protein in the supernatant was quantified using Bradford reagent (Figure 2B).[24] Using the calculations set up by Bai et al. dissociation constants were determined.[25] After a 3 minute heat challenge of 50.5 °C, 71 ± 3 % of the apo PPARγ LBD was aggregated. The addition of either rosiglitazone or MRL-871 protected the protein from unfolding. Rosiglitazone featured a K_D of 3.3 ± 1.2

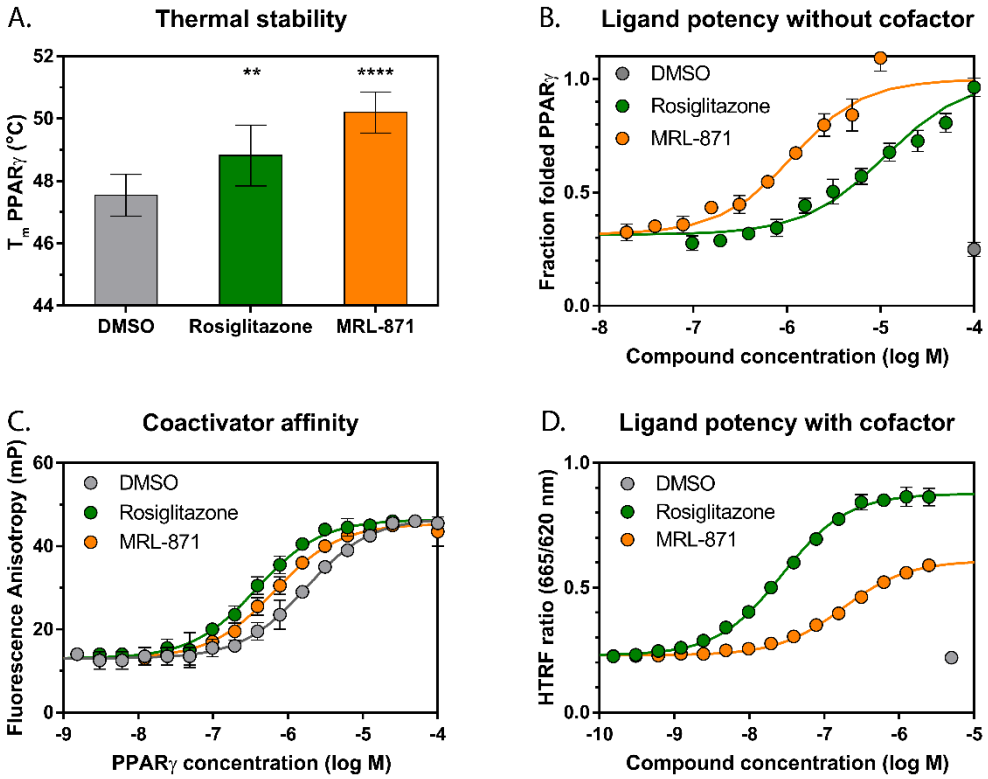

Figure 2 | MRL-871 interacts with PPARγ in biochemical assays. (*A*) Differential scanning fluorimetry assay of PPARγ LBD (3.5 µM) melting temperatures in absence and presence of rosiglitazone or MRL-871 (14 µM) ($n \geq 3$; mean ± s.d; significances between with and without compound assessed using unpaired t-test). (*B*) PPARγ LBD (600 nM) thermal stability assay using Bradford readout after a 3-minute heat-challenge at 50.5 °C ($n = 3$, representative data shown as mean ± s.d. of one experiment in duplicate). (*C*) Fluorescence anisotropy coactivator interaction assay between PPARγ LBD and fluorophore labelled PGC-1α peptide (10 nM) in absence (DMSO) or presence of rosiglitazone (10 µM) or MRL-871 (10 µM) ($n = 3$; representative data shown as mean ± s.d. of one experiment in triplicate). (*D*) HTRF coactivator recruitment of PPARγ LBD (10 nM) and PGC-1α peptide (200 nM) with ligand titration ($n = 3$, representative data shown as mean ± s.d. of one experiment in triplicate).

μM and MRL-871 had a ten-fold lower K_D value of 250 ± 110 nM. This low K_D testifies to the potential of MRL-871 as a high affinity PPARγ ligand. The weaker affinity of rosiglitazone in this assay reflects the strong preference of rosiglitazone to bind PPARγ in the presence of coactivators (vide infra).[26]

The agonistic activity of both compounds towards stabilizing the protein-protein interaction between PPARγ and coactivators was assessed using a fluorescence anisotropy (FA) assay. Here, PPARγ LBD was titrated to a fixed concentration of FITC-labeled peroxisome proliferator-activated receptor gamma coactivator 1-alpha (PGC-1α) peptide (Figure 2C). In absence of compound, the peptide bound to PPARγ with a K_D of 1.6 ± 0.1 μM. In the presence of rosiglitazone (10 μM) this K_D decreased to 370 ± 30 nM; a 4.4-fold increase of the PPARγ-PGC-1α affinity, indicating agonistic behavior. MRL-871 lowered the K_D to 710 ± 50 nM, representing a weaker 2.3-fold increase in affinity. Since rosiglitazone is classified as a full agonist, this indicates that MRL-871 acts as a partial agonist on this PPARγ–PGC-1α interaction.

Ligand potency towards the PPARγ-PGC-1α interaction was further assessed using a homogeneous time resolved fluorescence resonance energy transfer (HTRF) assay, which allows compound evaluation in a more befitting concentration window than FA (Figure 2D). Rosiglitazone featured an EC_{50} for PPARγ-PGC-1α stabilization of 26 ± 6 nM, while the EC_{50} of MRL-871 was 170 ± 10 nM. Importantly, and further testifying to a partial agonistic character of MRL-871 on the PPARγ-PGC-1α interaction, MRL-871 induced only a partial increase in the HTRF ratio. Thus while the MRL-871–PPARγ binding is strong, it does not very effectively induce a conformation of PPARγ to bind PGC-1α.

MRL-871 and rosiglitazone bind partly to similar parts of the PPARγ binding pocket (Figure 1D). The competitiveness of these binding modes was evaluated using a competition HTRF assay. MRL-871 was titrated to PPARγ in presence of fixed concentrations of rosiglitazone (Figure 3). An increased concentration of rosiglitazone shifted the EC_{50} values of MRL-871 to higher concentrations. Applying the Cheng-Prusoff equation, which corrects for the amount and affinity of rosiglitazone, showed that the calculated “inhibition constant” (Ki) of MRL-871 remained constant.[27] These results thus confirm that the two ligands cannot bind simultaneously to PPARγ.

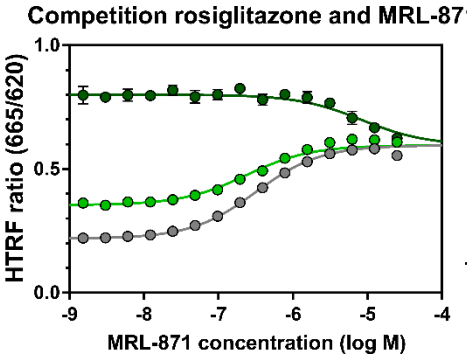

Concentration rosiglitazone	None	10 nM	1 µM
EC_{50}/IC_{50} (nM)	210 ± 100	230 ± 80	9100 ± 3700
K_i (nM)	210 ± 100	160 ± 60	230 ± 90

Figure 3 | MRL-871 competes for the binding location of rosiglitazone in HTRF. HTRF coactivator recruitment assay showing MRL-871 dependent change in PPARγ LBD (10 nM), PGC-1α peptide (200 nM) interaction in presence of fixed concentrations of rosiglitazone (*n* = 3, representative data shown as mean ± s.d. of one experiment in triplicate).

Certain ligands have been reported to be able to bind to the alternate site (Figure 1A) within the large PPARγ binding pocket even when the orthosteric binding site is occupied.[10,11,28] To further explore the behavior of MRL-871 in this matter, two tool compounds were covalently fused to the cysteine in the PPARγ ligand binding pocket (Figure 4A, Figure S2). GW9662 is known to block the orthosteric pocket of PPARγ, but leave enough room for compounds to bind to the alternate site.[10,29] SR16832 is bigger and specifically designed to simultaneously block both sites.[30] DSF and HTRF were used to quantify binding of MRL-871 to the covalently blocked PPARγ LBDs. In DSF (Figure 4B) the covalent blockers themselves lead to a thermal stabilization of 3.9 °C (P<0.0001) for GW9662 and 4.4 °C for SR16832 (P<0.0001). Addition of MRL-871 to the GW9662 modified PPARγ still caused an increase in PPARγ stability of 1.1 °C (P=0.03). When the LBD is covalently linked to SR16832, no significant change in thermal stability was observed (-0.6 °C, P=0.2) upon addition of MRL-871. In contrast, Rosiglitazone was not able to increase the thermal stability of PPARγ linked to GW9662 (0.0 °C, P=0.9) nor to SR16832 (-0.1 °C, P=0.6). Combined, this confirms that rosiglitazone only binds to the orthosteric binding site while MRL-871 can function by addressing a site distinct from the orthosteric site. This is further confirmed by HTRF experiments. PPARγ covalently ligated to GW9662 is hardly responsive to rosiglitazone anymore; rosiglitazone's EC_{50} decreases to 44 ± 35 µM, a more than 1800-fold loss (Figure 4C). Any residual binding might be caused by small amounts of unlinked PPARγ (Figure S2). In contrast, MRL-871 still has an EC_{50} of 1.3 ± 0.2 µM for PPARγ covalently ligated to GW9662, only an 8.1-fold decrease compared to apo PPARγ. SR16832 again inhibits the binding of both compounds (Figure 4D). Together these data show that even

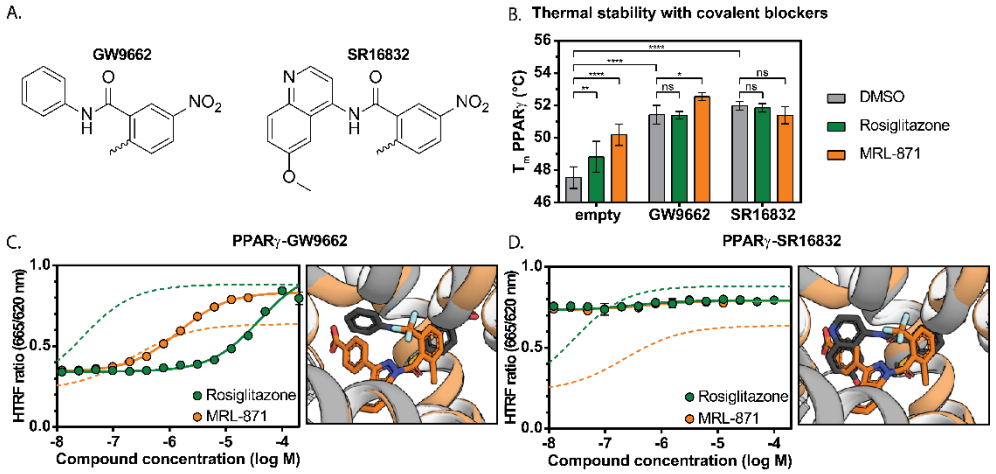

Figure 4 | MRL-871 still binds PPARγ with micromolar affinity when the orthosteric pocket is blocked by GW9662. (*A*) Molecular structures of covalent binders GW9662 and SR16832. (*B*) DSF melting temperatures of PPARγ LBD (3.5 µM) in absence and presence of rosiglitazone or MRL-871 (14 µM) and covalently bound to GW9662 or SR16832 ($n \geq 3$; mean ± s.d; significance difference between with and without compound assessed using unpaired t-test).(C-D) HTRF coactivator recruitment assay showing ligand dependent change in PPARγ LBD (10 nM), PGC-1α peptide (200 nM) interaction with the PPARγ LBD covalently bound to either (*C*) GW9662 or (*D*) SR16832. Dotted lines show HTRF curves without a covalent blocker ($n = 3$, representative data shown as mean ± s.d. of one experiment in triplicate).

when the orthosteric pocket is blocked, MRL-871 can bind to PPARγ. This distinct position is potentially, in part, generated by the GW9662 ligation, but provides entry points for chemical exploration.

In recent years, next to MRL-871, several other allosteric RORγt inverse agonists, with differing central scaffold structure, were developed. As a starting point to look into PPARγ vs RORγt selectivity of such compounds, we compared three allosteric RORγt inverse agonists (Figure 5).[31,32] In HTRF, the Glenmark compound 13 (CPD13) has a relatively similar EC_{50} as MRL-871 (300 ± 10 nM respectively 200 ± 80 nM) for PPARγ, while the EC_{50} of FM26 for PPARγ is significantly weaker (5.6 ± 0.8 µM) (Figure 5A). MRL-871 is also the most potent compound on RORγt, (4.7 ± 2.2 nM), but FM26 binds here a bit stronger than CPD13 (330 ± 100 nM respectively 620 ± 100 nM) (Figure 5B). In DSF, a similar pattern can be observed. MRL-871 and especially CPD13 efficiently stabilize PPARγ, while FM26 is not able to do so at the used concentration (Figure 5C). For RORγt, the increase in stability by MRL-871 is significantly larger than the increases caused by CPD13 and FM26. This

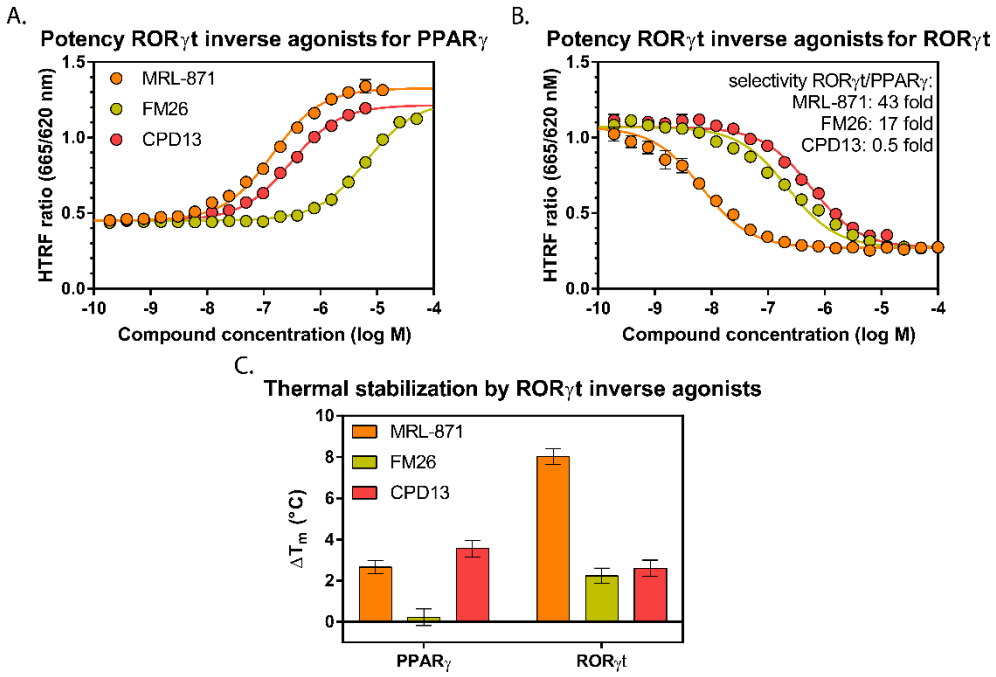

Figure 5 | PPARγ and RORγt selectivity. (*A*) Ligand dependent HTRF PPARγ-coactivator recruitment assay with PPARγ (10 nM), PGC-1α peptide (200 nM) ($n = 3$, representative data shown as mean ± s.d. of one experiment in triplicate). (*B*) Ligand dependent HTRF RORγt-coactivator recruitment assay with RORγt (20 nM), SRC1B2 peptide (100 nM) ($n = 3$, representative data shown as mean ± s.d. of one experiment in triplicate). (*C*) Differential scanning fluorimetry assay of PPARγ or RORγt LBD (3.5 µM) melting temperature increase induced by MRL-871, FM26 or CPD13 (14 µM) ($n \geq 3$; mean ± s.d).

differentiated binding profile for PPARγ and RORγt indicates that of these three compounds, CPD13 appears to be the most aselective. FM26 in contrast is most RORγt selective, while MRL-871 is the most potent compound on both NRs. These data thus indicate that PPARγ vs. RORγt selectivity can be tuned for these classes of compounds.

Conclusions

In conclusion, MRL-871 binds to PPARγ in a novel binding mode distinct to that previously found for other PPARγ ligands, including its most close counterpart the benzoyl 2-methyl indole compounds. The MRL-871 binding site in PPARγ is located between helices 3, 5, 7 and 11 and the beta sheet region with a hydrogen bond to Ser370 and without protrusion into branch I. This binding mode causes MRL-871 to bind with high affinity, independent of the presence of coactivator. MRL-871

features only weak coactivator stabilization for PPARγ. This partial agonism is highly desirable for novel compound development endeavors. PPARγ vs RORγt substype selectivity is tunable in these compounds classes, which provides a route towards a differentiated PPARγ pharmacology.

Experimental section

Protein expression and purification

General protocol

A pET15b vector containing the PPARγ LBD (residues 235-505) with an N-terminal His6-tag was transformed into BL21(DE3) competent Escheria Coli (Novagen) by heat shock. A pre-culture was initiated overnight at 37 °C, 250 rpm using a single colony in 8 mL LB medium with ampicillin (100 µg/mL). This culture was transferred to 2 L LB broth supplemented with ampicillin (100 µg/mL), and antifoam (0.05%), and incubated at 37 °C until OD600 of 1.0 was achieved. To induce expression, isopropyl β-D-thiogalactoside (IPTG) (0.5 mM) was added, and the culture was incubated at 18 °C, 180 rpm for 16 h. The bacteria were harvested using centrifugation (10,000 *g, 4 °C, 10 m) and dissolved in lysis buffer (50 mM Tris pH 8.0, 300 mM NaCl, 12.5 mM imidazole, 5% (v/v) glycerol, 1mM tris(2- carboxyethyl)phosphine (TCEP)). The bacteria were lysed using a homogenizer (Avestin Emulsiflex C3) at 15,000 psi with additional benzonase (1:10,000 v/v). The cell lysate was cleared by centrifugation (40,000 *g, 4 °C, 30 m) and purified via Ni^{2+} affinity column chromatography (QIAGEN, Ni-NTA Superflow Cartridge). Elution was done using elution buffer (50 mM Tris pH 8.0, 300 mM NaCl, 200 mM imidazole, 5% (v/v) glycerol, 1mM TCEP) and fractions containing high protein concentrations, determined using a NanoDrop Spectrophotometer, were combined and then split in two to prepare protein for both assays and crystallography.

Protein for assays

The purified protein was dialyzed against a storage buffer (25 mM Tris pH 8.0, 150 mM NaCl, 10% (v/v) glycerol, 5 mM DTT) overnight using 10K MWCO SnakeSkinTM dialysis tubing. Subsequently, the protein was concentrated using an Amicon Ultra centrifugal filter with a 10-kDa cutoff (Millipore), flash-frozen and stored at -80 °C until usage. Molecular weight and purity were confirmed using Quadrupole Time-of-Flight LC/MS and SDS-page (Figure S#).

Protein for crystallography

To remove the His-tag, 1 unit restriction grade thrombin (Novagen) was added per mg protein to before it being dialyzed against a storage buffer (25 mM Tris (pH 8.0), 150 mM NaCl, 10 v/v% glycerol, 5 mM DTT) overnight using 10K MWCO SnakeSkinTM dialysis tubing. Next, the protein was concentrated using Amicon Ultra centrifugal filter with a 10-kDa

cutoff (Millipore) and loaded on a Superdex 75 prep grade 16/60 size-exclusion column (GE Life Sciences) using filtered storage buffer (25 mM Tris pH 8.0, 150 mM NaCl, 10% glycerol and 5 mM DTT) as a running buffer. 3 mL fractions were collected and protein containing fractions that eluted around the volume typical for proteins of around 30 kDa (~75 mL) were combined. Subsequently, the protein was concentrated (>10 mg/mL) using an Amicon Ultra centrifugal filter with a 10-kDa cutoff (Millipore), flash-frozen and stored at -80 °C until usage. Molecular weight and purity were assessed using SDS-page (Figure S#). Because His-tag cleavage appeared to be incomplete, Ni2+ affinity column chromatography was used to capture the uncleaved protein and the eluted, non His-tagged, protein was again dialyzed against storage buffer (25 mM Tris pH 8.0, 150 mM NaCl, 10% (v/v) glycerol, 5 mM DTT) overnight using 10K MWCO SnakeSkinTM dialysis tubing. Subsequently, the protein was concentrated using an Amicon Ultra centrifugal filter with a 10-kDa cutoff (Millipore), flash-frozen and stored at -80 °C until usage. Molecular weight and purity were confirmed using Quadrupole Time-of-Flight LC/MS (Figure S#)

RORγt see chapter 2

Crystallography

Protein and compound were incubated together by adding PPARγ (10.52 mg/mL) and MRL-871 (in DMSO) in a 1:1 ratio with a final concentration of 2% DMSO. This mixture was incubated on ice for 1 hour. 75 µL of crystallization buffer (0.2 M ammonium nitrate, 20% (w/v) PEG3350) was added to each reservoir of a Swissci Polystyrene MRC 2-well Crystallization Plate™ (Molecular Dimensions, MD11-00-10/40/100) and 200 nL crystallization buffer and 200 nL protein and ligand sample were added to the sitting-drop pedestals. The crystal plate was placed at 4 °C. In seven days, hexagonal crystals grew. They were briefly cryoprotected with 30% (v/v) glycerol supplemented to the original crystallization buffer and immediately flash frozen. Protein crystals were measured at DESY PETRAIII synchrotron beamline P11 (DESY, Hamburg, Germany). The data was processed on the CCP4i2 (7.0.077) suite.[34] The dataset was indexed, integrated, and scaled using DIALS (1.14.11).[35] Anisotropic diffraction was analyzed and corrected using STARANISO followed by data reduction using Aimless.[36,37] Phaser was used for phasing with PDB ID 6FZP as a search model.[38,39] Thereafter, REFMAC5 and COOT were used in alternating cycles of refinement and model building.[40,41] The model was uploaded to PDB-REDO to perform a final model analysis and optimization and Phenix was used for final runs of refinement.[42,43] Figures were made using PyMOL (version 2.2.3, Schrödinger).[44]

Ligation

Ligations of PPARγ LBD to covalent compounds were done by incubating 80 µM protein with 2 equivalents GW9662 (10 mM in DMSO) or 3 equivalents SR16832 (10 mM in DMSO), in ligation buffer (50 mM Tris pH 8.0, 50 mM NaCl, 10 mM DTT) over at least 16h. PD

SpinTrapTM- G-25 spin columns (Cytiva) were used to exchange the buffer to storage buffer (25 mM Tris pH 8.0, 150 mM NaCl, 10% glycerol, 5 mM DTT). The ligated protein was centrifuged (11,000* g, 4°C, 5 m) to remove precipitated protein before the protein was aliquoted and flash-frozen and stored at -80 °C until usage. Full ligation was confirmed using Quadrupole Time-of-Flight LC/MS (Figure S#).

Differential scanning fluorimetry

Differential scanning fluorimetry (DSF) assays were performed using 40 µL samples containing 3.5 µM protein, 14 µM compound, and 2.5× SYPRO® Orange Protein Gel Stain (Sigma) in buffer containing 150 mM NaCl, 10 mM HEPES (pH 7.5), and 2% DMSO. The samples were heated from 35 °C to 65 °C at a rate of 0.3 °C per 15 s in a CFX96 touch real-time PCR detection system (Bio-Rad). Excitation (525/20 nm) and emission (570/20 nm) filters were used, and the reported melting values were calculated as the minimum in the negative derivative of the resulting melting curve. Reported T_m values are determined as means ± S.D. from at least 3 independent experiments performed in at least duplicate. ΔT_m values and significance are determined using an unpaired t-test with ΔT_m being the difference in means ± standard error of that difference.

Bradford thermal stability assay

Heat challenges were done in 50 uL volumes in PCR plates (Bio-rad #HSL9601) in at least duplicate with 600 nM protein in buffer containing 150 mM NaCl, 10 mM HEPES (pH 7.5) and a final concentration of 2% DMSO. Samples were heated for 3 minutes at the indicated heat challenge temperature, followed by cooling back to 25 °C for 3 minutes. Next, the plates were centrifuged to separate soluble from denatured protein (4700 rpm, 4°C, 15 m). 62.5 uL room temperature Coomassie (Bradford) Protein Assay Reagent (Thermo Scientific™, Pierce™ Coomassie (Bradford) Protein Assay Kit) was added to a clear, flat bottom 384-well plate (NUNC). After centrifugation, 37.5 uL supernatant was added to each well without touching the possible pellet at the bottom of the wells. 600 nM protein in buffer that did not undergo a heat-challenge or centrifugation was used as a positive control and buffer without protein was used as a negative control. The NUNC plate was then shaken for 10 seconds, followed by incubation for 10 minutes. Finally, absorbance at 595 nm was measured. The data were analyzed using GraphPad Prism and excel. Curve fitting was done by first determining the fraction of unfolded protein (fu0) after the heat challenge in absence of compound. Next, the data was reproduced using the exact model of Bai et al. where the standard deviation between the simulated and actual data was minimized to obtain the K_D.[25] The reported K_D values are the means ± S.D. from three individually fitted independent experiments performed in duplicate.

Fluorescence anisotropy

FA assays were performed in 10 µL volumes in duplicate in buffer containing 150 mM NaCl, 10 mM HEPES (pH 7.5), 5 mM DTT, 10 mM CHAPS, and 0.1%, m/v, BSA. FITC-labeled PGC-1α peptide (FITC- EAEEPSLLKLLLAPANTQ-NH2) (10 nM), compound (10 µM) and DMSO (1%) were present at fixed concentrations. His6-PPARγ LBD was titrated to this in round-bottom, nonbinding, black, 384-well plates (Corning, 4511) starting at 100 µM protein. The plates were measured in an Infinite F500 plate reader (Tecan) (excitation, 485 nm; emission, 535 nm). The data were then analyzed using GraphPad Prism software, where the curve-fitting was done via

$$y = \frac{B_{max} \times x}{K_d + x} + Background$$

Where Bmax is the maximum specific binding, K_D is the equilibrium dissociation constant, and background is the amount of nonspecific binding with no added protein. Background was assumed to be constant between constructs within each experiment. The reported K_D values are the means ± S.D. from three individually fitted independent experiments performed in duplo.

HTRF (also competition assay and RORγt)

HTRF assays were performed in 10 µL volumes in triplicate in buffer containing 150 mm NaCl, 10 mm HEPES (pH 7.5), 5 mm DTT, 10 mm CHAPS, and 0.1% (w/v) BSA. His6-protein, biotin-labeled coactivator peptide, terbium-labeled anti-His antibody (Cisbio, 61HISTLB), and D2-labeled streptavidin (Cisbio, 610SADLB) were present at fixed concentrations. Compounds dissolved in DMSO were titrated to this mixture in round-bottom, nonbinding, white, 384-well plates (Corning, 4513), keeping the DMSO concentration constant at 2%. The plates were measured in an Infinite F500 plate reader (Tecan) (excitation, 340 nm; emission, 665 nm and 620 nm). The data were then analyzed using GraphPad Prism software. The reported EC_{50}/IC_{50}/K_i values are the means ± S.D. from three individually fitted independent experiments performed in triplicate.

Specifics PPARγ

For assays measuring direct titrations towards (covalently ligated) PPARγ, His6-PPARγ LBD was used at 10 nM, biotin-PGC-1α peptide (Biotin-GTPPPQEAEEPSLLKLLLAPANTQ-NH2) at 200 nM, D2-labeled streptavidin at 25 nM and terbium-labeled anti-His antibody at 713 pM. Datapoints at high compound concentrations were omitted if the signal went down by more than 2.5% compared to the previous datapoint, since such effects are likely caused by precipitation which is independent of the affinity. The curve fitting was done via:

$$y = Bottom + \frac{x \times (Top - Bottom)}{EC_{50} + x}$$

Where Top and Bottom are the plateaus and EC_{50} is the concentration of agonist that gives a response halfway between Bottom and Top. Background was assumed to be constant within an experiment meaning the Bottom was constrained to be shared for all datasets (within the same construct) within an experiment.

Specifics competition assay

For the competition assay between MRL-871 and rosiglitazone, His6-PPARγ LBD was used at 10 nM, biotin- PGC-1α peptide (Biotin-GTPPPQEAEEPSLLKLLLAPANTQ-NH2) at 200 nM, D2-labeled streptavidin at 25 nM and terbium-labeled anti-His antibody at 713 pM. Also, rosiglitazone was present at fixed concentrations of 0, 10 nM or 1 µM. MRL-871 was titrated to this. EC50 values were fitted using:

$$y = Bottom + \frac{x \times (Top - Bottom)}{EC_{50} + x}$$

Where Top and Bottom are the plateaus and EC_{50} is the concentration of agonist that gives a response halfway between Bottom and Top. Top is set to be equal to the average signal over all rosiglitazone concentrations at 25 µM MRL-871.

The inhibition constant (K_i), which corrects for the concentration and affinity of rosiglitazone, is fitted, by first transforming the concentrations to logarithms and then using:

$$\log(EC_{50}) = \log\left(10^{logKi*\left(1+\frac{RadioligandNM}{HotKdNM}\right)}\right)$$

$$y = Bottom + \frac{Top - Bottom}{1 + 10^{x - \log(EC_{50})}}$$

Where EC_{50} is the concentration of MRL-871 that gives a response halfway between Bottom and Top. RadioligandNM is the concentration of rosiglitazone in nM. HotKdNM is the affinity of rosiglitazone. This was set to be 25.79 nM which is the EC determined from the direct titration HTRF experiments. Top and Bottom are the plateaus. Bottom is set to be equal to the average signal over all rosiglitazone concentrations at 25 µM MRL-871.

Specifics RORγt

For assays measuring direct titrations towards RORγt, His6-RORγt LBD was used at 20 nM, biotin-SRC1b2 peptide (Biotin-PSSHSSLTERHKILHRLLQEGSPSD-NH2) at 100 nM, D2-labeled streptavidin at 12.5 nM and terbium-labeled anti-His antibody at 733 pM.[33] Datapoints at high compound concentrations were omitted if the signal went up by more than 2.5% compared to the previous datapoint, since such effects are likely caused by precipitation which is independent of the affinity. The curve fitting was done via:

$$y = Bottom = \frac{Top - Bottom}{1 + \frac{x}{IC_{50}}}$$

Where Top and Bottom are the plateaus and IC_{50} is the concentration of inverse agonist that gives a response halfway between Bottom and Top. Background was assumed to be constant within an experiment meaning the Top was constrained to be shared for all datasets within an experiment. High concentrations of inverse agonist in theory lead to total dissociation between protein and coactivator, therefore Bottom was constrained to be equal to the signal in absence of protein.

Supporting information

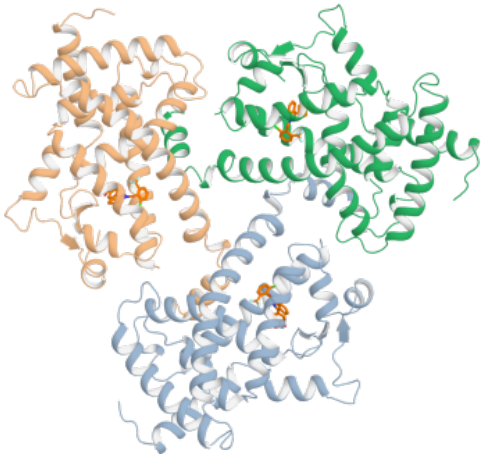

Figure S1 | **Symmetry mates for the PPARγ MRL-871 constructs.** Three symmetry mates are shown where you can see that helix 12 of one construct interacts with the cofactor binding groove of a second construct in a triangular manner.

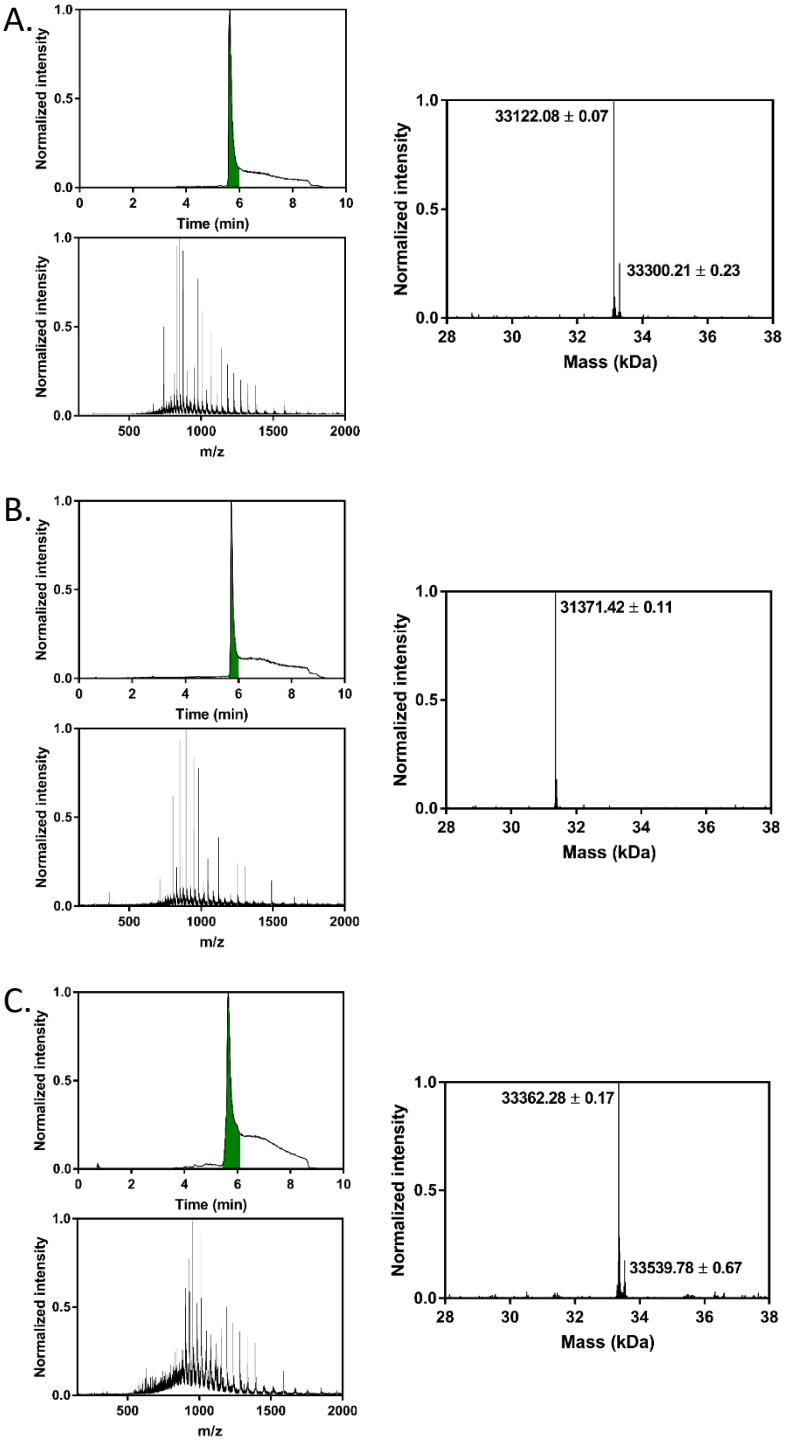
A.
Normalized intensity
Time (min)
m/z
33122.08 ± 0.07
33300.21 ± 0.23
Mass (kDa)
B.
31371.42 ± 0.11
C.
33362.28 ± 0.17
33539.78 ± 0.67

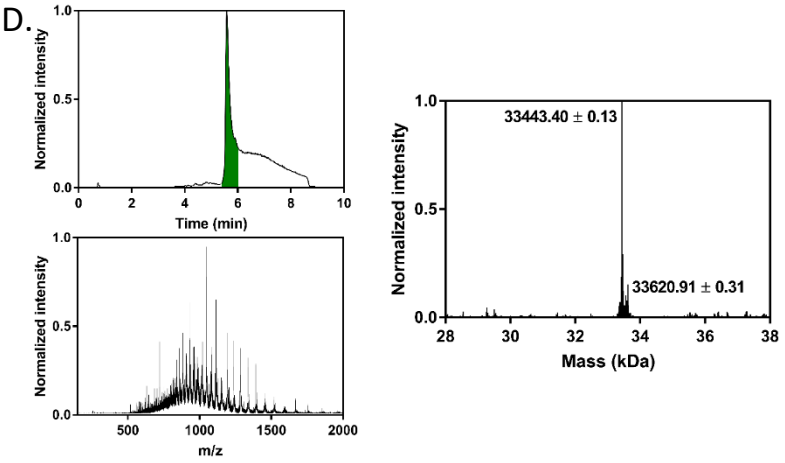

Figure S2 | **LC-MS Q-TOF analysis of all proteins.** For each protein, the total ion count chromatogram (top left), the m/z spectrum within the selected peak (bottom left), and the resulting deconvoluted mass spectrum (right) are shown. His-tagged PPARγ constructs show an additional peak at mass +178 Da which is caused by spontaneous α-*N*-6 gluconoylation at an amino group of the His6-tag.[1] (*A*) PPARγ assay construct, expected molecular weight (MW) 33122.2. (*B*) PPARγ crystallography construct, expected MW 31371.3. (*C*) PPARγ-GW9662, expected MW 33362.4), (*D*) PPARγ- SR16832, expected MW 33443.5.

Acknowledgments

Kim van Herk is acknowledged for her work on the initial setup of the assays and solving the crystal structure. Rens de Vries is greatly acknowledged for his help with the crystallography aspect of this chapter. Nicolaas is acknowledged for synthesizing the covalent compounds and optimizing ligation strategies.

References

1. Ahmadian, M. *et al.* PPARγ signaling and metabolism: The good, the bad and the future. *Nat. Med.* **19**, 557–566 (2013).
2. Lehmann, J. M. *et al.* An antidiabetic thiazolidinedione is a high affinity ligand for peroxisome proliferator-activated receptor γ (PPARγ). *J. Biol. Chem.* **270**, 12953–12956 (1995).
3. Kung, J. & Henry, R. R. Thiazolidinedione safety. *Expert Opin. Drug Saf.* **11**, 565–579 (2012).
4. Bruning, J. B. *et al.* Partial Agonists Activate PPARγ Using a Helix 12 Independent Mechanism. *Structure* **15**, 1258–1271 (2007).
5. Garcia-Vallvé, S. *et al.* Peroxisome Proliferator-Activated Receptor γ (PPARγ) and Ligand Choreography: Newcomers Take the Stage. *J. Med. Chem.* **58**, 5381–5394 (2015).

6. Kroker, A. J. & Bruning, J. B. Review of the Structural and Dynamic Mechanisms of PPARγ Partial Agonism. *PPAR Res.* **2015**, 816856 (2015).
7. Willems, S. *et al.* Endogenous vitamin E metabolites mediate allosteric PPARγ activation with unprecedented co-regulatory interactions. *Cell Chem. Biol.* **28**, 1489-1500.e8 (2021).
8. Choi, J. H. *et al.* Anti-diabetic drugs inhibit obesity-linked phosphorylation of PPARgamma by Cdk5. *Nature* **466**, 451–6 (2010).
9. Choi, J. H. *et al.* Antidiabetic actions of a non-agonist PPARγ ligand blocking Cdk5-mediated phosphorylation. *Nature* **477**, 477–481 (2011).
10. Hughes, T. S. *et al.* An alternate binding site for PPARγ ligands. *Nat. Commun.* **5**, 1–13 (2014).
11. Shang, J. *et al.* Cooperative cobinding of synthetic and natural ligands to the nuclear receptor PPARγ. *eLife* **7**, (2018).
12. Nolte, R. T. *et al.* Ligand binding and co-activator assembly of the peroxisome proliferator- activated receptor-γ. *Nature* **395**, 137–143 (1998).
13. Wang, L. *et al.* Natural product agonists of peroxisome proliferator-activated receptor gamma (PPARγ): a review. *Biochem. Pharmacol.* **92**, 73–89 (2014).
14. Fauber, B. P. *et al.* Discovery of imidazo[1,5-a]pyridines and -pyrimidines as potent and selective RORc inverse agonists. *Bioorg. Med. Chem. Lett.* **25**, 2907–2912 (2015).
15. Scheepstra, M. *et al.* Identification of an allosteric binding site for RORγt inhibition. *Nat. Commun.* **6**, 8833 (2015).
16. Acton, J. J. *et al.* Benzoyl 2-methyl indoles as selective PPARγ modulators. *Bioorg. Med. Chem. Lett.* **15**, 357–362 (2005).
17. Nolte, R. T. *et al.* Ligand binding and co-activator assembly of the peroxisome proliferator-activated receptor-gamma. *Nature* **395**, 137–143 (1998).
18. Chrisman, I. M. *et al.* Defining a conformational ensemble that directs activation of PPARγ. *Nat. Commun.* **9**, 1–16 (2018).
19. Pantoliano, M. W. *et al.* High-Density Miniaturized Thermal Shift Assays as a General Strategy for Drug Discovery. *J. Biomol. Screen.* **6**, 429–440 (2001).
20. Johnson, B. A. *et al.* Ligand-induced stabilization of PPARγ monitored by NMR spectroscopy: Implications for nuclear receptor activation. *J. Mol. Biol.* **298**, 187–194 (2000).
21. Hamuro, Y. *et al.* Hydrogen/deuterium-exchange (H/D-Ex) of PPARγ LBD in the presence of various modulators. *Protein Sci.* **15**, 1883–1892 (2006).
22. Matulis, D., Kranz, J. K., Salemme, F. R. & Todd, M. J. Thermodynamic stability of carbonic anhydrase: Measurements of binding affinity and stoichiometry using thermofluor. *Biochemistry* **44**, 5258–5266 (2005).
23. Niesen, F. H., Berglund, H. & Vedadi, M. The use of differential scanning fluorimetry to detect ligand interactions that promote protein stability. *Nat. Protoc.* **2**, 2212–2221 (2007).
24. Bradford, M. M. A rapid and sensitive method for the quantitation of microgram quantities of protein utilizing the principle of protein-dye binding. *Anal. Biochem.* **72**, 248–254 (1976).
25. Bai, N., Roder, H., Dickson, A. & Karanicolas, J. Isothermal Analysis of ThermoFluor Data can readily provide Quantitative Binding Affinities. *Sci. Rep.* **9**, 1–15 (2019).

26. Vink, P. de *et al.* Cooperativity as Quantification and Optimization Paradigm for Nuclear Receptor Modulators. *Chem. Sci.* (2022) doi:10.1039/D1SC06426F.
27. Yung-Chi, C. & Prusoff, W. H. Relationship between the inhibition constant (KI) and the concentration of inhibitor which causes 50 per cent inhibition (I50) of an enzymatic reaction. *Biochem. Pharmacol.* **22**, 3099–3108 (1973).
28. Laghezza, A. *et al.* Identification of the First PPARα/γ Dual Agonist Able To Bind to Canonical and Alternative Sites of PPARγ and To Inhibit Its Cdk5-Mediated Phosphorylation. *J. Med. Chem.* **61**, 8282–8298 (2018).
29. Leesnitzer, L. M. *et al.* Functional Consequences of Cysteine Modification in the Ligand Binding Sites of Peroxisome Proliferator Activated Receptors by GW9662. *Biochemistry* **41**, 6640–6650 (2002).
30. Brust, R. *et al.* Modification of the Orthosteric PPARγ Covalent Antagonist Scaffold Yields an Improved Dual-Site Allosteric Inhibitor. *ACS Chem. Biol.* **12**, 969–978 (2017).
31. Chaudhari, S. S., Thomas, A., Dhone, S. V., Khairatkar-Joshi, N. & Bajpai, M. Bicyclic Heterocyclic Compounds as ROR gamma Modulators. (2015) doi:WO2015008234A1.
32. Meijer, F. *et al.* Ligand-Based Design of Allosteric Retinoic Acid Receptor-Related Orphan Receptor γt (RORγt) Inverse Agonists. *J. Med. Chem.* acs.jmedchem.9b01372 (2019) doi:10.1021/acs.jmedchem.9b01372.
33. Leijten-van de Gevel, I. A. & Brunsveld, L. Delineation of the molecular determinants of the unique allosteric binding site of the orphan nuclear receptor RORγt. *J. Biol. Chem.* **295**, 9183–9191 (2020).
34. Potterton, L. *et al.* CCP 4 i 2: The new graphical user interface to the CCP 4 program suite. *Acta Crystallogr. Sect. Struct. Biol.* **74**, 68–84 (2018).
35. Clabbers, M. T. B., Gruene, T., Parkhurst, J. M., Abrahams, J. P. & Waterman, D. G. Electron diffraction data processing with DIALS. *Acta Crystallogr. Sect. Struct. Biol.* **74**, 506–518 (2018).
36. Tickle, I.J., Flensburg, C., Keller, P., Paciorek, W., Sharff, A. & Vonrhein, C., Bricogne, G. STARANISO. (2018).
37. Evans, P. R. & Murshudov, G. N. How good are my data and what is the resolution? *Acta Crystallogr. D Biol. Crystallogr.* **69**, 1204–1214 (2013).
38. McCoy, A. J. *et al.* Phaser crystallographic software. *J. Appl. Crystallogr.* **40**, 658–674 (2007).
39. Nolte, R. T. *et al.* Ligand binding and co-activator assembly of the peroxisome proliferator-activated receptor-gamma. *Nature* **395**, 137–143 (1998).
40. Murshudov, G. N. *et al.* REFMAC5 for the refinement of macromolecular crystal structures. *Acta Crystallogr. D Biol. Crystallogr.* **67**, 355–367 (2011).
41. Emsley, P., Lohkamp, B., Scott, W. G. & Cowtan, K. Features and development of Coot. *Acta Crystallogr. D Biol. Crystallogr.* **66**, 486–501 (2010).
42. Joosten, R. P., Long, F., Murshudov, G. N. & Perrakis, A. The PDB-REDO server for macromolecular structure model optimization. *IUCrJ* **1**, 213–220 (2014).
43. Adams, P. D. *et al.* PHENIX: A comprehensive Python-based system for macromolecular structure solution. *Acta Crystallogr. D Biol. Crystallogr.* **66**, 213–221 (2010).
44. The PyMOL Molecular Graphics System, Version 2.2.3. (2010).

Chapter 5

A Cheap and Label-free Thermal Stability Assay for Nuclear Receptor-Ligand Binding Constant Determination

Abstract

Nuclear receptors are a class of highly pursued drug targets for a range of diseases. When developing new compounds targeting these receptors, techniques to find dissociation constants are imperative. Currently, there is a range of assays available to quantify protein-ligand interactions. However, these techniques often use labels that can cause bias or require large quantities of material or expensive specialized equipment. This was the inspiration to develop a cheap and easy assay that can be done in every laboratory and provides dissociation constants in a label-free environment. The assay presented in this chapter is a thermal stability assay that measures the fraction of folded protein remaining after a heat challenge using Bradford reagent. As a proof of concept, the so-called Bradford thermal stability assay (BraTSA) is applied on peroxisome proliferator-activated receptor gamma (PPARγ), which is an important drug target for type 2 diabetes. The assay was able to identify PPARγ ligands that cause strong stabilization independent of cofactor presence which is the desired mode of action for compounds with insulin sensitizing effects without severe side effects.

This chapter will be submitted as: Leijten-van de Gevel, I. A. & Brunsveld, L. A cheap and label-free thermal stability assay for nuclear receptor-ligand binding constant determination .

Introduction

Nuclear receptors (NRs) are very attractive drug targets because they play a key role in a wide scale of physiological processes and, in connection with that, diseases.[1] In drug development, one of the first questions that needs to be answered for a compound is the affinity for its target protein. This affinity gives a first indication about the potency and the applicability to use this compound as a drug. For NRs, affinities are determined using various assays with associated advantages and disadvantages.[2] Displacement of radioactively-labeled specific ligands is a widely used and trusted manner to measure affinity.[3] Although being very sensitive, this type of assay requires very specific conditions for each individual NR and safety measurements and appropriate disposal need to be taken care of.[3] Furthermore, a displacement assay is only possible if there are ligands available for the site you want to investigate.[3] This means this technique is not able to identify ligands for orphan receptors or new allosteric pockets. The same limitations for allosteric or orphan receptor pocket finding hold for fluorometric assays using labeled ligands. These assays are safer and more environmentally friendly than radiometric assays, but they also come with their own challenges including where to place the, large, fluorogenic tag in the probe molecule and artefacts when screening optically active ligands. Fluorophores are not only placed directly on ligands but can also be coupled to cofactors which gives information about the results of compound binding. This eliminates the problem of fitting a fluorophore in the ligand binding pocket but does look at downstream effects that might not directly relate to binding affinity.

Besides displacement-based techniques, there is also a range of biophysical techniques that is being used to investigate ligand affinity in NRs. In surface plasmon resonance (SPR), on- and off-rates of binding are measured using changes in electromagnetic surface waves on a thin metal film.[4] This technique thus gives insight into binding kinetics in addition to the binding affinity.[5] While giving very valuable information, this technique requires specialized, expensive equipment. Also, it requires a lot of material and is labor-intensive to set up the assay for a new target. More recently, microscale thermophoresis (MST) was developed. This technique measures the influence of compounds on the motion of fluorescently labeled proteins in microscopic temperature gradients.[6] By doing so dissociation constants (K_d) can be determined. MST has only recently been adopted for use in NRs and is very promising. However, fluorescent labeling of the protein of interest

in necessary as well as specialized equipment. Isothermal titration calorimetry (ITC) measures the difference in heat absorbed in a protein containing and reference cell upon titration of ligand. This technique measures thermodynamic parameters and thus can differentiate between enthalpic and entropic binders. In addition, ITC can give information about whether a ligand binds using induced fit or conformational selection.[7,8] Unfortunately, also this technique has disadvantages mainly caused by low throughput and high sample consumption, but also by buffer limitations. When looking at the currently available techniques, there is a need for a label-free assay which can determine the binding affinity of ligands in NRs without being biased towards knowns pocket or requiring large quantities of material or expensive equipment that is not available in every lab.

A family of assays that could be very useful in this aspect are the assays based on thermal stability. A change in thermal stability results from a change in Gibbs free energy which is caused by the creation of new molecular interactions or conformational reordering.[9] There are multiple assay formats already available, including ITC, that make use of this principle. In Table 1 an overview is given of currently available techniques using thermal stability to look at protein ligand interactions.

Inspired by the thermal stability assays, we developed a new method to deduce K_d values of NRs in absence of fluorescent dye, expensive equipment, high protein concentration or strict amino acid composition requirements. The assay is inspired by the same principle the cellular thermal shift assay (CETSA) uses, being quantifying the fraction of folded protein remaining after a heat challenge (Figure 1).[10,11] However, instead of cells, purified protein is used. By doing so, the need to detect the protein of interest using specific antibodies is eliminated. Instead, a cheap and simple Coomassie-based read-out using Bradford reagent is utilized to quantify the folded protein.[12] To deduce K_d values, the effect of a range of compound concentrations on protein stability after a fixed heat challenge is measured and evaluated via the equations proposed by Bai *et al.*.[13] As a proof of concept, we applied the assay to peroxisome proliferator-activated receptor gamma (PPARγ), which is an important drug target for type 2 diabetes. Ligand-induced coactivator recruitment towards PPARγ leads to severe side effects.[14] However, ligands that inhibit a specific phosphorylation event by stabilizing the β-sheet region have insulin sensitizing effects.[15] The abilities of the Bradford thermal stability assay (BraTSA) to identify PPARγ ligands that cause strong stabilization

Method	Principle	Advantages	Limitations
Differential scanning fluorimetry (DSF) [9,13,16–18]	Monitors protein unfolding by measuring the change in fluorescence of a dye that increases emission upon binding to exposed hydrophobic patches using increasing temperature.	Easy to implement using standard equipment and minimal optimization; high throughput possible.	Requires fluorescent dye for detection; exposed hydrophobic parts can cause high initial fluorescence values.
Isothermal denaturation (ITD) [19,20]	Measures kinetics of protein unfolding for a prolonged time at constant temperature using a reporter dye.	More sensitive than DSF; discriminates compounds with similar melting temperatures but different thermal parameters; high throughput possible.	See DSF.
Nanoscale differential scanning fluorimetry (nanoDSF) [21,22]	Monitors protein unfolding by detecting changes in the intrinsic tryptophan fluorescence resulting from alterations of the protein structure using increasing temperature.	Requires no external probes; high throughput possible.	Requires aromatic amino acids; requires specialized instrument.
Thermal shift assay circular dichroism (CD) [23,24]	Monitors changes in CD at characteristic wavelengths as a function of temperature to follow protein unfolding.	Gives information about protein secondary structure; can provide thermal parameters.	Low throughput; works in limited buffer conditions.

Method	Principle	Advantages	Limitations
Differential static light scattering (DSLS) [25–27]	Monitors changes in scattered light intensity caused by protein aggregation upon heating by using a charge-coupled device camera.	Requires no external probes; fluorescent ligands are no problem; high throughput possible.	Proteins must form aggregates; specialized instrument required.
Differential scanning calorimetry (DSC)[28,29]	Monitors difference in energy needed to heat protein and reference cell at the same rate. Resulting heat absorption peak(s) can give heat capacity, enthalpy and melting temperatures.	Can provide information about free-energy surfaces and all associated folding microstates;	High sample consumption; exact protein concentration needed to be known; proper analysis is not straightforward; specialized instrument required.
Isothermal titration calorimetry (ITC)[30]	Monitors power required to remain equal temperatures between protein and reference cells upon ligand titration.	Provides thermal parameters, binding stoichiometry, and affinity.	Time consuming; high sample consumption; specialized instrument required.
Cellular thermal shift assay (CETSA) [10,31,32]	Monitors compound induced changes in target protein aggregation in a cellular context by quantifying the amount of soluble protein after a heat challenge.	Measures in a cellular context; high throughput possible	Need for expensive antibodies; extensive optimization for each target.

Table 1 | Overview of methods using the principles of thermal stabilization to look at protein-compound interactions

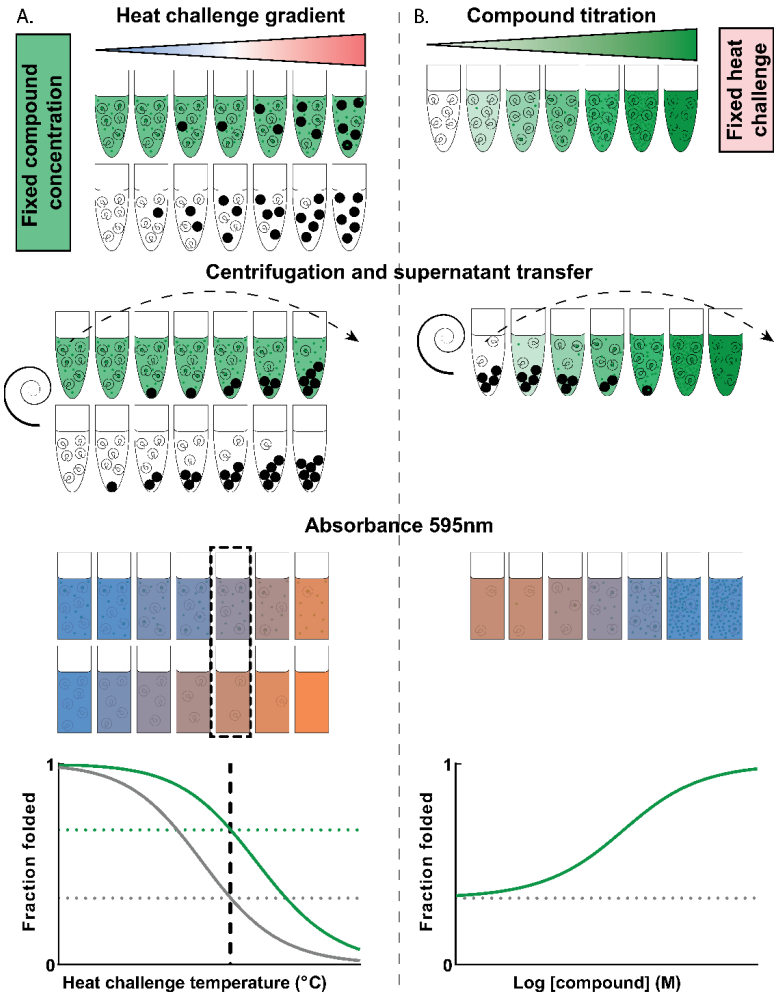

Figure 1 | Schematic representation of the assay. Folded and unfolded protein are represented as respectively white and black circles and compound is represented as green dots. (*A*) Outline heat challenge gradient experiment. Multiple aliquots at fixed compound concentration are subjected to a range of heat challenges in a PCR plate. Unfolded protein is precipitated using centrifugation and the supernatant is transferred to an optical plate with Bradford reagent after which absorbance at 595nm is measured. Absorbance is converted to fraction folded and a heat challenge temperature at which there is a big window between samples with and without compound is selected (dotted line). (*B*) Outline compound titration experiment. Aliquots with a range of compound concentrations are subjected to a heat challenge at a fixed temperature. Unfolded protein is precipitated using centrifugation and the supernatant is transferred to an optical plate with Bradford reagent after which absorbance at 595nm is measured. Absorbance is converted to fraction folded and the data is fitted using the model posed by Bai *et al*.[13]

independent of cofactor presence are shown here. Additionally, BraTSA is directly applied to the retinoic acid receptor related orphan receptor (ROR)γt without additional optimization. With this we showcase the easy implementation of BraTSA for new targets.

Results and Discussion

BraTSA can be done in two variants. The first variant of the assay, the heat challenge gradient, is mainly used to determine a suitable temperature for compound titrations. In this assay, a number of identical samples containing a fixed concentration of protein and compound or vehicle are subjected to a range of heat challenges. Each sample is identical but is heated to a different temperature for three minutes. Next, all samples are cooled down and centrifuged after which a portion of the supernatant, containing only folded protein, is transferred to an optical plate containing Bradford reagent. The measured absorbance at 595nm can then be converted to the fraction of folded protein left after the heat challenge by normalization using samples with non-heated protein as the maximum and buffer without protein as minimum. This results in an S-shaped curve with the fraction folded on the y axis, ranging from 0 to 1, and the heat challenge temperature on the x axis. This assay can be used to assess the degree of stabilization that a compound induces by looking at the shift of the melting temperature (T_m). Additionally, this assay can provide a suitable temperature for compound titrations which would be as low as possible, with a large assay window.

The second, and arguably most informative, assay is the compound titration. For this assay samples with a fixed protein concentration but increasing compound concentration are prepared. Each sample then undergoes a heat challenge at the chosen, fixed temperature after which the remaining folded protein is quantified by again centrifugation, transferring supernatant to Bradford reagent containing wells and measuring the absorbance at 595nm.

The equations described by Bai et al. are based on the competitive coupled equilibrium between protein folding-unfolding and ligand binding where both the unfolding and dissociation equilibrium constants are temperature dependent but constant at fixed temperature.[13] When combining this with mass conservation they deduce an equation for the fraction of folded protein (F_f) in terms of protein and compound concentration, F_f in absence of compound (F_{f0}) and K_d (see methods section).[13] In their original research, they used DSF to determine the F_f at a certain

temperature and compound concentration condition. We use the BraTSA as a label free and more intuitive alternative to determine F_f.

Optimizing conditions for the Bradford thermal stability assay (BraTSA)

The assay needed to be optimized regarding the protein and Bradford reagent concentrations. Protein concentration is both limiting the range of K_d values that can be fitted and is the most expensive component of the assay in most cases. Therefore, the optimal assay would use an as low amount of protein as possible, while maintaining a sufficiently high signal to background ratio (S/B) and Z' value.

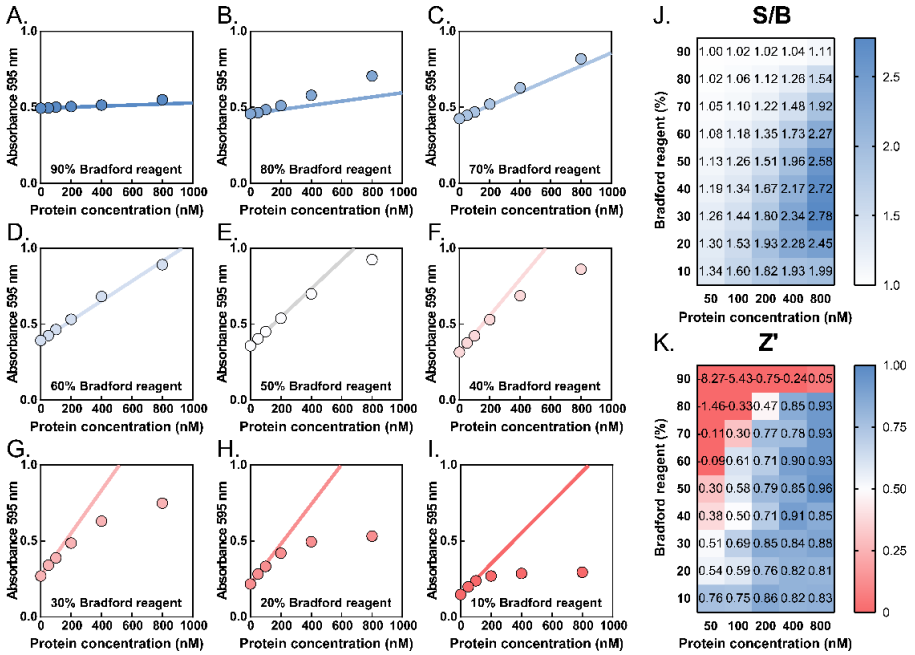

Figure 2 | Protein and Bradford reagent cross-titration optimization experiments. (A-*I*) Absorbance at 595 nm measured for all combinations. Each panel shows a fixed Bradford reagent percentage with varying PPARγ concentration. An extrapolated line through 0 and 50 nM protein is plotted to check if the absorbance scales linearly with the amount of protein added. (*J*) The signal to background (S/B) ratio is given for all measured conditions. This is determined by dividing the absorbance with protein by the absorbance without protein at the same Bradford reagent percentage. A dark blue color represents a high S/B ratio while white represents a S/B of 1. (*K*) Z' value of all measured conditions where the absorbance without protein at the same Bradford reagent percentage is used as the negative control. Red represents a low Z' value, white is a Z' value of 0.5 which is considered the threshold for a good assay, dark blue represents the perfect assay with Z'=1.0. All data shown are based on a single experiment with 3 independent replicates.

Furthermore, the absorbance should decrease linearly upon decrease in protein concentration as to directly correlate the absorbance and the fraction folded protein left after a heat challenge. For optimization, a cross-titration of Bradford reagent and protein solution was done at 9:1 through 1:9 ratios (Figure 2).

For all percentages of Bradford reagent, the signal, and with that also the S/B, increases upon increasing protein concentration. At high Bradford reagent percentages, this increase is only minor, leading to a small window unsuitable for the final assay. At very low Bradford reagent percentages, however, the absorbance change is only linear at protein concentrations that are too low for sufficient discrimination. The sweet spot for a linear assay seems to lie in the 50-70% Bradford reagent range. When minimizing the amount of protein, 60 or 70% is preferred. At 70% the S/B values are significantly lower, directing the choice to 60% Bradford reagent. By choosing a protein concentration of 600 nM, an excellent assay with Z'≥0.90 is ensured while still only using less than 120 µL of a 100 µM protein stock for a full 384-well plate.

Proof of concept of BraTSA using PPARγ with known ligands as a case-study

PPARγ is a nuclear receptor with a large binding pocket that has been shown to bind to ligands of diverse chemical nature.[33,34] In this study, PPARγ is used as a proof of concept to showcase the possibilities of the BraTSA for NRs. A heat challenge gradient was applied in presence and absence of 10 equivalents of 7 known ligands (Figure 3*A*) to decide upon a heat challenge temperature which ensures a large assay window. This yielded a melting temperature of 49.2 ± 0.3 °C for PPARγ by itself, while the compounds stabilized this to various extends towards 49.5 – 59.4 °C (Figure 3*C*). Based on these results, a heat challenge temperature of 50 °C was chosen for compound titrations. Compound titrations starting at 100 µM were made and all samples were subjected to a heat challenge at 50 °C (Figure 3*B*). For most compounds, S-shaped curves could be fitted via the calculations posed by Bai et al.[13] MRL24, which also induces a very strong thermal stabilization of 10.2 ± 0.4 °C (P<.001), binds too tightly to be fitted using the model ($EC_{50}<[P]_T$).[13] Bezafibrate, on the other hand, does not cause a significant stabilization in the heat challenge gradient experiment and also in the compound titration only causes minor stabilization at very high concentrations. When comparing the fitted K_d values with those previously measured using fluorescence polarization (FP) a clear correlation can be observed (Figure 3*D*).[35] In general, the affinities measured using BraTSA are

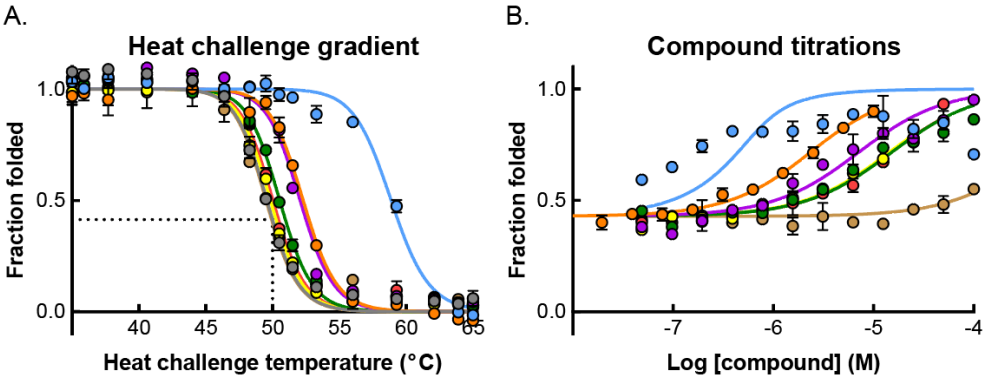

C.

	T_m (°C)	Log K_d (M)
DMSO	49.2 ± 0.3	X
MRL24	59.4 ± 0.6	<-6.8
MRL-871	53.0 ± 1.2	-6.4 ± 0.3
Tesaglitazar	51.6 ± 0.7	-5.9 ± 0.3
Rosiglitazone	50.6 ± 0.2	-5.3 ± 0.1
Troglitazone	50.1 ± 0.3	-5.2 ± 0.0
Telmisartan	50.2 ± 0.2	-5.0 ± 0.3
Bezafibrate	49.5 ± 0.0	>-3.7

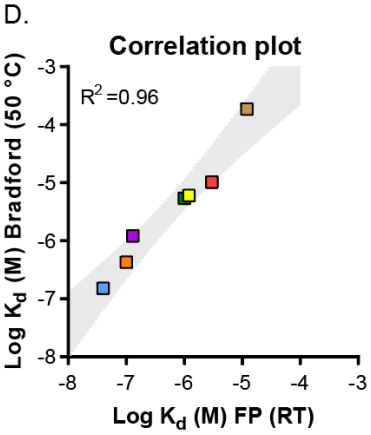

Figure 3 | Bradford reagent thermal stability assays executed on PPARγ. (*A*) Representative data of a heat challenge gradient experiment. 600 nM PPARγ was subjected a range of heat challenges in the presence or absence of 6 µM compound. 50 °C was selected as the temperature at which to perform compound titrations. (*B*) Representative data of a compound titration experiment. 600 nM PPARγ was incubated with a range of compound concentrations and subsequently subjected to a fixed heat challenge at 50 °C. The fraction folded was then calculated from the absorbance at 595 nm after transferring the supernatant after centrifugation to an optical plate with Bradford reagent. (*C*) Melting temperatures (T_m) and Log K_d values of PPARγ with all compounds. Reported values are mean and standard deviation of the fits of 3 independent experiments all run in triplicate. (*D*) Correlation between the data measured using the Bradford reagent thermal stability assay and previously published data of the same compounds on PPARγ measured with 2D FP titrations.

somewhat lower, but since they are measured at 50 °C instead of room temperature this can be explained by the temperature factor in the van 't Hoff equation.

Assessing the robustness of BraTSA against variations in protein concentration and temperature

To investigate the influence of protein concentration on the fitting of the data, MRL-871, Tesaglitazar and Rosiglitazone were titrated to 300, 600 and 1200 nM PPARγ (Figure 4*A*). Doubling the amount of protein, does not yield a significant change in the fitted K_d values. When comparing 300 and 1200 nM PPARγ for Tesaglitazar and MRL-871 there is a small but significant increase in K_d value measured (P<.001 resp P=0.007). One possible explanation for this could be the non-linear behavior observed at higher protein concentrations (Figure 2*D*). Based on these results, it might be interesting to execute the assay at lower concentrations for very strong binding compounds. However, the noise does increase (Figure S2) meaning care must be taken to ensure discrimination between folded and unfolded protein. A higher protein concentration can be used to get a bigger assay window if needed. In this situation, linearity must be ensured (Figure 2*D*). The influence of the heat-challenge temperature on the fitted K_d value is investigated as well. When applying a 48 °C heat challenge, the assay window gets very small, making it hard to reliably fit a K_d, resulting in large error bars (Figure S2, Figure 4*B*). However, overall, a clear trend is visible where for these compounds a

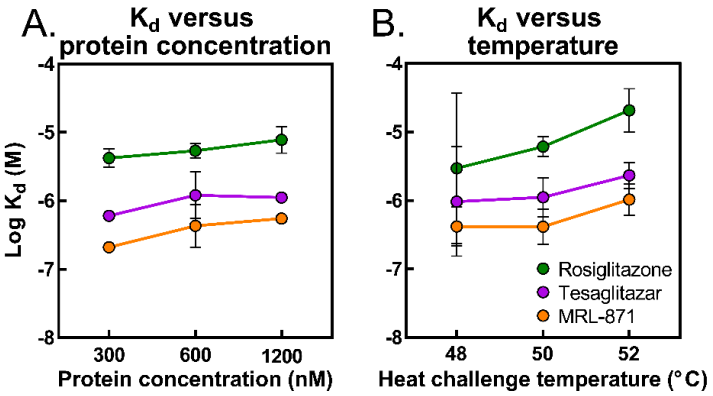

Figure 4 | Test robustness of the assay under varying conditions. (*A*) Upon alteration of protein concentration. (*B*) Upon alteration of the heat challenge temperature. The data shown are mean and standard deviation of the fits of 3 independent experiments all run in triplicate.

higher heat challenge temperature results in a weaker affinity. This is to be expected as dependent on the entropy of a protein-ligand interaction, the temperature should play a role in the measured K_d.

Showing the expandability of the assay by using BraTSA on RORγt

To illustrate the general applicability of the BraTSA assay towards other NR targets, also ligand binding to RORγt was studied. RORγt can be modulated by both agonists and inverse agonists. Additionally, RORγt has a second, allosteric binding site.[36] With the heat challenge gradient (Figure 5*A*,*C*) it can be seen that orthosteric agonist desmosterol stabilizes the NR to the greatest extent (+5.5 ± 0.5 °C, P<.001).

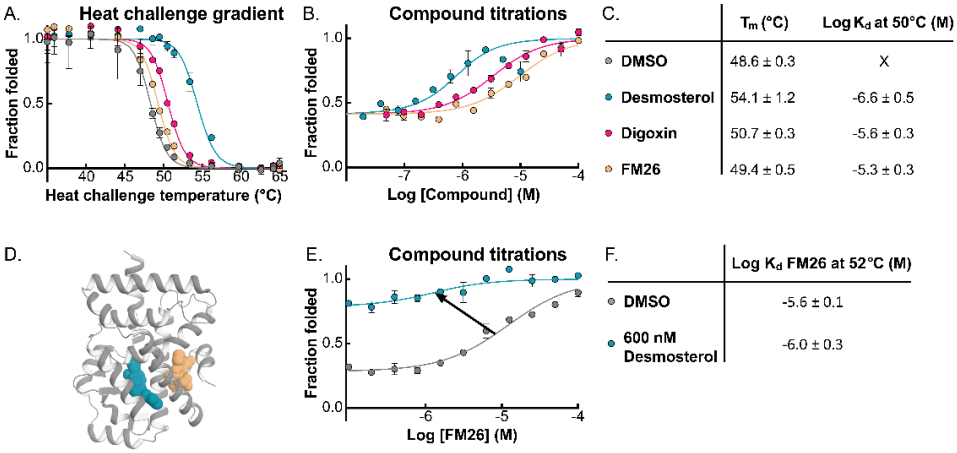

Figure 5 | Bradford reagent thermal stability assays executed on RORγt. (*A*) Representative data of a heat challenge gradient experiment. 600 nM RORγt was subjected a range of heat challenges in the presence or absence of 6 µM compound. 50 °C was selected as the temperature at which to perform compound titrations. (*B*) Representative data of a compound titration experiment. 600 nM RORγt was incubated with a range of compound concentrations and subsequently subjected to a fixed heat challenge at 50 °C. The fraction folded was then calculated from the absorbance at 595 nm after transferring the supernatant after centrifugation to an optical plate with Bradford reagent. (*C*) Melting temperatures (T_m) and Log K_d values of RORγt with all compounds. Reported values are mean and standard deviation of the fits of 3 independent experiments all run in triplicate. (*D*) Crystal structure of RORγt simultaneously bound to desmosterol and FM26 (PDB: 6T4J) protein is shown in grey, desmosterol in blue and FM26 in beige. (*E*) Representative data of a compound titration experiment. 600 nM RORγt was incubated with a range of FM26 concentrations in presence and absence of 600 nM desmosterol and subsequently subjected to a fixed heat challenge at 52 °C. (*F*) Melting temperatures (T_m) and Log K_d values of RORγt with FM26 in presence and absence of desmosterol. Reported values are mean and standard deviation of the fits of 3 independent experiments all run in triplicate.

Orthosteric inverse agonist digoxin also stabilizes RORγt (+2.1 ± 0.2 °C, P<.001) while the stabilization by allosteric inverse agonist FM26 is not significant (+0.8 ± 0.5 °C, P=.12) at 10 equivalents compound. 50 °C was selected as the temperature to do compound titrations, because this yielded the largest assay window. For all three compounds, K_d values in the high nanomolar to low micromolar range were found (Figure 5*B*,*C*). It is known that the presence of orthosteric agonist, can improve the affinity for allosteric inverse agonists in RORγt (Figure 5*D*).[36] When titrating FM26 in absence and presence of a fixed concentration of desmosterol, a significant increase in affinity is observed (P=0.02), illustrating the ability of this assay to indicate cooperative behavior (Figure 5*E,F*).

Perspectives on BraTSA

A possible concern was the question if BraTSA measures T_m or T_{agg} values and if that would impede the K_d calculation. However, assuming equilibria leads to very good to nearly perfect fits of the data that correlate really well with binding constants measured using different techniques (Figure 3*D*).[35] This would not have been possible if measuring irreversible aggregation. Also, the assumption that protein unfolding is a reversible monomolecular two-state reaction is made more often and did not result in data fitting problems in the past and literature shows that T_m and T_{agg} values are usually very comparable.[18,27,37]

Another label-free assay that could probably be used in combination with the equations of Bai *et al.* is nanoDSF. However, this technique requires the presence of tryptophan residues, nanoDSF in absence of tryptophan is only very scarcely reported, while Bradford reagent interacts with any basic amino acid.[21,38,39] The basic amino acids account for 13.3 % of the amino acid composition of proteins while tryptophan only has a 1.1% frequency making it much more probable that Bradford reagent would pick up the protein compared to nanoDSF.[40]

BraTSA measures K_d values at elevated temperatures. For the proteins and conditions used in this paper, we did isothermal experiments at ~13 °C above physiological temperature. This could lead to different K_d values than at physiological temperature. Most other biochemical assays are done at room temperature which is just as big of a deviation from physiological temperatures. In general, biochemical assays, including BraTSA, are mainly used for initial hit identification and hit to lead optimization of new compounds while the actual potency of ligands can only be determined in cells or whole organisms. In this

respect the low cost, easy implementation, and label-free conditions of BraTSA are, in our opinion, more important than the translation of the K_d values to physiological temperatures. For extrapolation of the binding data to lower temperatures, knowledge of the thermodynamic contributions of binding are required. Without resorting to other techniques, these could potentially be deduced by doing multiple compound titrations over a small range of temperatures and using a van 't Hoff plot. Alternatively, denaturants might be used to artificially lower the protein melting temperature.[13]

Conclusion

This chapter describes the development of BraTSA, a label-free thermal stability assay with the possibility to fit dissociation constants, and the application of this assay on NRs. We believe many of the assays based on protein thermal stability (Table 1) complement each other and can be used hand-in-hand to obtain additional information. The important aspects of BraTSA in this sense are that it can easily be implemented and that it does not require expensive specialized equipment, reagents or high amounts of material while still being able to measure K_d values in absence of possibly interfering labels.

In summary, BraTSA is a cheap and easy assay to obtain K_d values in a label-free environment. The assay could serve as a very easy first assay on a new protein without any optimization while still being able to derive binding constants especially in cases where cutting down on costs is important. In our own work on NRs we especially appreciate and use the ability to derive binding constants in absence of (labeled) cofactors. The data presented here serves merely as a proof of concept, while we envision a whole range of other possibilities for the future.

Experimental section

Protein expression and purification

PPARγ

A pET15b vector containing the PPARγ LBD (residues 235-505) with an N-terminal His6-tag was transformed into BL21(DE3) competent Escheria Coli (Novagen) by heat shock. A pre-culture was initiated overnight at 37 °C, 250 rpm using a single colony in 8 mL LB medium with ampicillin (100 µg/mL). This culture was transferred to 2 L LB broth supplemented with ampicillin (100 µg/mL), and antifoam (0.05%), and incubated at 37 °C until OD600 of 1.0 was achieved. To induce expression, isopropyl β-D-thiogalactoside (IPTG) (0.5 mM) was added,

and the culture was incubated at 18 °C, 180 rpm for 16 h. The bacteria were harvested using centrifugation (10,000 *g, 4 °C, 10 m) and dissolved in lysis buffer (50 mM Tris pH 8.0, 300 mM NaCl, 12.5 mM imidazole, 5% (v/v) glycerol, 1mM tris(2- carboxyethyl)phosphine (TCEP)). The bacteria were lysed using a homogenizer (Avestin Emulsiflex C3) at 15,000 psi with additional benzonase (1:10,000 v/v). The cell lysate was cleared by centrifugation (40,000 *g, 4 °C, 30 m) and purified via Ni2+ affinity column chromatography (QIAGEN, Ni-NTA Superflow Cartridge). Elution was done using elution buffer (50 mM Tris pH 8.0, 300 mM NaCl, 200 mM imidazole, 5% (v/v) glycerol, 1mM TCEP) and fractions containing high protein concentrations, determined using a NanoDrop Spectrophotometer, were combined. The purified protein was dialyzed against a storage buffer (25 mM Tris pH 8.0, 150 mM NaCl, 10% (v/v) glycerol, 5 mM DTT) overnight using 10K MWCO SnakeSkinTM dialysis tubing. Subsequently, the protein was concentrated using an Amicon Ultra centrifugal filter with a 10-kDa cutoff (Millipore), flash-frozen and stored at -80 °C until usage. Molecular weight and purity were confirmed using Quadrupole Time-of-Flight LC/MS and SDS-page.

RORγt

A pET15b vector containing the RORγt LBD (residues 265-518) with an N-terminal His6-tag was transformed into BL21(DE3) competent Escheria Coli (Novagen) by heat shock. A pre-culture was initiated, using a single colony in 8 mL LB medium supplemented with ampicillin (100 µg/mL), overnight at 37 °C 250 rpm. This culture was transferred to 500 mL TB medium with ampicillin (100 µg/mL), MgCl2 (0.5 mM), and antifoam (0.05 %), and incubated at 37 °C until OD600 nm = 1.0 was reached Isopropyl β-D-thiogalactoside (IPTG) (0.5 mM) was then added to induce expression, and the culture was incubated at 18 °C 150 rpm for 16 h. The bacteria were harvested using centrifugation (10,000 *g, 4 °C, 10 m) and dissolved in lysis buffer (50 mM Tris pH 8.0, 300 mM NaCl, 20 mM imidazole, 10 v/v% glycerol, 1mM tris(2-carboxyethyl)phosphine (TCEP)). The cells were lysed using a homogenizer (Avestin Emulsiflex C3) at 15,000 psi with additional cOmplete™, EDTA-free Protease Inhibitor Cocktail (1 tablet/50 mL buffer) and benzonase (1:10,000 v/v). The cell lysate was cleared by centrifugation (40,000 *g, 4 °C, 30 m) and purified via Ni2+ affinity column chromatography (QIAGEN, nickel-nitrilotriacetic acid (Ni-NTA) Superflow Cartridge). Elution fractions containing the protein of interest were afterwards dialyzed against a storage buffer (20 mM Tris pH 8.0, 150 mM NaCl, 10 v/v% glycerol, 5 mM DTT) overnight and, subsequently, stored at -80 °C until usage. Molecular weight and purity were assessed using Quadrupole Time-of-Flight LC/MS and SDS-page.

Bradford-reagent-based thermal stability assay

Protein concentration and Bradford reagent percentage cross titration

For the cross titration, a 1:2 serial dilution of protein was made in assay buffer (150 mM NaCl, 10 mM HEPES, pH 7.5) starting at 3.2 µM. Protein and Bradford reagent were combined in a clear, non-treated, flat bottom 384-well plate (Nunc™) with a total volume of 100 µL in each well. The volumes of both components ranged from 10 to 90 µL with 10 µL increments. All combinations were prepared in triplicate. The plate was shaken for 10 seconds and incubated for 10 minutes as described by the supplier of the Bradford reagent after which absorbance at 595 nm was measured using 75 flashes per well(Tecan spark™ 10M). Linearity plots were made by fitting a straight line through the mean of the datapoints at 0 and 50 nM protein of each Bradford reagent percentage. Deviations from this line were inspected visually. The signal to background ratio (S/B) of each combination was determined by dividing the average absorbance at 595 nm by the average absorbance at the same Bradford percentage in absence of protein. Z' values were determined via:

$$Z' = 1 - \frac{3 * (\sigma_{sample} + \sigma_{background})}{\left|\mu_{sample} - \mu_{background}\right|}$$

Where σ_{sample} and $\sigma_{background}$ are the standard deviations of the samples respectively with and without protein at the same Bradford reagent percentage. μ_{sample} and $\mu_{background}$ are the average absorbances with and without protein at the same percentage of Bradford reagent. Both S/B and Z' were determined for every combination of protein concentration and Bradford percentage.

Centrifuge time and speed check

Centrifuge time and speed were compared to the standard used in cellular thermal shift assays (CETSA) (20 minutes, 20,000*g). 60 µL Bradford reagent was added to each well of a clear, non-treated, flat bottom 384-well plate (Nunc™). Protein was diluted to 600 nM in assay buffer (150 mM NaCl, 10 mM HEPES, pH 7.5). Multiple 50 µL samples of both protein solution and plain buffer were added to two clear, rigid 96-well PCR plates (B70671, BIOplastics). One of these plates was subjected to a heat challenge of 60 °C for three minutes followed by 25 °C for three minutes in a CFX96 Touch Real-Time PCR Detection System (Bio-Rad). After the heat challenge, 3*40 µL of both protein and plain buffer from both the heated and the non-heated PCR plate were directly transferred to separate wells of the optical plate with Bradford reagent for absorbance determination without centrifugation. 4*40 µL protein from the heated plate was combined in an Eppendorf tube for high-speed centrifugation. 160 µL of non-heated protein and buffer were added to a second and third Eppendorf tube. The three Eppendorf tubes were centrifuged in a precooled Eppendorf centrifuge (20,000*g, 4 °C, 20 m). Both PCR plates were centrifuged

in a precooled tabletop centrifuge with plate inserts (4700 rpm/3818*g, 4 °C, 15 m). 3*40 µL of all centrifuged conditions were transferred to separate wells of the optical plate with Bradford reagent without touching the bottom of the PCR plate or Eppendorf tube. The optical plate was shaken for 10 seconds and incubated for 10 minutes after which absorbance at 595 nm was measured using 75 flashes per well (Tecan spark™ 10M). The mean and standard deviation of the triplicates were calculated and plotted.

Heat challenge gradient

Stocks with 600 nM protein, optionally 6 µM compound and a final concentration of 2% DMSO were prepared in assay buffer (150 mM NaCl, 10 mM HEPES, pH 7.5). Of each stock, 50 µL samples were transferred to two columns and all rows of two clear, rigid 96-well PCR plates (B70671, BIOplastics). Both plates were subjected to a three-minute heat challenge followed by three minutes at 25 °C in a CFX96 Touch Real-Time PCR Detection System (Bio-Rad). For the first plate, the heat challenges ranged from 35 till 49.5 °C with lower heat challenges for the bottom rows and gradually higher heat challenge temperatures for the top rows. For the second plate a similar protocol ranging from 50.5 till 65 °C was used. Both plates were subsequently centrifuged (4700 rpm/3818*g, 4 °C, 15 m). 60 µL Bradford reagent was added to all used wells of a clear, non-treated, flat bottom 384-well plate (Nunc™). After centrifugation, 40 µL out of every well of the PCR plates was transferred to Bradford reagent containing wells of the optical plate with special attention to not touch the bottom of the wells during aspiration. The optical plate was shaken for 10 seconds and incubated for 10 minutes after which absorbance at 595 nm was measured using 75 flashes per well (Tecan spark™ 10M).

Compound titrations

1:2 serial dilutions of compound to 600 nM protein were made in non-binding, flat bottom 96-well plates (150 mM NaCl, 10 mM HEPES, pH 7.5, 2% DMSO) with a final volume of 160 µL per well. Out of each well, two times 50 µL was transferred to a clear, rigid 96-well PCR plate (B70671, BIOplastics). The PCR plate was subjected to a three-minute heat challenge at a previously determined, fixed temperature, followed by three minutes at 25 °C in a CFX96 Touch Real-Time PCR Detection System (Bio-Rad). The plate was subsequently centrifuged (4700 rpm/3818*g, 4 °C, 15 m). 60 µL Bradford reagent was added to all used wells of a clear, non-treated, flat bottom 384-well plate (Nunc™). After centrifugation, 40 µL out of every well of the PCR plate was transferred to Bradford reagent containing wells of the optical plate with special attention to not touch the bottom of the wells during aspiration. The optical plate was shaken for 10 seconds and incubated for 10 minutes after which absorbance at 595 nm was measured using 75 flashes per well (Tecan spark™ 10M).

Data fitting and K_d determination

Data fitting of the BraTSA data was done in two steps. First, raw absorbance data was transformed to fraction folded protein (Ff) by normalization via:

$$F_f = \frac{A_{sample} - A_{no\ protein}}{A_{no\ heat} - A_{no\ protein}}$$

In this equation A_{sample} is the absorbance of a sample with known heat challenge temperature and compound concentration. $A_{no\ protein}$ is the average absorbance of three samples with just buffer, used as a negative control. $A_{no\ heat}$ is the absorbance of a sample at the same compound concentration as the sample, but without application of a heat challenge.

Next, for the heat challenge gradient experiments, S-shaped curves are fitted in GraphPad Prism via:

$$Y = \frac{1}{1 + \frac{T_m}{X}^{Hillslope}}$$

where T_m is the melting temperature and $Hillslope$ is the slope of all curves. The Hillslope is restricted to be shared for all melting curves measured withing a single experiment. The bottom and top of the curve are fixed at respectively 0 and 1 indicating that a low enough temperature would leave all protein folded while a high temperature could unfold all protein.

For the compound titrations, the expression described by Bai *et al*. was used for the fit of K_d values. This was done in GraphPad Prism via:

$$Y = 1 - \frac{1}{1 + \frac{F_{f0}}{1 - F_{f0}} * \left(1 + \frac{\frac{1}{2} * \left(\left(X - [P]_T - K_d * \left(1 + \frac{1 - F_{f0}}{F_{f0}}\right)\right) + \sqrt{\left([P]_T - X + K_d * \left(1 + \frac{1 - F_{f0}}{F_{f0}}\right)\right)^2 + 4 * X * K_d \left(1 + \frac{1 - F_{f0}}{F_{f0}}\right)}\right)}{K_d}\right)}$$

where F_{f0} is the fraction of folded protein in absence of compound. This factor is constrained to be shared for all curves measured withing a single experiment. $[P]_T$ is the concentration of protein (in molar) used in an experiment. This value needs to be entered before fitting the curve. Finally, K_d is the dissociation constant in molar and is fitted for each individual compound. All experiments were performed three times in duplicate and the reported values are the geometrical mean and standard deviation of the combined fits of the three experiments.

Supporting information

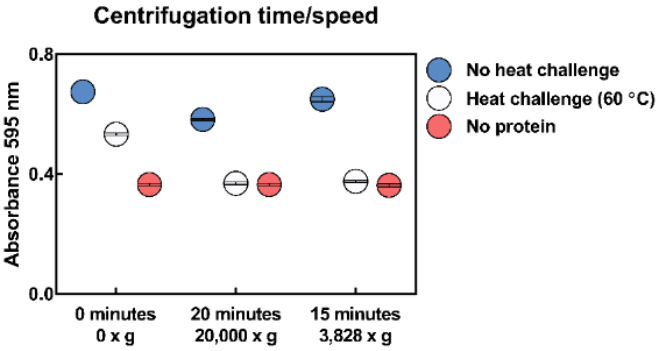

Figure S1 | Centrifuge time and speed check. PPARγ (600 nM) with and without a heat challenge at 60 °C is centrifuged and the protein in the supernatant is quantified using Bradford reagent to determine if this effectively pellets unfolded protein. The centrifuge time and speed mostly used for CETSA purposes (20 minutes at 20,000 *g) is compared to one more suitable for BraTSA (15 minutes at 3828 *g).

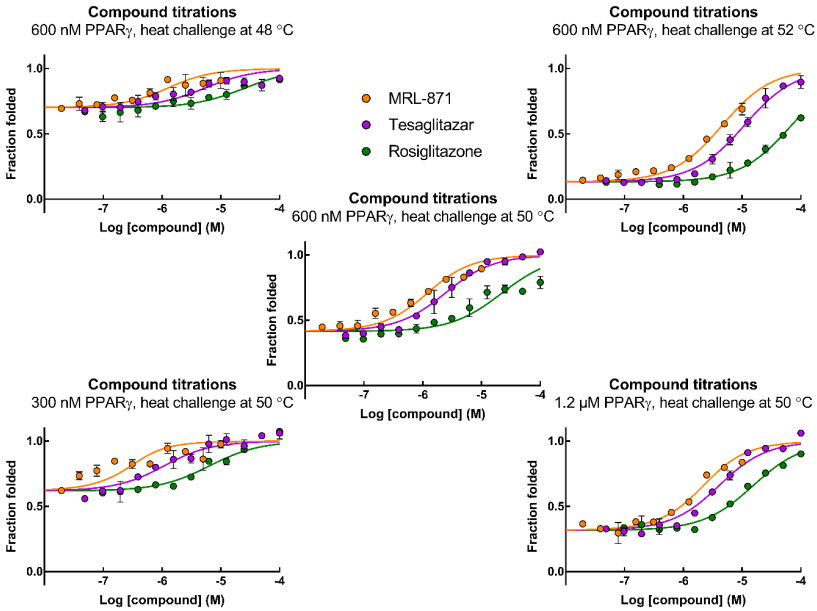

Figure S2 | Test robustness of the assay under varying conditions. Representative data of compound titration experiments. 300, 600 or 1200 nM PPARγ was incubated with a range of compound concentrations and subsequently subjected to a fixed heat challenge at 48, 50 or 52 °C. The fraction folded was then calculated from the absorbance at 595 nm after transferring the supernatant after centrifugation to an optical plate with Bradford reagent. *Top*, altering the heat challenge temperature. *Bottom*, altering the protein concentration.

References

1. Zhao, L., Zhou, S. & Gustafsson, J.-Å. Nuclear Receptors: Recent Drug Discovery for Cancer Therapies. *Endocr. Rev.* **40**, 1207–1249 (2019).
2. Zhang, C. *et al.* Allosteric binding on nuclear receptors: Insights on screening of non-competitive endocrine-disrupting chemicals. *Environ. Int.* **159**, 107009 (2022).
3. Liu, X. *et al.* Receptor-binding affinities of bisphenol A and its next-generation analogs for human nuclear receptors. *Toxicol. Appl. Pharmacol.* **377**, 114610 (2019).
4. Homola, J., Yee, S. S. & Gauglitz, G. Surface plasmon resonance sensors: review. *Sens. Actuators B Chem.* **54**, 3–15 (1999).
5. Cheskis, B. & Freedman, L. P. Modulation of Nuclear Receptor Interactions by Ligands: Kinetic Analysis Using Surface Plasmon Resonance. *Biochemistry* **35**, 3309–3318 (1996).
6. Jerabek-Willemsen, M., Wienken, C. J., Braun, D., Baaske, P. & Duhr, S. Molecular Interaction Studies Using Microscale Thermophoresis. *ASSAY Drug Dev. Technol.* **9**, 342–353 (2011).
7. Zhou, H.-X. From Induced Fit to Conformational Selection: A Continuum of Binding Mechanism Controlled by the Timescale of Conformational Transitions. *Biophys. J.* **98**, L15–L17 (2010).
8. Shang, J. & Kojetin, D. J. Structural mechanism underlying ligand binding and activation of PPARγ. *Struct. Lond. Engl. 1993* **29**, 940-950.e4 (2021).
9. Gao, K., Oerlemans, R. & Groves, M. R. Theory and applications of differential scanning fluorimetry in early-stage drug discovery. *Biophys. Rev.* **12**, 85–104 (2020).
10. Molina, D. M. *et al.* Monitoring Drug Target Engagement in Cells and Tissues Using the Cellular Thermal Shift Assay. *Science* **341**, 84–87 (2013).
11. Shaw, J. *et al.* Determining direct binders of the Androgen Receptor using a high-throughput Cellular Thermal Shift Assay. *Sci. Rep.* **8**, 1–11 (2018).
12. Bradford, M. M. A rapid and sensitive method for the quantitation of microgram quantities of protein utilizing the principle of protein-dye binding. *Anal. Biochem.* **72**, 248–254 (1976).
13. Bai, N., Roder, H., Dickson, A. & Karanicolas, J. Isothermal Analysis of ThermoFluor Data can readily provide Quantitative Binding Affinities. *Sci. Rep.* **9**, 1–15 (2019).
14. Kung, J. & Henry, R. R. Thiazolidinedione safety. *Expert Opin. Drug Saf.* **11**, 565–579 (2012).
15. Choi, J. H. *et al.* Antidiabetic actions of a non-agonist PPARγ ligand blocking Cdk5-mediated phosphorylation. *Nature* **477**, 477–481 (2011).
16. Pantoliano, M. W. *et al.* High-density miniaturized thermal shift assays as a general strategy for drug discovery. *J. Biomol. Screen.* **6**, 429–440 (2001).
17. Lo, M.-C. *et al.* Evaluation of fluorescence-based thermal shift assays for hit identification in drug discovery. *Anal. Biochem.* **332**, 153–159 (2004).
18. Niesen, F. H., Berglund, H. & Vedadi, M. The use of differential scanning fluorimetry to detect ligand interactions that promote protein stability. *Nat. Protoc.* **2**, 2212–2221 (2007).
19. Sarver, R. W., Rogers, J. M. & Epps, D. E. Determination of Ligand-MurB Interactions by Isothermal Denaturation: Application as a Secondary Assay to Complement High Throughput Screening. *J. Biomol. Screen.* **7**, 21–28 (2002).

20. Senisterra, G. A., Soo Hong, B., Park, H.-W. & Vedadi, M. Application of High-Throughput Isothermal Denaturation to Assess Protein Stability and Screen for Ligands. *J. Biomol. Screen.* **13**, 337–342 (2008).
21. Baaske, P. & Duhr, S. System and method for a seal-free tempering of capillaries. (2016).
22. Magnusson, A. O. *et al.* nanoDSF as screening tool for enzyme libraries and biotechnology development. *FEBS J.* **286**, 184–204 (2019).
23. Greenfield, N. J. Using circular dichroism collected as a function of temperature to determine the thermodynamics of protein unfolding and binding interactions. *Nat. Protoc.* **1**, 2527–2535 (2006).
24. Létourneau, D., LeHoux, J.-G. & Lavigne, P. Determination of Ligand Binding Affinity and Specificity of Purified START Domains by Thermal Shift Assays Using Circular Dichroism. in *Intracellular Lipid Transport: Methods and Protocols* (ed. Drin, G.) 293–306 (Springer, 2019). doi:10.1007/978-1-4939-9136-5_20.
25. Kurganov, B. I. Kinetics of Protein Aggregation. Quantitative Estimation of the Chaperone-Like Activity in Test-Systems Based on Suppression of Protein Aggregation. *Biochem. Mosc.* **67**, 409–422 (2002).
26. Senisterra, G., Markin, E., Yamazaki, K. & Hui, R. Methods and apparatuses for characterizing stability of biological molecules. (2004).
27. Senisterra, G. A. *et al.* Screening for Ligands Using a Generic and High-Throughput Light-Scattering-Based Assay. *J. Biomol. Screen.* **11**, 940–948 (2006).
28. Sanchez-Ruiz, J. M. Probing free-energy surfaces with differential scanning calorimetry. *Annu. Rev. Phys. Chem.* **62**, 231–255 (2011).
29. Johnson, C. M. Differential scanning calorimetry as a tool for protein folding and stability. *Arch. Biochem. Biophys.* **531**, 100–109 (2013).
30. Velázquez-Campoy, A., Ohtaka, H., Nezami, A., Muzammil, S. & Freire, E. Isothermal Titration Calorimetry. *Curr. Protoc. Cell Biol.* **23**, 17.8.1-17.8.24 (2004).
31. Jafari, R. *et al.* The cellular thermal shift assay for evaluating drug target interactions in cells. *Nat. Protoc.* **9**, 2100–2122 (2014).
32. Seashore-Ludlow, B. *et al.* Quantitative Interpretation of Intracellular Drug Binding and Kinetics Using the Cellular Thermal Shift Assay. *Biochemistry* **57**, 6715–6725 (2018).
33. Wang, L. *et al.* Natural product agonists of peroxisome proliferator-activated receptor gamma (PPARγ): a review. *Biochem. Pharmacol.* **92**, 73–89 (2014).
34. Garcia-Vallvé, S. *et al.* Peroxisome Proliferator-Activated Receptor γ (PPARγ) and Ligand Choreography: Newcomers Take the Stage. *J. Med. Chem.* **58**, 5381–5394 (2015).
35. Vink, P. de *et al.* Cooperativity as Quantification and Optimization Paradigm for Nuclear Receptor Modulators. *Chem. Sci.* (2022) doi:10.1039/D1SC06426F.
36. de Vries, R. M. J. M., Meijer, F. A., Doveston, R. G., Leijten-Van de Gevel, I. A. & Brunsveld, L. Cooperativity between the orthosteric and allosteric ligand binding sites of RORγt. *Proc. Natl. Acad. Sci. U. S. A.* **118**, (2021).
37. Kopec, J. & Schneider, G. Comparison of fluorescence and light scattering based methods to assess formation and stability of protein–protein complexes. *J. Struct. Biol.* **175**, 216–223 (2011).

38. nanoDSF thermal unfolding analysis of proteins without tryptophan residues. https://resources.nanotempertech.com/application-notes/application-note-nt-pr-007-unfolding-without-tryptophan?locale=en_us.
39. Real-Hohn, A., Groznica, M., Löffler, N., Blaas, D. & Kowalski, H. nanoDSF: In vitro Label-Free Method to Monitor Picornavirus Uncoating and Test Compounds Affecting Particle Stability. *Front. Microbiol.* **11**, 1442 (2020).
40. Itzkovitz, S. & Alon, U. The genetic code is nearly optimal for allowing additional information within protein-coding sequences. *Genome Res.* **17**, 405–412 (2007).
41. Layton, C. J. & Hellinga, H. W. Thermodynamic Analysis of Ligand-Induced Changes in Protein Thermal Unfolding Applied to High-Throughput Determination of Ligand Affinities with Extrinsic Fluorescent Dyes. *Biochemistry* **49**, 10831–10841 (2010).

Chapter 6

Epilogue

Abstract

In this thesis several topics surrounding allosteric pockets of nuclear receptors are investigated using mutagenesis and assay development as the major tools. With this, the uniqueness of the allosteric pocket of RORγt was confirmed, an attempt of creating such a pocket in RORα and RORβ as a chemical biological tool was made, a novel and promising compound binding mode in PPARγ was discovered and a new thermal stability assay for nuclear receptors was developed. This final chapter aims to review the obtained results and suggest future possibilities arising from these findings. This way the path is laid out to create a novel assay format for discovering allosteric RORγt binders, a new approach is suggested for pocket insertion into RORα and RORβ, advise is given for the development of selective compounds for either RORγt or PPARγ and additional possibilities for BraTSA are described.

Introduction

The allosteric modulation of NRs is a promising strategy for selectively influencing NR regulated processes. In this thesis we aimed to increase our understanding about the functioning of allosteric pockets and develop methods to investigate them. One of the receptors standing central in this thesis is RORγt. This receptor is a very interesting target for inhibition in case of autoimmune disorders.[1] An allosteric pocket in RORγt was found and a lot of effort is put into the development of inverse agonist that bind this pocket. Our aim was to take a step back and first look into the formation of this pocket.

In **chapter 2** we used mutagenesis to find the most crucial residues for pocket formation. The combination of a glutamine residue at position 487 and a long H11' appeared essential for forming the allosteric pocket. This combination is unique for RORγt within the NR superfamily and with this the uniqueness of this is proven. In **chapter 3** we then tried to incorporate a similar pocket into the highly similar RORα and RORβ. This could yield an alternative strategy of blocking the functions of these receptors giving more opportunities to study the physiological functions of these receptors. Both rational design and extensive mutagenesis were unsuccessful in creating such a pocket, putting extra emphasis on the uniqueness of the pocket in RORγt.

In **chapter 4** we investigated the off-target activity of RORγt inverse agonist MRL-871 on PPARγ. Understanding the reasons for these unselective effects could potentially help with the development of more selective compounds for RORγt in the future. The binding mode of MRL-871 in PPARγ was elucidated and did not resemble any existing compound binding modes in this receptor. Additionally, MRL-871 stabilizes PPARγ effectively with only limited cofactor binding yielding a very interesting starting point for potential type II diabetes treatment.

Finally, a large issue for looking at protein target interactions is finding the best assay for the intended purpose. Thermal shift assays give information about the protein stability increase caused by a ligand. Additionally, they could be used to quantify binding affinity. Various assays already exist, all coming with their individual pros and cons. In **chapter 5** we expanded the toolbox with an additional assay, BraTSA, which as a proof of concept was shown to work very well on NR ligand interactions. This assay uses the same thermodynamical principles of other

thermal stability assays, but does not rely on labels, potentially interfering with compound binding, or expensive machines.

In this last chapter, I want to reflect on the research done in these previous chapters and give some recommendations for future projects.

Mutagenesis as a tool for selective allosteric compound discovery in RORγt

In **chapter 1**, it was described that one of the difficulties with finding allosteric modulators for NRs is the lack of assays that are specifically designed to identify allosteric ligands. If one would screen a library of compounds on a typical NR, ligands that can bind both to the orthosteric and allosteric sites could potentially be found. The discrimination between both binding sites, based on assay output, would typically not be possible (Figure 1, *top*). The very nature of the orthosteric binding site, evolutionary developed to bind to small molecules, will typically overrule observations of ligand binding events to the allosteric site. A possible way to prevent this, is by blocking the orthosteric pocket. This would make it impossible for compounds to bind to this pocket, forcing compound effects to function solely via the allosteric site. In an assay featuring such a RORγt construct with an occluded orthosteric site, compounds thus must bind allosterically (Figure 1, *bottom*).

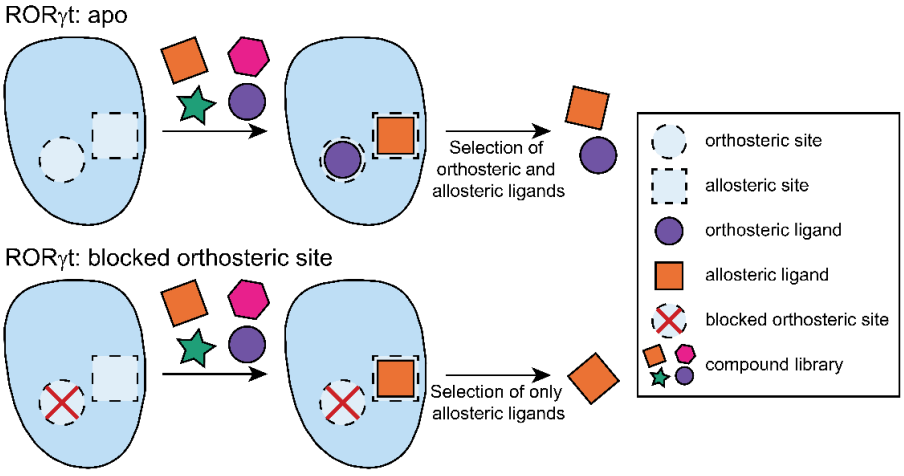

Figure 1 | Schematic representation of the effect of RORγt orthosteric site occlusion. *Top,* When both binding sites are available, both orthosteric and allosteric ligands will be identified. *Bottom,* When the orthosteric pocket is blocked, only allosteric ligands will be selected.

One strategy to block the orthosteric pocket is via covalent attachment of a molecular probe that fills the pocket. This strategy was first applied to PPARγ and later expanded to RORγt.[2–4] Meijer *et al.* discovered that covalent attachment of GW9662 inspired compounds to Cys-320 in the LBD of RORγt resulted in a protein incapable of being targeted by orthosteric compounds. Allosteric compounds remained able to bind and sometimes even showed increased affinities, probably caused by the cooperativity between the orthosteric and allosteric binding pockets of RORγt.[5] Two of the difficulties of the method to block the orthosteric pocket of RORγt with a chemically reactive probe, is that the ligation needs to be 100% complete and without affecting other cysteine residues. Therefore, I would like to propose a different strategy for blocking the orthosteric binding pocket of RORγt, by utilizing mutagenesis.

Mutagenesis could be used to replace small amino acids pointing into the orthosteric pocket by larger residues creating bulk and preventing compounds from binding. In a preliminary study, Val-376 and Ile-400 were identified in addition to Cys-320, which has already proven to be an interesting site for orthosteric pocket occlusion, as residues that could be promising to apply this strategy (Figure 2*A*). These residues are relatively small and point into the orthosteric pocket from three different directions. Additionally, they do not seem to have important interactions with other amino acids which would make them essential for proper folding or functioning. To find out if creating bulk at these positions would lead to a protein with a dysfunctional orthosteric pocket, but capable of binding allosteric ligands, a series of mutants was made where individual residues and various combinations were mutated to phenylalanine's (Figure 2*B*).

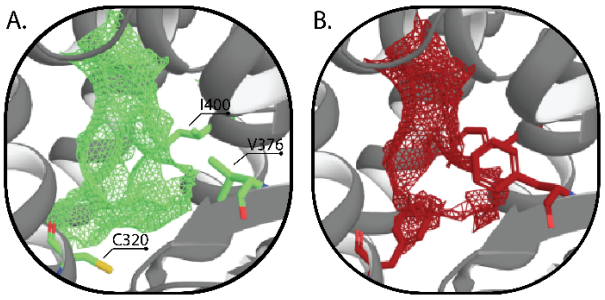

Figure 2 | Close up of the orthosteric binding site of RORγt. Small residues that point into the pocket are indicated. The available cavity is shown as a mesh. (*A*) The native orthosteric site with interesting residues indicated in green. (*B*) Model of the mutated orthosteric site where the residues are mutated to phenylalanines (red).

To assess the functioning of these proteins, HTRF protein titrations were done using fixed concentrations of labeled SRC1b2 peptide or MRL-871 probe (Figure 3). When titrating the proteins to the peptide a clear decrease in affinity is seen upon increasing mutations. This means that the mutations have a negative effect on the constitutive activity of RORγt. Such a lower constitutive activity could lead to a smaller assay window for inverse agonist screening and is therefore undesirable. The C320F mutation only has a small effect, but addition of V376F or especially I400F strongly lowers the cofactor affinity of RORγt. Titrating protein to the allosteric probe AlexaFluor-MRL leads to an increase in signal for all proteins, implying continued functionality of the allosteric pocket. The affinity seems slightly decreased compared to the wildtype protein, but since these proteins would be used merely as a tool to identify interesting compounds and not for affinity determination this does not have to be an issue.

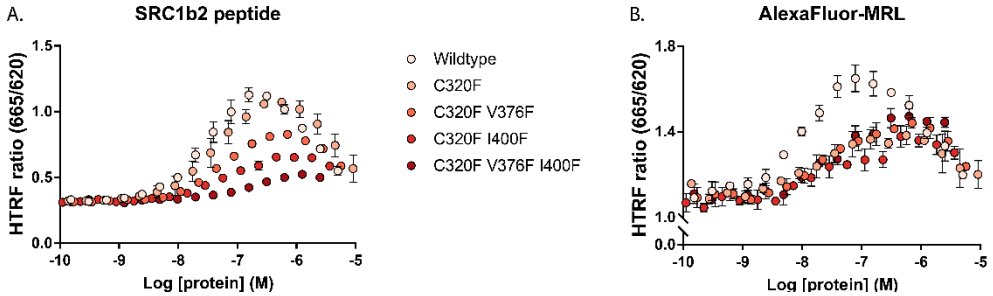

Figure 3 | Homogeneous time-resolved FRET (HTRF) protein binding curves verify cofactor and fluorescent probe binding. (*A*) HTRF assay where RORγt (mutant) is titrated to biotin-SRC1b2 peptide (100 nM). Affinity and total intensity are reduced upon increasing mutations. (*B*) HTRF assay where RORγt (mutant) is titrated to AlexaFluor-MRL (100 nM).

After establishing cofactor binding, HTRF compound titrations to a fixed concentration of peptide and protein (100 nM) could be done (Figure 4). For the wildtype, all compounds, both orthosteric and allosteric, show the expected changes in signal and affinities. The C320F mutant shows a slightly decreased baseline signal as can be explained by the slightly lower cofactor affinity (Figure 3*A*). The orthosteric agonists still bind, although with a ~20-fold decrease in potency. This means this mutation is not enough to fully block the orthosteric pocket. Digoxin, an orthosteric inverse agonist that is roughly twice as large as cholesterol, is completely blocked from binding, indicating that bigger compounds are inhibited by this mutation. When looking at the allosteric compounds, their affinity is barely affected by this mutation. MRL-871 binds with really similar potency as for the

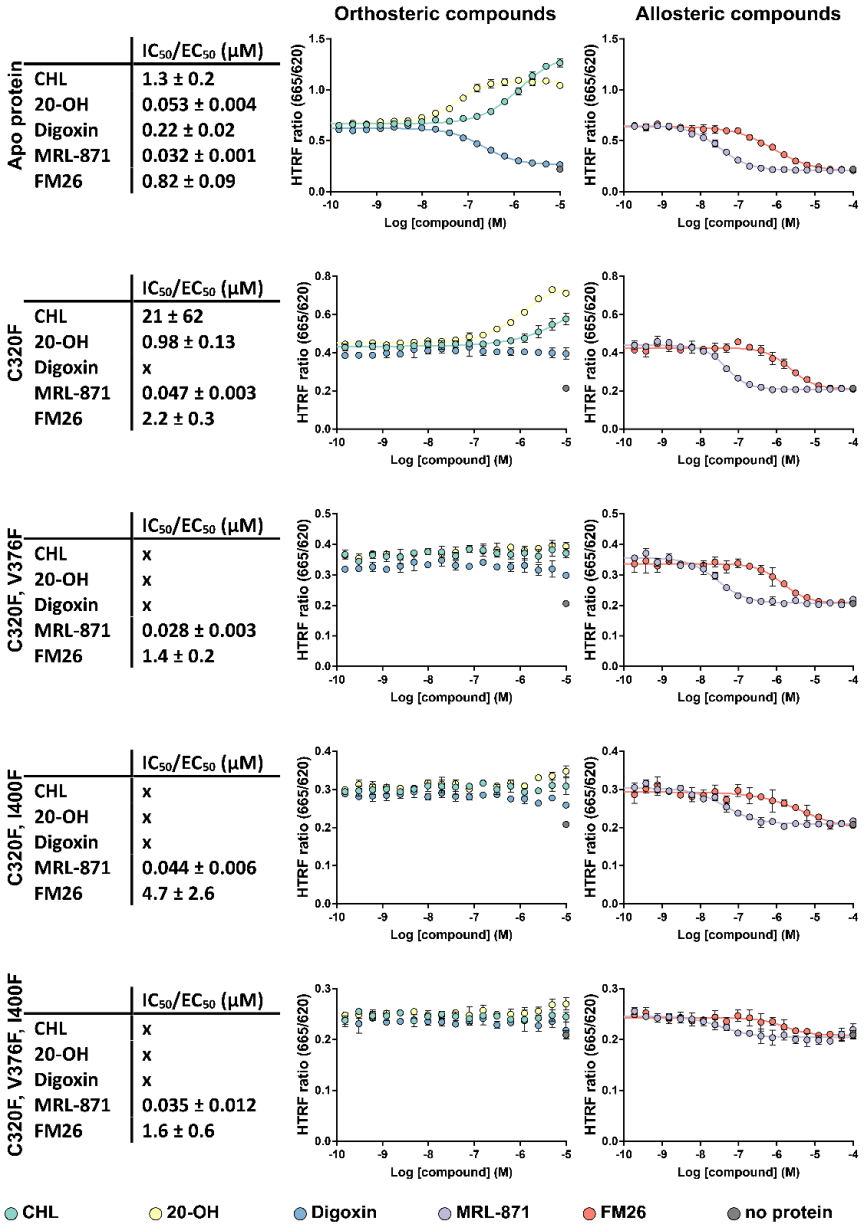

Figure 4 | Homogeneous time-resolved FRET (HTRF) compound binding curves show mutations effectively block the orthosteric binding pocket. HTRF coactivator recruitment of RORγt (mutant) LBD (100 nM) and SRC1b2 peptide (100 nM) with ligand titration. *Top*, apo protein binds both orthosteric and allosteric compounds. *Middle and bottom*, mutations in the orthosteric pocket increasingly block orthosteric pocket binding and decrease the assay window while allosteric compounds keep binding with high affinity. (*n* = 1, data shown as mean ± s.d. of one experiment in triplicate).

wildtype protein. The affinity of FM26 is slightly decreased which could be caused by the pyrrole group of FM26 that lies in closer proximity to the orthosteric pocket.[6] The other mutants show really similar behavior, but are capable of fully blocking orthosteric compound binding. However, since their cofactor affinity is even lower, the assay window is decreased. This means that these constructs could probably benefit from using a higher protein concentration.

In summary, these results give a nice first indication for the usefulness of mutagenesis to block the orthosteric pocket for allosteric compound hit finding. For future research I would suggest optimizing the HTRF assay for the specific mutants in order to potentially increase the assay windows. Furthermore, I would look into the isolated V376F and I400F mutants as opposed to only assessing them in combination with C320F. Additionally, it could be interesting to look into different amino acids for the point mutations. Right now, phenylalanine is chosen as the replacement for all residues, but potentially other large residues such as tyrosine or tryptophan could also work.

Exploring the difference in the allosteric region of the ROR isoforms in a systematic manner

In **chapters 2 and 3** the determinants of the allosteric region of RORγt were investigated using mutagenesis and an attempt was made to create a similar pocket into RORα and RORβ. These chapters made clear that the allosteric pocket as present in RORγt cannot readily be formed in RORα or RORβ. However, it would still be interesting to artificially create such a pocket in these receptors as a tool to investigate their physiological functions. For this purpose, and with the knowledge gained in these chapters, I would advise for a more systematic approach to create an allosteric pocket in RORα and RORβ.

For RORβ a rational approach was taken where presumably crucial residues were pinpointed and changed to their RORγt counterparts. This resulted in functional receptors, presumably due to the relatively small changes, but did not yield allosteric pocket formation. For RORα a blunter approach was taken, where whole regions of RORγt were inserted into this receptor. This approach led to severely mutated proteins that were hard to express and purify and lost functionality. Through this experience we learned that both extreme approaches were unsuccessful to create an allosteric pocket into these receptors. For this reason, a

more systematic approach, where big changes are reduced to their necessary elements, is suggested.

In **chapter 2**, crucial residues for allosteric pocket formation were elucidated, leading to proving the uniqueness of this pocket for RORγt. However, it is very much possible that there are more residues or regions where certain alterations are incompatible with allosteric pocket formation. By incorporating regions of RORα or RORβ into RORγt, the compatibility of these stretches with allosteric pocket formation can be easily tested. An example for this is testing the compatibility of all residues in the H11' (Figure 5). For these experiments, the whole H11' of RORβ was swapped for that of RORγt and vice versa. Next, their binding to SRC1b2 peptide and AlexaFluor-MRL probe were tested using HTRF. It can be concluded that the affinity for SRC1b2 peptide is not affected majorly by these mutations. However, when titrating each protein to AlexaFluor-MRL, only the unaltered RORγt protein shows binding. This means that there are residues within the H11' of RORβ that are incompatible with allosteric pocket formation, but just inserting the H11' of RORγt does not yield a RORβ protein with a functioning allosteric pocket.

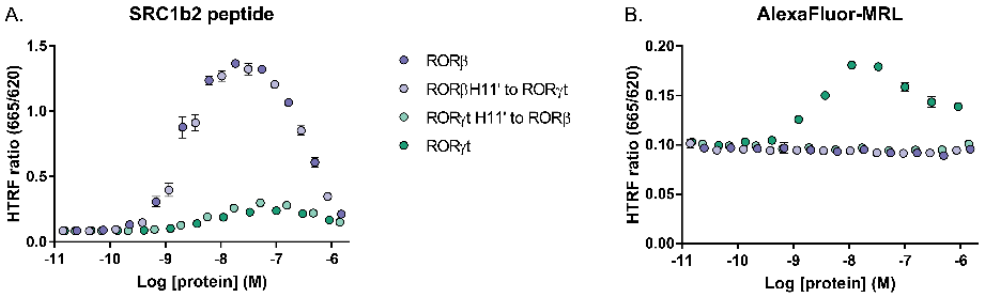

Figure 5 | Homogeneous time-resolved FRET (HTRF) protein binding curves check cofactor and fluorescent probe binding. (*A*) HTRF assay where protein is titrated to biotin-SRC1b2 peptide (20 nM). The mutations only minorly change the affinity of the proteins. (*B*) HTRF assay where protein is titrated to AlexaFluor-MRL (100 nM). Only native RORγt is able to bind this probe.

By only inserting the H11' of RORγt into RORβ, the conclusion would have been that there might be important residues in this stretch, but these alone are not able to create a functional allosteric pocket. By looking from the side of RORγt, way more information is gained. This valuable information can be used to pinpoint the important residues more sophisticatedly. I would suggest using this approach on both RORα and RORβ and exchange more regions within proximity of the allosteric

pocket with RORγt (Figure 6). I would not recommend doing these mutations additively, but instead explore one site at a time. This way the chance of creating malfunctioning receptors is reduced. Furthermore, I would suggest incorporating the Glu-487 residue in each construct, since this amino acid has been proven to be crucial.[7]

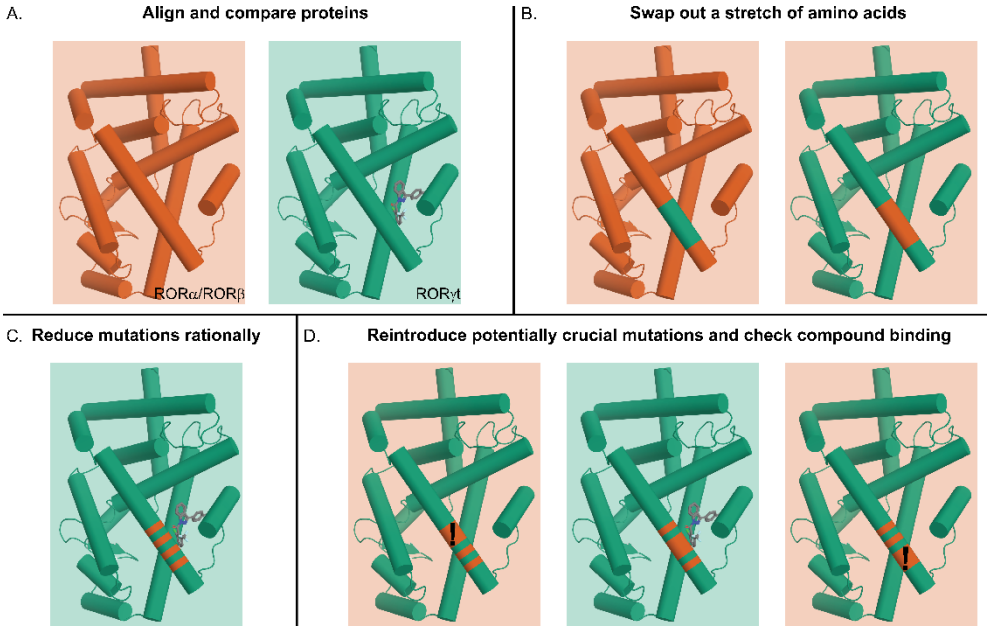

Figure 6 | Schematic representation of the approach to increase the chances to successfully implement an allosteric pocket into RORα or RORβ. (*A*) Protein sequences are compared to indicate how the residues align. (*B*) A stretch of amino acids is swapped between both proteins and allosteric compound binding is checked. (*C*) The mutations are reduced rationally to restore allosteric compound binding. (*D*) Potentially crucial mutations are reintroduced to indicate which ones are incompatible with allosteric compound binding.

After important stretches are elucidated, the next step would be to reduce the number of mutated residues to only crucial ones. For this I would suggest using a rational approach for the first step. Using visual inspection of the available crystal structures, residues that are likely to be less important for pocket formation, for instance because their side chains are directed out of the pocket, can be indicated. Then, I would suggest making a new RORγt mutant where again part of the H11' of RORβ is inserted, but now only residues seemingly unimportant from visual inspection are included (Figure 6C). If this still leads to an unfunctional allosteric pocket, this means that these presumably unimportant residues have a bigger

effect than expected and need further investigation. If the allosteric pocket is still functional, this reduces the potentially important residues significantly meaning they can be investigated one by one (Figure 6D). By applying this method to each region in proximity of the allosteric pocket in RORγt, hopefully similar pockets can be created in RORα and RORβ.

Tuning the selectivity of MRL-871 and related compounds towards PPARγ

In **chapter 4** the binding mode and effects of MRL-871 on PPARγ were studied. For therapeutic purposes, it is important that RORγt allosteric inverse agonists have minimal off target effects. Therefore, tuning the selectivity of RORγt over PPARγ is interesting. In the chapter, three RORγt inverse agonists were tested on RORγt and PPARγ simultaneously. While these compounds have highly similar substituents, their central core structures differ. MRL-871 features an indazole core while FM26 and CPD13 respectively have a trisubstituted isoxazole and a thienopyrazole core. These differences result to having significant effects on the preference for either RORγt or PPARγ. The largest difference in affinity in HTRF is featured by MRL-871. However, since this compound binds with very high affinity to RORγt, also its binding in PPARγ is in the nanomolar regime. As such, this compound would potentially not be ideal for targeting RORγt in autoimmune disorders. FM26could be a more promising candidate regarding this aspect. Its affinity to RORγt is lower than that of MRL-871, but in PPARγ binding is only seen at very high concentrations. Optimization around this core could therefore yield stronger RORγt inverse agonists with lower PPARγ off-target activity. Recently, work has been published that highlights the potential of this.[8]

Future possibilities for BraTSA

BraTSA, as described in **chapter 5**, is a simple and cheap assay that can provide binding constants for NRs. However, what is described in this chapter merely serves as a proof of concept and in theory could potentially be applied in a plethora of situations. One of these situations, that I would like to describe in more detail, is the application of this assay for unpurified proteins (Figure 7). In many situations, especially when assessing libraries of mutants, the protein purification process is a hurdle that is very labor and material intensive, especially when these mutants end up not harboring the desired compound binding. For this reason, it could be useful to have a cheap and quantitative ligand binding assay that can be applied on

mixtures of proteins. For this purpose, I would suggest a modified version of BraTSA using Coomassie staining of SDS-page gels for read-out. In this modified version, after overexpression of the target protein, cell lysate would be divided into samples which could be treated with a range of compound concentrations. After this a fixed heat challenge is applied to all samples leading to (partial) denaturation of most proteins. As with normal BraTSA, centrifugation could then be applied to separate denatured from folded protein. Next, a normal SDS-page protocol could be applied on the folded protein where samples are combined with buffer, denatured and charge separated in an electrophoresis chamber. Coomassie staining, that is based on the same principle as the Bradford protein assay could then be used to visualize the proteins on the gel. With overexpression, normally there is a clear band at the molecular weight of this protein. Using suitable software, the intensity of this band can be quantified and can be compared between the samples before and after the heat challenge with varying compound concentrations. When plotting these intensities, the calculations by Bai *et al*. can again be used to fit dissociation constants.[9] Alternatively, western blotting could be used to, even more specifically, visualize and quantify the protein of interest.

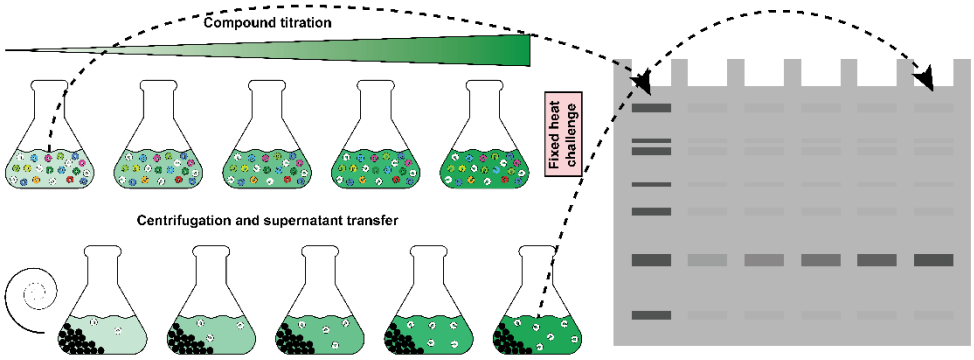

Figure 7 | Schematic representation of SDS-page based TSA to look at compound induced thermal stabilization in bacterial lysate. Bacterial lysate is split into samples and treated with a range of compound concentrations. A fixed heat challenge is then applied after which centrifugation pellets unfolded protein. Supernatant is denatured and run using SDS-page after which staining is done using Coomassie. Intensity of the overexpression band is used to quantify the amount of folded protein before and after the heat challenge.

Another, logical, next step for BraTSA is the application to other target classes. Up till now, NRs are used for proof-of-concept studies. However, in theory, the assay could be applied to any protein. Especially in cases where functional assays are not

available, BraTSA could yield a nice alternative where little to no baseline information about the functions of such proteins within the cell is needed.

Furthermore, inspired by Bai *et al*., denaturing agents might be used to artificially lower the melting temperature of proteins. This way it might be possible to measure BraTSA at physiological temperatures.

Closing thoughts

The research described in this thesis, provides us with novel insights into ligand binding in NRs and especially in the allosteric pocket of RORγt. It also gives us novel tools and methods to investigate such a system. Hopefully, the knowledge that the allosteric pocket of RORγt is unique gives extra motivation to develop compounds binding this pocket that could benefit patients suffering from autoimmune diseases. Additionally, knowing the binding mode and effects of MRL-871 in PPARγ could yield a starting point for developing more selective compounds for both RORγt and PPARγ. For PPARγ these strong binders in the β-sheet region without major agonistic effects could be very interesting for developing drugs for type II diabetes. Finally, I hope BraTSA will be adopted in more labs as a cheap and easy to set up assay to measure binding affinities of various proteins and ligands that could be challenging to investigate using alternative assays.

Experimental section

Site-directed mutagenesis

Point mutations (C320F, V376F, I400F and combinations) were introduced using the QuikChange Lightning Multi Site-Directed Mutagenesis Kit (Agilent) in accordance with the protocols described in the kit manual. The parental DNA for this was a pET15b vector containing the RORγt LBD (residues 265-518) with an N-terminal His6-tag. Single primers designed to hybridize with the parental DNA containing 1 mismatch were utilized for this.

The primers for the H11' swap constructs were prepared via the method described by Liu and Naismith.[10] In short, primers with overlap on the 5' end (pp) were designed in such a way that the swap was in the pp region while the 3' ends (no) could hybridize to the DNA efficiently. For the PCR reaction, 0.2 ng/µL parental DNA was combined with 1 µM of both primers and 1X Phusion polymerase in HF buffer (Thermo Scientific). The reaction started with denaturation (1 min, 98 °C) followed by 18 amplification steps. Each of these steps started with denaturation (10 s, 98 °C), followed by annealing (1 min, T_m no -5 °C) and extension (2:30 min, 72 °C). The method ended with a final annealing (1 min, T_m pp -5 °C) and extension (30 min, 72 °C) step.

For all mutagenesis reactions, the parental DNA was digested using DpnI followed by transformation into XL10-Gold Ultracompetent Cells (Agilent) by heat shock. Small cultures were initiated, using single colonies in 5 mL LB medium supplemented with ampicillin (100 µg/mL), overnight at 37 °C 250 rpm. DNA was isolated using the QIAprep® Spin Miniprep Kit (Qiagen) in accordance with the supplied protocol. The mutations were confirmed by sequencing using T7 promoter and T7 terminator primers (BaseClear).

Expression and purification of the RORγt and RORβ constructs

His6-RORγt LBD constructs were expressed and purified as described in chapter 2. The His6-RORβ LBD construct was expressed and purified as described in chapter 3.

Homogeneous time-resolved FRET (HTRF)

Protein titrations were done as described in chapter 3. Compound titrations were done as described in chapter 2. All assays were done as a proof of concept and only measured once in triplicate.

References

1. Ivanov, I. I. *et al.* The Orphan Nuclear Receptor RORγt Directs the Differentiation Program of Proinflammatory IL-17+ T Helper Cells. *Cell* **126**, 1121–1133 (2006).
2. Leesnitzer, L. M. *et al.* Functional consequences of cysteine modification in the ligand binding sites of peroxisome proliferator activated receptors by GW9662. *Biochemistry* **41**, 6640–6650 (2002).
3. Brust, R. *et al.* Modification of the Orthosteric PPARγ Covalent Antagonist Scaffold Yields an Improved Dual-Site Allosteric Inhibitor. *ACS Chem. Biol.* **12**, 969–978 (2017).
4. Meijer, F. A., van den Oetelaar, M. C. M., Doveston, R. G., Sampers, E. N. R. & Brunsveld, L. Covalent Occlusion of the RORγt Ligand Binding Pocket Allows Unambiguous Targeting of an Allosteric Site. *ACS Med. Chem. Lett.* **12**, 631–639 (2021).
5. de Vries, R. M. J. M., Meijer, F. A., Doveston, R. G., Leijten-Van de Gevel, I. A. & Brunsveld, L. Cooperativity between the orthosteric and allosteric ligand binding sites of RORγt. *Proc. Natl. Acad. Sci. U. S. A.* **118**, (2021).
6. Meijer, F. *et al.* Ligand-Based Design of Allosteric Retinoic Acid Receptor-Related Orphan Receptor γt (RORγt) Inverse Agonists. *J. Med. Chem.* acs.jmedchem.9b01372-acs.jmedchem.9b01372 (2019) doi:10.1021/acs.jmedchem.9b01372.
7. Gevel, I. A. L. de & Brunsveld, L. Delineation of the molecular determinants of the unique allosteric binding site of the orphan nuclear receptor RORγt. *J. Biol. Chem.* **295**, 9183–9191 (2020).
8. Meijer, F. A. *et al.* Structure–Activity Relationship Studies of Trisubstituted Isoxazoles as Selective Allosteric Ligands for the Retinoic-Acid-Receptor-Related Orphan Receptor γt. *J. Med. Chem.* **64**, 9238–9258 (2021).
9. Bai, N., Roder, H., Dickson, A. & Karanicolas, J. Isothermal Analysis of ThermoFluor Data can readily provide Quantitative Binding Affinities. *Sci. Rep.* **9**, 1–15 (2019).

10. Liu, H. & Naismith, J. H. An efficient one-step site-directed deletion, insertion, single and multiple-site plasmid mutagenesis protocol. *BMC Biotechnol.* **8**, 91–91 (2008).

Understanding Allosteric Modulation of Nuclear Receptors by Engineering Proteins and Assays

Nuclear receptors (NRs) are proteins that reside within cells and translate molecular input into transcriptional output. Usually, target-molecules enter the cell and bind to the classical, orthosteric pocket within the ligand binding domain (LBD) of a NR. However, in recent years alternate ligand binding sites have been discovered which can be highly relevant for therapeutically targeting NRs. These allosteric binding sites are less conserved among NRs which highlights possibilities for increased selectivity. Additionally, in some cases, these sites are also available when the orthosteric pocket is already occupied, making it interesting for cases where endogenous compounds block the classical pocket. Currently, a lot of effort is put into the development of compounds that bind such allosteric sites. The research described in this dissertation investigates the mechanisms behind the formation of allosteric pockets in NRs via the development of engineered proteins and novel assays.

Retinoic acid receptor-related orphan receptor-γt (RORγt) is a constitutively active NR that positively regulates the expression of interleukin-17 in T helper 17 cells, resulting in an inflammatory reaction. In autoimmune diseases, inhibiting this receptor has proven to be effective in reducing inflammation. In 2015, a novel, allosteric binding site was found withing the LBD of RORγt. In chapter 2, the molecular determinants of the allosteric binding site of RORγt were determined using multiple-sequence alignment, mutagenesis and several biochemical assays. Based on these results we could conclude that this pocket is unique within the NR superfamily.

RORα and RORβ are the two additional members of the ROR superfamily. In contrast to RORγt, few molecules are available for these receptors making it difficult to evaluate their functions or attempt to target them. Because these receptors are highly related to RORγt, but do not possess all critical residues needed for allosteric pocket formation, in chapter 3, we tried to engineer an allosteric pocket into RORα and RORβ using mutagenesis. Unfortunately, both bottom-up and top-down mutagenesis strategies did not yield allosterically targetable NRs, meaning there are even more necessities making this pocket unique for RORγt.

One of the first identified RORγt allosteric inverse agonists, MRL-871, shows significant off target binding to peroxisome proliferator-activated receptor gamma (PPARγ). In chapter 4, we investigated the binding mode of this compound to PPARγ. We showed that MRL-871 binds in a unique way within the LBD of this NR and with that stabilizes the LBD without inducing strong agonism. This binding mode could potentially uncouple insulin sensitizing actions from adverse effects.

Current techniques to quantify NR-ligand interactions often use labels that can cause bias or require large quantities of material or expensive specialized equipment. In chapter 5 we developed a novel biochemical assay to study ligand binding quantitatively. This assay is based on the principle that interaction between a protein and a ligand can lead to a change in thermal stability. By measuring the amount of soluble protein that is left after a heat-challenge, we can create compound binding curves. From the data of the Bradford thermal stability assay (BraTSA) we can deduce dissociation constants in a cheap, label-free manner. As a proof of principle, the assay is successfully applied to both PPARγ and RORγt.

Finally, in chapter 6 ongoing efforts and future opportunities are highlighted based on the findings of the previous chapters. This way the path is laid out to create a novel assay format for discovering allosteric RORγt binders, a new approach is suggested for pocket insertion into RORα and RORβ, advise is given for the development of selective compounds for either RORγt or PPARγ and additional possibilities for BraTSA are described.

Together, the data described in this dissertation has provided novel insights into the allosteric modulation of NRs by using mutagenesis and engineering assays.

Allostere Modulatie van Kernreceptoren Begrijpen door het Ontwikkelen van Eiwitten en Analysemethodes

Kernreceptoren zijn eiwitten die zich binnenin de cel bevinden en moleculaire input vertalen naar output in de vorm van eiwittranscriptie. Normaal gesproken komen moleculen de cel binnen en binden aan de klassieke, orthostere pocket binnen het ligand bindende domein (LBD) van een kernreceptor. De laatste jaren zijn er alternatieve ligand bindende plaatsen ontdekt welke zeer relevant kunnen zijn voor het therapeutisch benaderen van kernreceptoren. Deze allostere bindingsplaatsen zijn minder bewaard gebleven tussen verschillende kernreceptoren wat mogelijkheden brengt voor het verhogen van selectiviteit. Verder zijn deze plaatsen in sommige gevallen ook beschikbaar wanneer de orthostere bindingsplaats al bezet is. Dit maakt het interessant voor gevallen waar endogene liganden de klassieke pocket bezetten. Op dit moment wordt er veel energie gestoken in de ontwikkeling van moleculen die in allostere pockets binden. Het werk dat wordt beschreven in dit proefschrift onderzoekt de mechanismes achter het vormen van allostere pockets in kernreceptoren via de ontwikkeling van gemanipuleerde eiwitten en nieuwe analysemethodes.

De Retinoic acid receptor-related orphan receptor-γt (RORγt) is een constitutief actieve kernreceptor die de expressie van interleukine -17 in T helper 17 cellen positief reguleert wat leidt tot ontstekingsreacties. Binnen auto-immuunziektes is gebleken dat het inhiberen van deze receptor ontstekingen kan verminderen. In 2015 werd een nieuwe, allostere bindingsplaats ontdekt binnen het LBD van RORγt. In hoofdstuk 2 werden de moleculaire determinanten van de allostere bindingsplaats in RORγt bepaald met behulp van multiple-sequence alignment, mutagenese en meerdere biochemische analysemethodes. Gebaseerd op deze resultaten konden we concluderen dat de pocket uniek is voor RORγt binnen de superfamilie van kernreceptoren.

RORα en RORβ zijn de andere twee leden van de ROR superfamilie. In tegenstelling tot RORγt zijn er maar weinig moleculen beschikbaar voor deze receptoren wat het evalueren van functies en therapeutisch benaderen van deze receptoren bemoeilijkt. Omdat deze receptoren in hoge mate verwant zijn aan RORγt, maar niet alle kritische residuen benodigd voor allostere pocket formatie bezitten,

hebben we in hoofdstuk 3 geprobeerd om een allostere bindingsplaats in RORα en RORβ te construeren met behulp van mutagenese. Helaas waren zowel “bottom-up” als “top-down” mutagenese strategieën onsuccesvol in het creëren van allosteer te benaderen receptoren. Dit betekent dat er nog meer factoren zijn die de pocket uniek maken voor RORγt.

Een van de eerste allostere inverse agonisten die werd gevonden voor RORγt, MRL-871, laat significante binding zien aan peroxisome proliferator-activated receptor gamma (PPARγ). In hoofdstuk 4 hebben we de manier van binden van dit molecuul in PPARγ onderzocht. We lieten zien dat MRL-871 bindt op een unieke manier binnen het LBD van deze receptor en op deze manier het LBD stabiliseert zonder het induceren van sterke activatie. Deze manier van binden kan mogelijkerwijs de insuline sensibiliserende acties loskoppelen van de bijwerkingen.

Hedendaagse technieken die interacties tussen kernreceptoren en liganden kwantificeren, gebruiken vaak labels die de resultaten in een bepaalde richting sturen of hebben grote hoeveelheden materiaal of dure specialistische apparatuur nodig. In hoofdstuk 5 hebben we een nieuwe biochemische analysemethode ontwikkeld die ligand binding kwantitatief kan bestuderen. Deze methode is gebaseerd op het principe dat interactie tussen een eiwit en een ligand kan leiden tot een verandering in thermische stabiliteit. Door het meten van de hoeveelheid oplosbaar eiwit die over is na een “heat-challenge”, kunnen we bindingscurven voor moleculen maken. Vanuit de data van dit Bradford thermische stabiliteit assay (BraTSA) kunnen we dissociatie constanten deduceren op een goedkope en labelvrije manier. Als “proof of principle” hebben we deze techniek succesvol toegepast op zowel PPARγ als RORγt.

Als laatste worden in hoofdstuk 6 voortdurende inspanningen en toekomstige kansen uitgelicht gebaseerd op de bevindingen van de eerdere hoofdstukken. Op deze manier wordt het pad uitgestippeld voor het maken van een nieuwe analysemethode voor het ontdekken van allostere RORγt binders, een nieuwe aanpak wordt voorgesteld voor het creëren van een allostere pocket in RORα en RORβ, advies wordt gegeven voor het ontwikkelen van selectieve moleculen voor ofwel RORγt ofwel PPARγ en extra mogelijkheden voor BraTSA worden uitgewerkt.

Samengenomen beschrijft de data in dit proefschrift nieuwe inzichten in de allostere modulatie van kernreceptoren door het gebruik van mutagenese en het ontwikkelen van analysemethodes.

Curriculum Vitae

Iris Leijten-van de Gevel werd geboren op 3 februari 1994 in Rosmalen. Na het *cum laude* behalen van haar VWO-diploma aan het Theresialyseum in Tilburg begon zij aan haar studie Biomedische Technologie aan de Technische Universiteit Eindhoven. Haar bachelorgraad (BSc) behaalde ze in 2015 *met grote waardering* waarna ze doorstroomde naar de masteropleiding Biomedical Engineering. Tijdens haar master heeft ze deelgenomen aan een eenjarig honors programma van de "Netherlands Research School of Chemical Biology" (NRSCB). Als afstudeerproject heeft ze, onder begeleiding van prof.dr.ir. Luc Brunsveld en dr. Christian Ottmann gewerkt aan het karakteriseren van de interactie tussen 14-3-3 en kernreceptoren. Hierna heeft ze een externe stage uitgevoerd binnen de assay development afdeling van AstraZeneca in Göteborg, Zweden. Na het behalen van haar mastergraad (MSc) *met grote waardering* in 2017 is ze gestart aan haar promotieonderzoek onder begeleiding van prof.dr.ir. Luc Brunsveld in de Chemische Biologie groep aan de Technische Universiteit Eindhoven. Het doel van haar onderzoek was het begrijpen van de allostere modulatie van kernreceptoren door middel van het ontwikkelen van eiwitten en analysemethodes.

Iris Leijten-van de Gevel was born on February 3rd, 1994 in Rosmalen, the Netherlands. After completing her pre-university education *cum laude* at the Theresialyceum in Tilburg he started studying Biomedical Engineering at the Eindhoven University of Technology. In 2015 she obtained her Bachelor of Science (BSc) degree *with great appreciation* after which she continued with the Master program Biomedical Engineering. During her Master education she participated in a 1-year honor program of the "Netherlands Research School of Chemical Biology" (NRSCB). As graduation project she characterized the interaction between 14-3-3 and nuclear receptors under supervision of prof.dr.ir. Luc Brunsveld and dr. Christian Ottmann. After this she did an externship at the assay development department of AstraZeneca in Gothenburg, Sweden. After obtaining her Master of Science (MSc) *with great appreciation* in 2017 she started her PhD project under supervision of Luc Brunsveld in the Chemical Biology group of the Eindhoven University of Technology. The goal of her research was to understand the allosteric modulation of nuclear receptors by engineering proteins and assays.

List of Publications

I.A. Leijten-van de Gevel & L. Brunsveld. A Cheap and Label-free Thermal Stability Assay for Nuclear Receptor-Ligand Binding Constant Determination. *In preparation.*

I.A. Leijten-van de Gevel, K.H.N. van Herk, R.M.J.M. de Vries, N.J. Ottenheym, C. Ottmann & L. Brunsveld. Indazole MRL-871 Interacts with PPARγ via an Unique Unanticipated Binding Mode. *Submitted*.

R.M.J.M. de Vries*, F.A. Meijer*, R.G. Doveston, **I.A. Leijten-van de Gevel** & L. Brunsveld. Cooperativity between the orthosteric and allosteric ligand binding sites of RORγt. *Proc. Natl. Acad. Sci. U. S. A.* **118**, (2021).

E. Sijbesma*, B.A. Somsen*, G.P. Miley, **I.A. Leijten-van de Gevel**, L. Brunsveld, M.R. Arkin & C. Ottmann. Fluorescence Anisotropy-Based Tethering for Discovery of Protein–Protein Interaction Stabilizers. *ACS Chem. Biol.* **15**, 3143–3148 (2020).

I.A. Leijten-van de Gevel & L. Brunsveld. Delineation of the molecular determinants of the unique allosteric binding site of the orphan nuclear receptor RORγt. *J. Biol. Chem*. **295**, 9183–9191 (2020).

I.A. Leijten-van de Gevel*, F.A. Meijer*, R.M.J.M. de Vries* & L. Brunsveld. Allosteric small molecule modulators of nuclear receptors. *Mol. Cell. Endocrinol.* **485**, 20–34 (2019).

Acknowledgements

Ineens is het zover: na bijna 10 jaar komt mijn tijd op de TU/e ten einde. In 2012 startte ik, vers van het VWO, vol goede moed aan mijn bachelor. Eerst nog een kleine omzwerving naar de technische wiskunde, maar al snel helemaal op mijn plek bij biomedische technologie. In die tijd heb ik ontzettend veel mogen leren, steeds meer in de richting van de chemische biologie, maar ben ik ook persoonlijk veel gegroeid. Ik schrijf dit dankwoord dan ook in ons tweede eigen huis, met twee katten die af en toe miauwen achter de deur, terwijl ik straks onze dreumes van de opvang mag gaan halen. Deze ontwikkelingen op persoonlijk en wetenschappelijk vlak had ik nooit alleen kunnen maken en daarom wil ik graag een aantal mensen bedanken.

Als eerste is daar mijn promotor **Luc**. Tijdens de eerstejaarscolleges biochemie maakte je al indruk en introduceerde je mij in de wondere wereld van de eiwitten. De fascinatie die je toen op mij hebt overgebracht, is nooit verdwenen. Dankjewel dat je mij de kans en vrijheid hebt gegeven om mezelf te ontwikkelen. Jij zag altijd kansen wanneer ik dacht dat het allemaal niet meer goed kwam en vooral de wekelijkse meetings tijdens het laatste jaar van mijn promotie heb ik enorm gewaardeerd. Dankjewel dat je altijd plaats voor mij wist te maken in je drukke schema. En ook bedankt voor je geduld in tijden waarin ik zoekende was naar de balans en waar onderzoek misschien niet op de eerste plaats stond. De Chemical Biology groep groeit soms sneller dan ik bij kan houden en dat je daarbij ook nog AmbAgon zeer succesvol hebt weten op te richten vind ik heel indrukwekkend.

Ook de rest van mijn promotiecommissie wil ik van harte bedanken. **Christian**, bij het eerste college dat ik van je had was ik een tikkeltje afgeleid door de combinatie van spieren en wetenschap. In de jaren daarna heb ik je leren kennen als een enorm bevlogen wetenschapper die het liefst al zijn aandacht geeft aan dat ene wondere eiwit, 14-3-3. Toch was je de eerste jaren van mijn promotie altijd aanwezig bij de nuclear receptor meetings en had je altijd hele waardevolle inzichten. Dankjewel dat je wil optreden als mijn tweede promotor. Bedankt ook **prof. Zwart** en **dr. Kalkhoven** voor het lezen van mijn proefschrift en bijwonen van mijn verdediging. Tijdens de jaarlijkse nuclear receptor research network meetings heb ik u allebei al een beetje mogen leren kennen en afgelopen november hebben we daar zelfs de discussie over mijn onderzoek al voorzichtig opgestart. Ik kijk er naar uit om deze discussie voort te zetten. Thank you **prof. Merk** for taking the time to travel all the way from München. I am very curious about your viewpoint on my research. I also want to thank **dr. Grisoni** and **dr. Van Zanten** for their critical assessment of my dissertation and their participation in the defense ceremony. Als laatste **Maarten**, bedankt voor het voorzitten van de zitting en voor alle vragen tijdens chemical biology meetings die me steeds weer aan het denken hebben gezet.

Natuurlijk wil ik ook mijn paranimfen **Femke** en **Suzanne** bedanken. Als eerste Femke: wij leerden elkaar kennen tijdens NRSCB en kwamen er meteen achter dat we heel veel raakvlakken hebben. Zoveel, dat we ons bijna niet kunnen voorstellen dat we elkaar tijdens onze jeugd in buurdorpen Bavel en Gilze nooit eerder zijn tegengekomen. Zeker omdat onze onderwerpen aan elkaar gerelateerd waren, hebben we tijdens onze promoties veel samen mee mogen maken. De hoogtepunten hierbij waren toch wel de conferenties (vakanties?) in Ljubljana en Heidelberg samen met Rens. Buiten het werk heb je me al eens eerder met veel succes bijgestaan als bruidsmeisje, dus ik weet zeker dat ik mijn verdediging goed doorkom met jou aan mijn zij. **Suzanne**, toen ik startte aan mijn promotie was jij ook net een paar maanden bezig. Ik heb altijd enorm genoten van onze gezellige theekransjes en kon altijd heerlijk met je sparren, een beetje over werk, maar ook zeker over onze creatieve projecten. Ook in de laatste jaren waarin we elkaar niet heel veel hebben gezien, hield je altijd de vinger aan de pols om te checken hoe het met me ging. Hiervoor ben ik je ontzettend dankbaar! Heel fijn en bijzonder dat wij nu kort na elkaar allebei deze periode mogen afronden.

Als ik één ding heb geleerd tijdens de afgelopen vier jaar is het dat samen altijd fijner is dan alleen. Daarom wil ik ook graag de mensen bedanken met wie ik samen heb mogen werken aan het onderzoek in dit proefschrift. **Femke**, nogmaals, en **Rens**, vanaf het begin van mijn promotie vormden wij samen de zelf benoemde “NR kerngroep”. Hoewel we het onderzoek allemaal vanaf een hele andere kant benaderden, konden we altijd fijn met elkaar sparren en hebben we samen onder andere een review geschreven. Het was altijd wonderbaarlijk om te merken hoe goed wij elkaar aanvulden, ook op onze conferentiereisjes. Rens, bedankt dat er altijd plek was op de drukbezette kruk op jouw kantoor voor uitgebreide “vrijdagmiddagdiscussies”. Hoofdstuk 3 en 4 hadden niet bestaan zonder mijn fantastische club aan masterstudenten. **Laureen**, ik was pas net begonnen aan mijn PhD toen ik jou al onder mijn hoede kreeg. Jouw enorme drive en onuitputtelijke enthousiasme is aanstekelijk en je hebt ontzettend veel gedaan om een lastig en niet automatisch succesvol project zo goed mogelijk te doorgronden. Dankjewel hiervoor en succes verder bij Synaffix waar ze enorm boffen met jou. **Nicolaas**, het was wat zoeken in het begin om de juiste verhouding tussen ons te vinden, maar ik vond het heel leuk om naast jou te mogen staan tijdens de laatste fase van je afstuderen waarbij je mij hebt geïntroduceerd aan het wondere eiwit PPARγ. Je grondigheid en plezier in het opzetten en analyseren van assays deel ik met je. Je hebt er echt voor gezorgd dat je resultaten naar een hoger niveau werden getild. Heel passend dan ook dat je nu bij het PPSC werkt, wat een goede match! **Kim**, ik vond het heel leuk om jou te mogen begeleiden. Je trekt graag je eigen plan, maar ik ben blij dat ik je hierbij toch heb mogen ondersteunen. Dankjewel voor het voortzetten van het PPARγ project. Zonder jouw kristalstructuur hadden we nu niet zo’n mooi verhaal te vertellen gehad. Nog veel geluk bij Symeres. **Twan**, jij had de

zware taak om met de mega dataset van Laureen aan de slag te gaan en dat terwijl ik in het begin amper tijd had om je te begeleiden. Hoewel er veel gebeurde in mijn wereld en in de wereld om ons heen (trouwen, verhuizen, zwanger, pandemie) ben jij altijd vrolijk en stug doorgegaan. Dankjewel voor je doorzettingsvermogen en voor het geven van een stabiele factor in die snel veranderende wereld. Je hebt je enorm (snel!) ontwikkeld tijdens je afstuderen en ik ben ervan overtuigd dat je je eigen PhD met glans gaat volbrengen. **Justin**, **Lisanne** en **Ingrid** wat was het leuk om jullie samen met Femke te begeleiden tijdens jullie bachelor eind project. Ik vond het leuk om jullie in die korte periode kennis te laten maken met heel veel verschillende technieken op het lab. Hoewel jullie project nogal abrupt werd afgekapt, hebben we samen toch een leuke start kunnen maken aan een mooi project. Succes met jullie afstudeerprojecten!

Bente, onze onderzoeken hebben elkaar meerdere keren gekruist. Ik vind het superleuk dat jij en je studenten het werk dat ik in mijn master heb gestart, doorzetten met zulke goede resultaten, dankjewel daarvoor! Ook bedankt voor je hulp met het frustrerende PPARγ fosforylatie verhaal, zonder jou had ik dat veel eerder opgegeven. En natuurlijk bedankt voor de gezelligheid, onder andere tijdens ons tripje naar Leiden voor de Dutch Medicine Days samen met Femke en Emira. Daarvoor wil ik **Emira** natuurlijk ook bedanken. Jou leerde ik kennen als “de andere studente van Eline”. Inmiddels ben je natuurlijk wel meer dan dat. Ik heb heel veel respect voor het uithoudingsvermogen waarmee je onderzoek en leven op twee locaties combineert. **Guido** en **Maxime**, ik kan niet anders dan jullie in een adem bedanken. Ik vind het heel leuk dat ik jullie vanaf de zijlijn heb mogen zien groeien en dat jullie intussen alweer tot over je oren in het PhD bestaan zijn beland. Maxime, bedankt voor de persoonlijke interesse die je altijd hebt getoond. Ik vond het altijd heel leuk om je eventjes te spreken en ook in het lab heb ik je altijd met veel plezier geholpen tijdens je master. Guido, ook naast jou heb ik wat uurtjes in het lab mogen doorbrengen. Ik vond het heel leuk om je de fijne kneepjes van de NR expressie bij te brengen en vind het heel gaaf en bewonderingswaardig hoe jij alles jezelf eigen maakt. **Pim**, jouw inzichten tijdens meetings, maar ook gezellig in discussie op kantoor, hebben me altijd aan het denken gezet, dankjewel hiervoor. Zonder jouw aanmoediging had ik nooit de moed gehad om het BraTSA verhaal werkelijkheid te laten worden, bedankt! Ik ben heel benieuwd wat jouw carrière allemaal nog gaat brengen, want ik ken niemand met zo’n brein als jij. **Auke**, jou wil ik bedanken als mijn PPARγ collega. Wat fijn dat je het stokje van dat project hebt overgenomen toen het voor mij te “chemisch” werd. Ik vind het heel gaaf dat daar zulke interessante resultaten uitkomen en ben benieuwd wat de toekomst zal brengen. **Peter**, I would like to thank you for everything you do for the group. I also really liked getting to know you a little better over our shared interest of bouldering and I appreciate the interest you always show in me and my family. Good luck with the rest of your career you’re working so hard on. **Sylvia**, ten eerste bedankt voor

het overnemen van mijn Qtof verantwoordelijkheid. Maar natuurlijk ook voor de gezelligheid door de jaren heen. Ik herinner me nog steeds ons gesprek van inmiddels bijna 3 jaar geleden bij de verdediging van Sebastian Andrei over het wel of niet krijgen van kinderen tijdens je PhD waarbij jij zei dat je goed bij mij zou afkijken. Hoe leuk dat ik nu een dreumes heb rondlopen en jij hoogzwanger bent! Veel geluk met je gezin en succes met de rest van je promotie. **Eline** wil ik ook heel graag bedanken. Al tijdens mijn bachelor leerde ik jou kennen doordat jij ons begeleidde bij mijn eerste project in het lab. Ik heb in die tijd zelfs "in jouw oude kamer" gewoond en later heb jij mij begeleid bij mijn afstudeerproject. Bedankt voor alle begeleiding en inspiratie de afgelopen jaren. Ik vind het leuk dat wij allebei ons eigen pad bewandelen, maar toch steeds parallellen blijven houden. Heel veel geluk met je gezin en carrière. **Tim**, jou wil ik graag bedenken voor de gezelligheid in het lab, helemaal tussen de lockdown periodes door. Ik vond het heel gezellig om jouw lab-buur te zijn, maar ook om een keertje te baby-daten. Succes met je carrière! Ook de rest van de huidige en vroegere **Chemical Biology group** wil ik bij dezen bedanken voor de fijne input tijdens de meetings, maar ook de leuke gesprekken in het lab, op de gang en bij conferenties en uitjes.

Ik wil ook heel graag de "bitterbalbarbecue" groep bedanken voor alle gezelligheid tijdens koffie, thee- en lunchpauzes op de universiteit, maar ook daarbuiten. We zijn met zijn negenen gestart en inmiddels hoort een heel groot deel daarvan inmiddels bij de club van doctors. Femke, Suzanne en Rens heb ik al eerder benoemd, maar de rest wil ik bij dezen ook bedanken. **Simone**, bedankt dat je vanaf dag een je best hebt gedaan om mij me thuis te laten voelen. In je drukke schema wist je gelukkig altijd tijd te maken voor een gezellige kop thee en ook om 12uur met de lunch was je er altijd bij. Zo'n stabiele factor is heerlijk, dankjewel daarvoor! Ik heb altijd met veel bewondering aanschouwd hoe hard jij kunt werken, maar ook hoe goed jij bent in de begeleiding van studenten. Ze boffen maar met jou bij AbSano! Ik hoop dat je daar net zo goed tot je recht komt. **Lenne**, ook jij zorgde ervoor dat ik mij al heel snel thuis voelde als PhD'er. Niet alleen je manier van werken, maar ook je balans tussen werk en vrije tijd is inspirerend. Bedankt dat je me daarin het goede voorbeeld hebt gegeven! Ik zal nooit meer de middag vergeten waarin je steeds mensen apart ophaalde om vervolgens te laten raden met wie je aan het daten was en ik ben nog steeds enthousiast over de conclusie: **Maaike**! Maaike, jou leerde ik kennen tijdens de eerste ietwat ongemakkelijke TGIF borrel van onze PhD's. We zijn praktisch tegelijk gestart en het was daardoor ook leuk om jouw weg vanaf de zijlijn te mogen volgen. Inmiddels heb jij je al bij de club van doctors gevoegd en hoop ik snel je voorbeeld te gaan volgen! Lenne en Maaike, heel veel geluk zowel persoonlijk als in jullie werk. **Daan**, als mede STO3.25 afstudeerder kende ik jou al een beetje toen ik aan mijn PhD begon. Het was dus letterlijk vanaf dag een meteen gezellig zoals ook de bekende, enthousiaste karaoke foto's niet aan de verbeelding overlaten. Ik ken weinig mensen die zo serieus en

doelgericht kunnen werken als jij, hopelijk kun je dit snel weer oppakken! **Wiggert**, hoewel we in hetzelfde jaar met BMT zijn gestart, en ook nog met sommige dezelfde mensen zijn omgegaan in die tijd, leerden we elkaar toch pas echt kennen tijdens onze PhD's. Met jou op kantoor was het nooit saai! Of het nou wetenschappelijke discussies of kattenfoto's waren, er was altijd wel wat om over te kletsen. Bedankt voor alle gezelligheid en succes met de allerlaatste loodjes.

Niet alleen met Wiggert en Pim, maar ook met **Anniek**, **Eva** en **Lieuwe** heb ik ontzettend geboft als kantoorgenootjes. Bedankt voor alle leuke gesprekken en nodige afleiding tijdens drukke schrijf- of nakijkdagen en natuurlijk bedankt voor de gezellige kantoordates die we hebben gehouden.

Ik wil ook graag een aantal mensen bedanken zonder wie "de derde verdieping" niet zo gestroomlijnd zou lopen als hij nu doet. **Tanja**, bedankt voor al het werk dat jij doet achter de schermen om de Chemical Biology groep te ondersteunen. Wat fijn dat het altijd mogelijk was om binnen te komen wandelen als er iets nodig was. **Joost**, bedankt voor al het geduld dat je met me hebt gehad in de tijd dat ik de eiwitten mat op de Qtof. Ik weet dat het niet altijd van harte ging, maar ik kon altijd erg lachen (soms pas achteraf) om de stiekem best vriendelijke steken onder water. Sylvia en **Sebastian**, bedankt voor het meten van de Qtof samples. Ik weet wat voor verantwoordelijkheid dit is, maar bij jullie is deze in hele goede handen! **Yan Ni**, thanks for keeping all machines up and running and trying to create some order in the peptide chaos. **Christine**, bedankt voor het schoonhouden van de kantoren en labs, maar ook bedankt voor alle fijne gesprekjes. Ik vond het altijd leuk om je even te spreken in de gang en waardeer je oprechte interesse. Verder, heel belangrijk, **Peggy**. De manier waarop jij het Biolab in goede banen weet te krijgen is echt bewonderingswaardig. Ik vond het ook leuk om je een beetje te leren kennen tijdens het begeleiden van de studenten op het lab met biochemie. Bedankt ook dat je mijn vertrouwenspersoon was tijdens het prille begin van mijn zwangerschap, het was heel fijn om dat aan iemand te kunnen vertellen. Ik wil ook de rest van het **Biolab** bedanken voor de fijne werksfeer en de gezelligheid.

De ICMS animatie studio, en meer specifiek **Koen** en **Milan** wil ik bedanken voor het realiseren van mijn kaft. Je zult maar iemand voor je krijgen die graag wil dat d'r proefschrift er uitziet als een kinderjurkje! Jullie hebben ontzettend goed geluisterd en dit mooier gedaan dan ik me had kunnen voorstellen. De "pockets"/'zakjes" van elk hoofdstuk zijn heel goed gelukt: het zoeken naar de specifieke vereisten van een pocket ("Hoe lang moet die 'naad' zijn?", "Kunnen we hier iets 'loshalen' en werkt het dan nog?"), het vanuit het niets creëren van een soortgelijke pocket in een ander eiwit, het bepalen van de exacte bindingsplaats van een molecuul (MRL-871) binnen de grote pocket van een eiwit (PPARγ) en als laatste het met behulp van een assay kijken of er eigenlijk wel iets in een pocket zit.

Ik vind het heel fijn dat jullie de opdracht zo serieus hebben genomen en ben heel blij met het eindresultaat.

Ook buiten de universiteit zijn er mensen zonder wie de laatste 4,5 jaar er anders, en minder fijn, uit hadden gezien. Daarom wil ik graag ook mijn vrienden en familie bedanken. Als eerste mijn “oudste” vriendin **Jeanine**. We leerden elkaar al in de kleuterklas kennen en zijn de rest van de basisschool als soort Siamese tweeling door het leven gegaan. Misschien maar goed ook dat we vanaf de middelbare school alleen maar AL onze hobby’s samendeden. Van dansen tot klarinet spelen bij het orkest en van hardlopen tot volleybal: we zorgden er altijd voor dat we elkaar regelmatig zagen. En gelukkig lukt dat nog steeds! Ook al wonen we al lang niet meer bij elkaar in de buurt, toch blijven we tijd voor elkaar maken en kan ik altijd op je steun rekenen. Of je nou een krabbeltje moet zetten tijdens mijn bruiloft (dankjewel getuige) of een muurtje schildert in ons huis. Ik ben heel dankbaar dat je altijd tijd maakt in je drukke schema en dat je er ook bij deze mijlpaal weer bij bent! Ook **Daniek** en **Ilona** wil ik natuurlijk bedanken. Wij leerden elkaar tijdens onze bachelor kennen en er ontstond meteen een soort drie-eenheid. Ondanks dat we alle drie een ander leven leiden en een eindje uit elkaar wonen, lukt het toch om eens in de paar maanden af te spreken. Steeds als we dit doen, voelt het alsof we elkaar gisteren nog hebben gesproken. Bedankt voor alle gezelligheid en ik kijk ernaar uit dat we elkaar al onze nieuwe huizen kunnen showen binnenkort. Tijdens de afstudeerprojecten ontstond er ineens nog een complete vriendengroep. Een deel kwam vanuit Gemini en de rest van Helix vloer 3 of vloer 4, maar iedere dag werd er weer geappt: “lunchen?” en kwamen we met zijn allen bij elkaar. Inmiddels vormen we alweer een heel aantal jaar samen de “pauzeapp”, die inmiddels beter de “spellenavondapp” of wat later de “bruiloften, baby’s, huizen en verdedigingen app” had kunnen heten, want dat zijn de momenten dat we elkaar nu zien. **Marjolein**, **Sandra**, **Melanie**, **Nick**, **Saskia** en **Pascal**, bedankt voor de gezelligheid tijdens alle maandelijkse spellenavonden tijdens de eerste periode van mijn PhD. En ook bedankt dat we toen de pandemie uitbrak elkaar zijn blijven volgen en steunen bij alle grote mijlpalen die we stuk voor stuk hebben doorgemaakt. Zo leuk om te zien dat we allemaal vanuit het stel studenten dat we waren zulke grote stappen hebben doorgemaakt en ons inmiddels midden in het volwassen leven bevinden! Vanuit dezelfde groep zijn daar natuurlijk ook **Sanne**, **Mathijs**, **Tom**, en **Nimke**. Ook wij kennen elkaar pas een jaar of zes echt, maar wat hebben we al veel met elkaar meegemaakt! Onze vriendschap is heel snel gegroeid en al vrij snel kozen we ervoor om in hetzelfde mooie dorp te gaan wonen. Hier hebben we met onze eigen, gekozen “familie” onze gezinnen zien groeien. Zo mooi om dit met elkaar te beleven! Maar ook zo gezellig om gewoon samen boodschappen te doen, een kop thee te drinken of een spelletje te doen. Inmiddels hebben wij jullie helaas verlaten voor onze échte familie, maar ik ben blij dat we elkaar nog steeds

regelmatig zien en hoop dat onze kinderen altijd die neefjes/nichtjes band zullen houden.

En dan als laatste natuurlijk die échte familie waar ik het net al over had. Ik kom uit een enorm warm nest en heb het geluk gehad om met mijn schoonfamilie in net zo'n nest te zijn beland. Ik wil daarom ook echt álle oma's, opa, ooms, tantes, neefjes en nichtjes bedanken voor hun gezelligheid en interesse. Hoewel mijn werk aan de universiteit voor sommigen nogal een ver van jullie bed show was, heb ik altijd alleen veel trots ervaren. Andersom heb ik ook altijd heel veel respect gehad voor en inspiratie gehaald uit wat jullie allemaal doen en met hoeveel liefde en gedrevenheid dat gaat. Ik vind het heel leuk hoe verschillend iedereen is, maar hoe vertrouwd en fijn het ook voelt om bij elkaar te zijn. Na wat omzwervingen naar Eindhoven en Eersel zijn we sinds kort weer "thuis" in Gilze beland en het voelt heerlijk om iedereen weer om ons heen te hebben: we zijn echt in een warm bad beland.

Nog even in het kort bij naam mijn schoonouders en -broertjes, **Michel**, **Desirée**, **Jim** en **Thijn**. Het is alweer 13 jaar geleden dat ik voor het eerst bij jullie binnenstapte. Vanaf moment één heb ik me altijd welkom gevoeld ook al is het met de bekende "puberperikelen" echt niet altijd makkelijk geweest. Bedankt voor het geven van een extra thuis, niet alleen voor mij, maar natuurlijk ook voor Lisse. Hoe hard jullie werken is ook echt bewonderingswaardig en inspirerend. Ik wist niet dat er zo veel liefde in een supermarkt kon gaan. Heel veel geluk ook gewenst straks in jullie mooie, nieuwe huis.

Natuurlijk verdient ook mijn eigen gezin een heel bijzonder plekje in dit dankwoord. **Papa**, 28 jaar geleden had ik de eer om jouw meest bijzondere verjaardagscadeau ooit te mogen zijn. Ik blijf het leuk vinden dat we die dag samen delen en het wordt vast makkelijker om het ook weer samen te vieren nu we weer vlakbij elkaar wonen. Bedankt dat je me altijd als stille kracht hebt uitgedaagd om het beste uit mezelf te halen. Bedankt ook voor de onvermoeibaarheid waarmee je altijd voor mij en m'n gezin klaarstaat. En, Lisse heeft echt een super-opa! **Mama**, door de jaren heen wordt het alleen maar duidelijker hoeveel wij op elkaar lijken, of, zoals Krezip zingt, "I'll grow up to be just like you". Je bent een fantastisch voorbeeld voor het op een verstandige manier kiezen voor de dingen waar je echt gelukkig van wordt. We hebben intussen ook een leeftijd bereikt waarbij je niet alleen mijn moeder bent, maar ook een hele lieve vriendin waartegen ik alles kan zeggen en ook gewoon weleens lekker kan zeuren. Bedankt dat je altijd mijn klankbord wil zijn. "Ome" **Mees**, wat draag je die titel op een heerlijke manier. Kleine broertjes worden groot en daar ben ik nog steeds niet helemaal aan gewend. Wat een leuke kerel ben jij geworden zeg! Geen wonder dat je zo'n grote en gevarieerde groep aan lieve vrienden om je heen hebt verzameld. Ik heb veel bewondering voor hoe hard je werkt en hoe onmisbaar je jezelf hebt gemaakt op je werk. En voor een "man

alleen" heb je echt het aller gezelligste en mooiste appartement dat ik ken waar ook nog eens de meest fantastische dingen op tafel worden getoverd. Je bent een topper en ik ben blij dat we weer zo dicht bij elkaar wonen.

En als laatste zijn daar natuurlijk **Koert** en **Lisse**. Lieve Koert, wat kennen we elkaar al lang en wat hebben we al veel meegemaakt samen. We waren pas 14 toen we verliefd werden en inmiddels zijn we alweer een half leven verder! We zijn niet meer hetzelfde jongetje en meisje als toen, maar ik ben heel blij en trots op waar we nu staan als man en vrouw, met een fantastische dochter! Bedankt dat je me altijd hebt gesteund ook al snapte jij net zo weinig van mijn eiwit "snoeren" als ik van jouw kabels in de garage. Ik weet nog goed dat je me een keer trots vertelde dat je had geleerd dat aminozuren een soort puzzelstukjes waren waarmee je eiwitten kunt maken. Bedankt voor je interesse en al je pogingen om iets te begrijpen van wat ik doe. Bedankt ook voor je onuitputtelijke vertrouwen in mij, zelfs als ik dat soms zelf een beetje verloren was. En natuurlijk bedankt voor alle liefde en voor het zijn van een fantastische papa voor Lisse. Lieve Lisse, jou wil ik als allerlaatste bedanken. Jij was het perfecte lichtpuntje tijdens de soms lastige laatste twee jaar van mijn PhD. Wanneer de wereld soms stil leek te staan, maakte jij gigantische sprongen in je ontwikkeling en liet ons keer op keer weer lachen met je gekke streken. Het is prachtig om je te zien groeien van een kleine afhankelijke baby, naar een lieve peuter met een duidelijke eigen wil en groot gevoel voor humor. Dankjewel dat ik jouw mama mag zijn.

Dan is nu toch het moment gekomen om dit verhaal af te ronden. Niet alleen ruim 4,5 jaar PhD, maar ook bijna 10 jaar aan de TU/e komen nu echt ten einde. Nog één keer bedankt voor alle lieve mensen die ik heb genoemd, maar ook voor iedereen die ik nog vergeten ben. Op naar het volgende avontuur!

Iris